Novel Aspects of Platelet Signaling and of the Pathogenesis of Immune Thrombocytopenia

• • •

Neue Aspekte in Signalwegen von Blutplättchen und in der Pathogenese der Immunthrombozytopenie

Doctoral thesis for a doctoral degree
at the Graduate School of Life Sciences,
Julius-Maximilians-Universität Würzburg,
Section Biomedicine

submitted by

David Stegner

from Lichtenfels

Würzburg, 2011

Submitted on:

Members of the *Promotionskomitee*:

Chairperson:	**Prof. Dr. Manfred Gessler**
Primary Supervisor:	**Prof. Dr. Bernhard Nieswandt**
Supervisor (Second):	**Prof. Dr. Georg Krohne**
Supervisor (Third):	**Prof. Dr. Johan W. M. Heemskerk**
Date of Public Defense:	**_____**
Date of receipt of Certificates:	**_____**

Table of Contents

Summary

This work summarizes the results of studies on three major aspects of platelet signaling and of the pathogenesis of immune thrombocytopenia. Therefore, this thesis is divided into three parts.

i) Platelet activation and subsequent thrombus formation at sites of vascular injury is crucial for normal hemostasis, but it can also trigger myocardial infarction and stroke. The initial capture of flowing platelets to the injured vessel wall is mediated by the interaction of the *glycoprotein* (GP) Ib-V-IX complex with *von Willebrand factor* (vWF) immobilized on the exposed subendothelial *extracellular matrix* (ECM). The central importance of GPIb for platelet adhesion is well established, whereas GPV is generally considered to be of minor relevance for platelet physiology and thrombus formation. This study intended to clarify the relevance of this receptor during thrombus formation using *Gp5*$^{-/-}$ mice and mice with different double-deficiencies in GPV and in other platelet receptors. It was found that GPV and the collagen receptor integrin $\alpha 2\beta 1$ have partially redundant functions in collagen-triggered platelet aggregation. Further, it was revealed that GPV limits thrombus formation and impairs hemostasis *in vivo*. The data presented here demonstrate that the protective effect of GPVI-deficiency (another platelet collagen receptor) in arterial thrombosis and ischemic stroke depends on the expression of GPV. Moreover, it was demonstrated that lack of GPV restores the hemostatic function of mice lacking both GPVI and $\alpha 2\beta 1$ or mice lacking GPVI and the *C-type lectin receptor 2* (CLEC-2). Conclusively, GPV-depletion or blockade might have the potential to treat hemorrhagic disease states.

ii) Platelets contain the two *phospholipase* (PL) D isoforms, PLD1 and PLD2, both of which presumably become activated upon platelet stimulation. However, the function of PLD in the process of platelet activation and aggregation has not been definitively explored. Thus, PLD-deficient mice were analyzed. Mice lacking PLD1 or PLD2 were viable, fertile and had normal platelet counts. PLD1 was found to be responsible for the inducible PLD-activity in platelets and to contribute to efficient integrin activation under static conditions. Moreover, flow adhesion experiments revealed that PLD1 is essential for efficient GPIb-mediated integrin activation. Consequently, *Pld1*$^{-/-}$ mice were protected from arterial thrombosis and ischemic brain infarction without affecting tail bleeding times. Hence, inhibition of PLD1 might be a novel approach for antithrombotic therapy.

iii) Cellular activation of platelets or immune cells results in increased cytosolic *calcium* (Ca^{2+}) levels. *Store-operated calcium entry* (SOCE) via the STIM1-Orai1 axis is the main route of Ca^{2+} entry downstream of *immunoreceptor tyrosine-based activating motif* (ITAM) receptor stimulation in mast cells and T cells. However, the requirement of Ca^{2+}-mobilization in *Fc*γ

receptor (FcγR)-signaling and the relevance of STIM2 for T cell SOCE have been unclear. To address these questions, genetically modified mice lacking central molecules of the SOCE machinery were analyzed. Ca^{2+}-measurements revealed that both STIM isoforms contribute to Ca^{2+}-mobilization downstream of T cell receptor activation. Additionally, it was found that FcγR stimulation results in SOCE and is mediated by STIM1 and probably Orai1. Animal models of *immune thrombocytopenia* (ITP) revealed that SOCE is essential for platelet clearance and that both STIM isoforms contribute to the pathology of ITP. Moreover, in this work it was also demonstrated that STIM1 and Orai1 are essential in IgG-mediated systemic anaphylaxis. STIM2 contributes to IgG-mediated, but not to IgE-mediated anaphylaxis. The data indicate that interference with SOCE might become a new strategy to prevent or treat IgG-dependent autoimmune diseases.

Zusammenfassung

Diese Arbeit fasst Untersuchungen von drei wesentlichen Aspekten der Signalwege von Blutplättchen und der Pathogenese der Immunthrombozytopenie zusammen. Daher ist diese Doktorarbeit in drei Teile unterteilt.

i) Die Aktivierung von Blutplättchen und die anschließende Thrombusbildung in Folge vaskulärer Verletzungen sind für die normale Hämostase elementar, sie können aber auch Herzinfarkt oder Schlaganfall verursachen. Die anfängliche Adhäsion zirkulierender Blutplättchen an der verletzten Gefäßwand wird durch die Wechselwirkung des *Glykoprotein* (GP) Ib-V-IX Komplexes mit dem auf der freigelegten subendothelialen Matrix immobilisierten *von Willebrand Faktor* (vWF) vermittelt. Die zentrale Bedeutung von GPIb für die Adhäsion von Blutplättchen ist lange bekannt, wohingegen GPV allgemein als unbedeutend für die Physiologie von Blutplättchen oder die Thrombusbildung angesehen wird. Das Ziel dieser Arbeit war, die Bedeutung dieses Rezeptors für die Thrombusbildung zu überprüfen. Hierfür wurden GPV-defiziente Mäuse und mehrere Mauslinien, denen neben GPV ein weiterer Plättchenrezeptor fehlte, analysiert. Es wurde festgestellt, dass GPV und der Kollagenrezeptor Integrin $\alpha 2\beta 1$ teilweise redundante Funktionen in der Kollagen-vermittelten Plättchenaggregation haben. Des Weiteren wurde gezeigt, dass GPV die Thrombusbildung begrenzt sowie die Wundstillung reguliert. Die hier gezeigten Daten belegen, dass GPV überraschenderweise für den Schutz vor arterieller Thrombose oder ischämischem Schlaganfall, der aus dem Fehlen des wichtigsten Kollagenrezeptors GPVI resultiert, benötigt wird. Außerdem wurde gezeigt, dass die Abwesenheit von GPV die Hämostase in Mäusen, denen GPVI und $\alpha 2\beta 1$ oder GPVI und CLEC-2 (von *C-type lectin receptor 2*) fehlt, wieder herstellt. Folglich, könnte die pharmakologische Herabregulierung der GPV-Expression oder die Blockade des Rezeptors eine neue Behandlungsmöglichkeit von hämorrhagischen Krankheitszuständen darstellen.

ii) Blutplättchen exprimieren die beiden *Phospholipase* (PL) D Isoformen PLD1 und PLD2, die vermutlich beide im Zuge der Blutplättchenstimulation aktiviert werden. Allerdings wurde die Rolle von PLD in der Thrombozytenaktivierung und -aggregation noch nicht abschließend untersucht. Daher wurden PLD-defiziente Mäuse analysiert. Mäuse, denen entweder PLD1 oder PLD2 fehlt, sind lebensfähig, fertil und haben normale Thrombozytenzahlen. Es zeigte sich, dass PLD1 für den induzierbaren Anteil der PLD-Aktivität in Blutplättchen verantwortlich und an der Integrinaktivierung unter statischen Bedingungen beteiligt ist. Des Weiteren ergaben Adhäsionsexperimente unter Flussbedingungen, dass PLD1 für die GPIb-vermittelte Integrinaktivierung von zentraler Bedeutung ist. Folglich sind Mäuse mit einer genetischen Ablation von PLD1 vor arterieller Thrombusbildung und ischämischem Schlaganfall

geschützt. Da die Blutungszeiten dieser Tiere nicht verlängert waren, könnte die Inhibition von PLD1 einen anti-thrombotischen Therapieansatz darstellen.

iii) Die zelluläre Aktivierung von Thrombozyten oder Immunzellen geht mit einem Anstieg der zytosolischen Kalziumkonzentration einher. Der sogenannte Speicher-vermittelte Kalziumeinstrom (*store-operated calcium entry*, SOCE) über die STIM1-Orai1-Achse ist der wichtigste Kalziumeinstrommechanismus in Folge der Stimulation von Rezeptoren mit einem *immunoreceptor tyrosine-based activating motif* (ITAM) in Mastzellen und T-Zellen. Allerdings ist die Notwendigkeit eines Kalziumeinstroms in Fcγ Rezeptor (FcγR)-vermittelten Signalprozessen sowie die Relevanz von STIM2 hierbei noch unklar. Daher wurden gentechnisch veränderte Mäuse, denen zentrale Moleküle des SOCE-Apparats fehlen, untersucht. Kalziummessungen zeigten, dass beide STIM-Isoformen an der Kalziummobilisierung in Folge der T-Zellrezeptorstimulation beteiligt sind. Außerdem wurde gezeigt, dass die Stimulation von FcγRs zu SOCE führt, der von STIM1 und vermutlich auch von Orai1 vermittelt wird. Die Daten aus dem *Immunthrombozytopenie* (ITP) Tiermodell belegen, dass SOCE für die Zerstörung von Plättchen essentiell ist. Weiterhin sprechen die hiervorliegenden Ergebnisse für eine Rolle beider STIM Isoformen in der Pathologie der ITP. Außerdem konnte in dieser Arbeit nachgewiesen werden, dass STIM1 und Orai1 entscheidende Faktoren für IgG-vermittelte systemische Anaphylaxie sind. STIM2 ist ebenfalls an der IgG-vermittelten, nicht jedoch an der IgE-vermittelten Anaphylaxie beteiligt. Diese Ergebnisse legen nahe, dass Eingriffe in den SOCE eine neue Strategie in der Behandlung von IgG-abhängigen immunologischen Erkrankungen sein könnten.

1 Introduction

Platelets are the smallest circulating cells in the human blood with a diameter of just 3-4 µm (1-2 µm in mice). One microliter blood contains about 150,000-300,000 of these anucleated discoid-shaped cells, which have a lifespan of about ten days (mice have approximately 1,000,000 platelets/µl with a lifespan of 5 days). Aged platelets are constantly removed from the circulation by macrophages in spleen and liver. New platelets have to be permanently produced via fragmentation of megakaryocytes in order to maintain high platelet levels. Impaired platelet production or increased platelet clearance (e.g. caused by autoantibodies) may result in low platelet counts, termed thrombocytopenia (e.g. heparin-induced or immune thrombocytopenia).

Platelets “monitor” the integrity of the vascular system and most platelets never undergo firm adhesion before they are finally cleared from the circulation. Only in response to altered vascular surfaces, like upon traumatic injury or pathological alteration of the endothelial layer, such as found in atherosclerosis, platelets rapidly become activated, secrete their granule contents and interact with one another to form a plug that seals the wound.

Platelet activation, coagulation and resulting thrombus formation are crucial to limit blood loss after tissue trauma. However, in diseased arteries these processes may lead to thrombotic vessel occlusion with obstruction of blood flow, loss of oxygen supply and subsequent tissue damage [1], such as in myocardial infarction and ischemic stroke. Since these pathologies represent leading causes of mortality and severe disability worldwide, platelet inhibition is one major strategy in treating these diseases.

1.1 Platelet Activation and Thrombus Formation

Exposure of the subendothelial *extracellular matrix* (ECM) upon vascular injury induces the rapid deceleration of circulating platelets, enabling sustained contacts of platelet receptors with components of the ECM, e.g. collagen, laminin and fibronectin and leading to platelet activation. This activation causes a rapid remodeling of the cytoskeleton and a morphological change of the cells from discoid to spheric shape followed by spreading on the reactive surface. Platelet activation also triggers the exocytosis of α- and dense granules, which are small intracellular vesicles that are only found in platelets and their progenitors.

Platelet activation and thrombus formation following vascular injury are complex signaling processes, which can be divided into three major steps: (I) adhesion, (II) activation and (III)

aggregation (Figure 1-1). The mechanisms of platelet adhesion at sites of injury depend to a great extent on the local rheological conditions. Blood flow has a greater velocity in the center of the vessel than near the wall thereby generating shear forces between adjacent layers of fluid that become maximal at the wall. At high shear rates (> 1000 s^{-1}) the interaction between *glycoprotein* (GP) Ib and its ligand *von Willebrand factor* (vWF), immobilized on collagen of the exposed ECM, is essential to mediate platelet adhesion [2]. The GPIb-vWF interaction causes the deceleration and rolling of platelets along the vessel wall, a process termed “tethering”. The rolling of platelets enables other platelet receptors, such as GPVI, to interact with their ligands resulting in cellular activation. The direct collagen binding of the major platelet activating collagen receptor GPVI triggers tyrosine phosphorylation cascades downstream of the receptor-associated *immunoreceptor tyrosine activation motif* (ITAM) bearing *Fc receptor* (FcR) γ-chain (Figure 1-2) [3]. GPVI-ITAM or hemITAM-signaling via the *C-type lectin receptor 2* (CLEC-2), whose ligand remains to be identified, results in the activation of several effector molecules, most notably *phospholipase* (PL) Cγ2 [4]. PLCγ2 cleaves *phosphatidylinositol-4,5-bisphosphate* (PIP_2) into *inositol-1,4,5-trisphosphate* (IP_3) and *diacylglycerol* (DAG). DAG activates *protein kinase C* (PKC), while IP_3 triggers calcium (Ca^{2+}) mobilization from the intracellular stores and subsequent *store operated calcium entry* (SOCE) via Ca^{2+} channels in the plasma membrane [5]. All platelet signaling events converge in the “final common pathway” of platelet activation, the functional upregulation of integrin adhesion receptors (Figure 1-2), leading to stable adhesion on the ECM and platelet aggregation. Integrin adhesion receptors are heterodimeric transmembrane proteins composed of an α– and a β–chain. Platelets express three β1 integrins and two β3 integrins. Among them, αIIbβ3 is considered the most important as it mediates adhesion to the subendothelium [6] and platelet aggregation by binding to fibrinogen [7].

Platelet activation also triggers the secretion of adhesive proteins, like vWF and fibrinogen from α-granules, which also contain growth and coagulation factors and *second wave mediators* like *adenosine diphosphate* (ADP) and serotonin from dense granules along with the production and release of *thromboxane* A_2 (TxA_2). Second wave mediators contribute to the recruitment and activation of additional platelets into the growing thrombus [1].

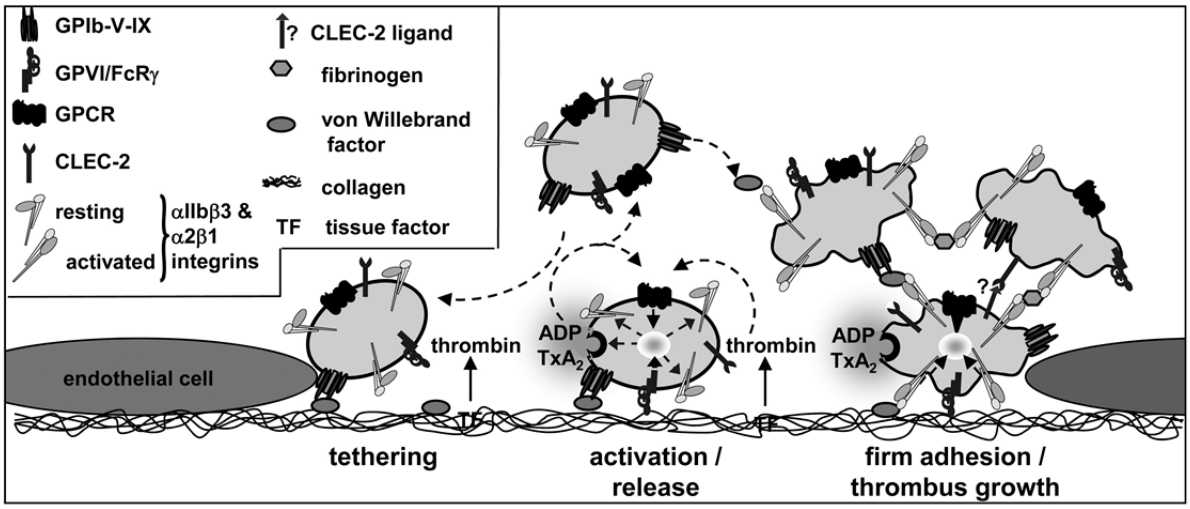

Figure 1-1: Model for platelet adhesion to the subendothelial matrix at sites of vascular injury and subsequent thrombus formation. The initial contact (tethering) to the ECM is mediated predominantly by GPIb–vWF interactions. In a second step GPVI–collagen interactions initiate cellular activation resulting in the shift of integrins to a high-affinity state and the release of second-wave agonists, most importantly ADP, ATP and TxA_2. In parallel, exposed *tissue factor* (TF) locally triggers the formation of thrombin, which in addition to GPVI, mediates cellular activation. Finally, firm adhesion of platelets to collagen through activated α2β1 (directly) and αIIbβ3 (indirectly via vWF or other ligands) results in sustained GPVI signaling, enhanced release of soluble agonists and procoagulant activity. Released ADP, ATP and TxA_2 amplify integrin activation on adherent platelets and mediate thrombus growth by recruiting and activating additional platelets. The forming thrombus is stabilized by signaling through CLEC-2, whose ligand / counter-receptor remains to be identified. Taken from Stegner and Nieswandt, 2011 [8].

Vascular injury also triggers the coagulation cascade leading to thrombin generation and ultimately to fibrin formation. The interaction between activated plasma factor VII and *tissue factor* (TF) initiates the extrinsic pathway of blood coagulation, leading to the activation of *coagulation factors* (F) X, XI and prothrombin. Blood coagulation is further promoted by the scramblase-mediated exposure of negatively charged *phosphatidylserine* (PS) on the surface of activated platelets, which enhances the assembly and activity of two major coagulation factor complexes [9, 10]. The intrinsic coagulation pathway is initiated via the contact activation system when FXII comes into contact with negatively charged surfaces, such as polyphosphates or extracellular RNA [11, 12]. This pathway generates active thrombin via FXII, FXI and FX. Locally generated thrombin activates platelets through *protease-activated receptors* (PARs). These receptors convert an extracellular proteolytic cleavage event, which unmasks a new N-terminus acting as tethered ligand [13, 14], into an intracellular signal via several G proteins [15]. Like thrombin, also the second wave mediators TxA_2 and ADP, which are released from damaged endothelial cells and activated platelets, stimulate receptors that couple to heterotrimeric G proteins (GPCR, Figure 1-2) and induce distinct downstream signaling pathways [reviewed in 15]. G_{12}/G_{13} proteins regulate multiple pathways, of which the Rho/Rho-kinase pathway, leading to myosin light chain phosphorylation and platelet shape change, is the best studied one [16]. The α-subunit of G_i

family proteins inhibits adenylyl cyclase, while its βγ-complexes can regulate several channels and enzymes, most notably *phosphoinositide-3-kinases* (PI3K) [17]. Gq proteins activate PLCβ [18] leading to calcium mobilization and PKC activation (see above). Again, these signaling events converge in a shift of platelet integrins from a low affinity to a high affinity state (Figure 1-2). This process, termed "inside-out" signaling enables integrins to efficiently bind their ligands [19] thus promoting firm adhesion of the platelets via binding to collagen (through integrin α2β1, GPIa/IIa) and vWF (through integrin αIIbβ3, GPIIb/IIIa). Following this, interaction of platelets is mediated by binding of activated αIIbβ3 to plasma fibrinogen and vWF.

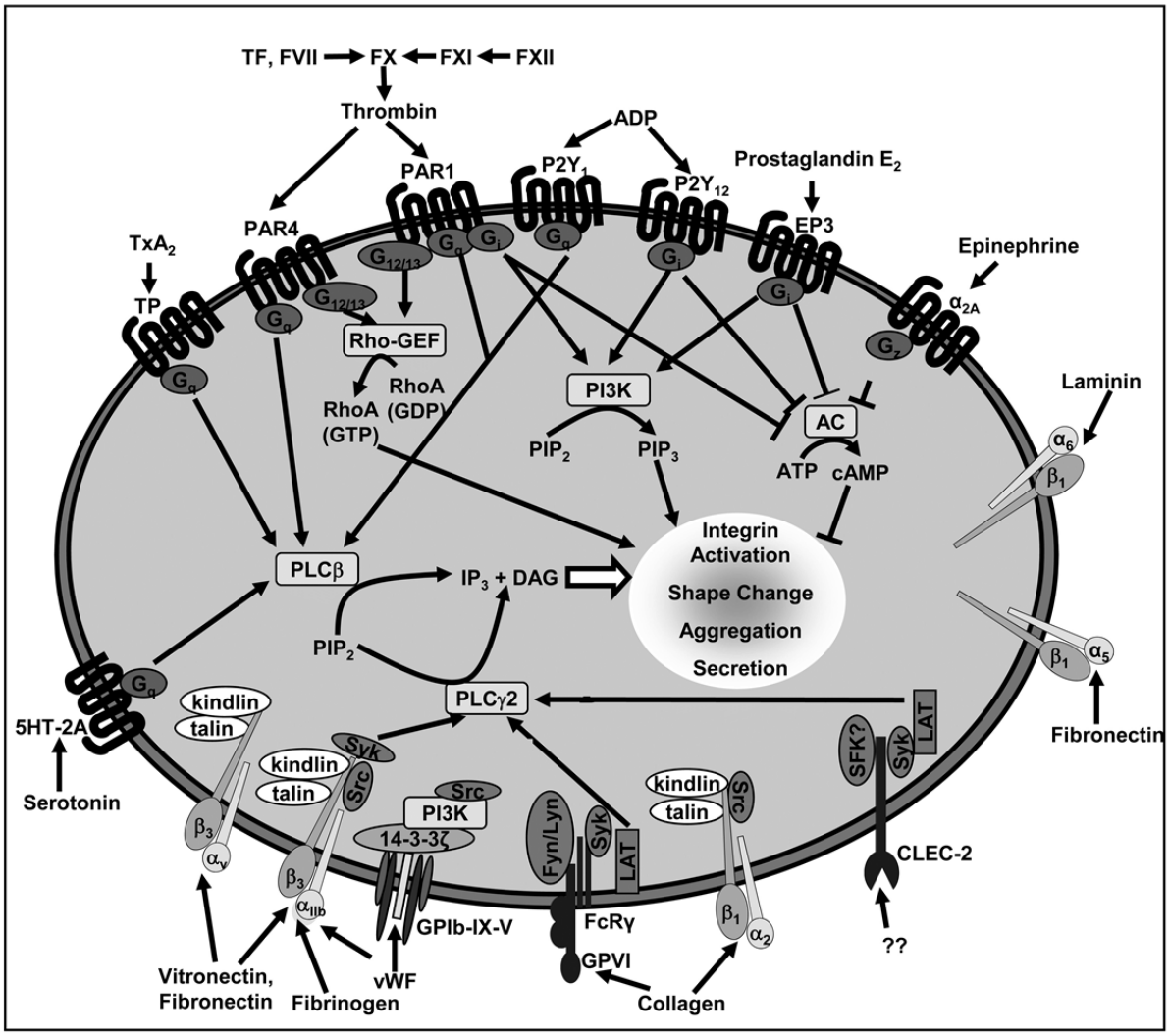

Figure 1-2: Platelet receptors and important signaling molecules leading to platelet activation. Soluble agonists stimulate G protein-coupled receptors, activating the corresponding G proteins. G_q proteins stimulate PLCβ, while $G_{12/13}$ trigger Rho activation and G_i and G_z inhibit the *adenylyl cyclase* (AC). Crosslinking of GPVI or CLEC-2 results in activation of PLCγ2. TF indicates *tissue factor*; TxA_2, *thromboxane A2*; TP, *TxA2 receptor*; PAR, *protease-activated receptor*; RhoGEF, *Rho-specific guanine nucleotide exchange factor*; PI3K, *phosphoinositide-3-kinase*; PIP_2, *phosphatidylinositol-4,5-bisphosphate*; PIP_3, *phosphatidylinositol-3,4,5-trisphosphate*; IP_3, *inositol-1,4,5-trisphosphate*; DAG, *diacylglycerol*. Modified from Stegner and Nieswandt, 2011 [8].

1.2 The GPIb-V-IX Complex

The GPIb-V-IX complex is a structurally unique and highly abundant receptor complex, exclusively expressed in megakaryocytes and platelets. Four different genes encode the receptor complex, namely the α- and β-subunits of GPIb (CD42b & CD42c), GPV (CD42d) and GPIX (CD42a). They all belong to the *leucine-rich repeat* (LRR) protein superfamily [20]. Two GPIbβ (25 kD) subunits are linked via disulfide-bonds to GPIbα (135 kD) [21], which bears most ligand binding sites of the whole complex. GPIX (22 kD) is non-covalently associated to GPIb and two GPIb-IX complexes associate to one GPV subunit (82 kD, see Figure 1-3) [22]. In humans, loss or dysfunction of this receptor complex causes the *Bernard-Soulier syndrome* (BSS), a congenital bleeding disorder characterized by mild thrombocytopenia and giant platelets [20]. A similar phenotype can be reproduced in mice deficient in GPIbα [23] or GPIbβ [24]. Notably, no GPV-deficient patients have been reported to date and GPV-deficiency in mice did not cause a BSS-like phenotype [25], while loss of function mutations and subsequent BSS has been reported for all other receptor subunits [26].

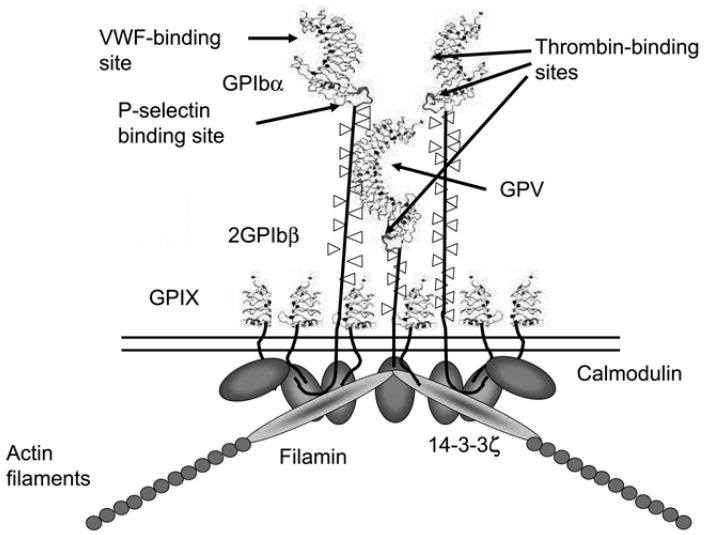

Figure 1-3: The GPIb-V-IX complex. Platelet GPIb-V-IX is composed of four different transmembrane polypeptides: GPIbα, GPIbβ, GPIX and GPV in a 2:4:2:1 stoichiometry. Each member of the complex contains one or multiple leucine-rich repeats in the extracellular domain and GPIbα and GPV are poly-glycosylated (white triangles).

Many extracellular ligands interact with GPIb-V-IX, mostly by binding to a domain on the N-terminal region of GPIbα. Binding sites of the three most prominent ligands are depicted.

The cytoplasmic domains of the single subunits interact with a number of proteins, including filamin, calmodulin and the 14-3-3ζ protein. Modified from Clemetson, 2007 [26].

1.2.1 GPIb-Signaling

The GPIb-V-IX complex has many ligands, namely vWF, thrombin, P-selectin (CD62P), *macrophage-1 antigen* (Mac-1), coagulation factors XI and XII, *high-molecular-weight kininogen* (HMWK), thrombospondin-I and protein C [26, 27]. Basically all of them interact with the N-terminal extracellular part of GPIbα. The C-terminal cytoplasmic tail of GPIbα is composed of 96 amino acids and contains binding sites for putative signaling molecules, such as 14-3-3ζ and for proteins of the platelet cytoskeleton, like actin-binding protein and filamin [22]. Calmodulin binds to the cytoplasmic tail of all receptor subunits, except for GPIX. However, the only known function of this interaction is the prevention of receptor shedding via *a disintegrin and metalloproteinase* 17 (ADAM17) [28, 29].

In addition to the established role of GPIbα to bind vWF, which enables platelet rolling and subsequent platelet receptor ligand interactions (see above) another function for GPIb was suggested: Under extremely high shear rates (> 10,000 s^{-1}), such as found in stenosed arteries, GPIb-dependent platelet adhesion and subsequent aggregation can occur independently of integrin activation [30-32]. This hypothesis is supported by the notion that platelets lacking the extracellular part of GPIbα – unlike platelets lacking the αIIbβ3 integrin – failed to incorporate into a growing arterial thrombus in wildtype mice [33].

Apart from its mandatory role as central adhesion receptor, a signal transducing role of the GPIb-V-IX complex has been assumed for a long time [26]. However, studies on GPIb-mediated signaling in platelets have been hampered by the fact that the receptor induces only weak signaling and does not interact with its principal ligand, vWF, under static conditions, but only in the presence of high shear conditions [34]. The antibiotic ristocetin [35] and the snake venom protein botrocetin [36] have been used to induce interactions between human GPIb and vWF under static conditions. The latter substance also works on mouse platelets, leading to platelet agglutination and, reportedly, GPIb-specific signaling events [37-39]. This is, however, not accompanied by detectable αIIbβ3 integrin activation and fibrinogen binding in suspension, excluding this assay for studies on GPIb-induced αIIbβ3 integrin activation [40]. Similarly, clustering of mouse GPIb by antibodies leads to platelet agglutination *in vitro* and thrombocytopenia *in vivo* in the absence of αIIbβ3 integrin activation [41]. Despite these difficulties in addressing pathways downstream of GPIb, several molecules have been proposed to be involved in GPIb signaling [22, 42]. It was demonstrated that the *adhesion and degranulation promoting adapter protein* (ADAP) is important in GPIb-induced integrin activation [43], while protein kinase A-mediated phosphorylation of GPIbβ at Ser166 impairs vWF-binding to GPIb [44]. One model links GPIb to ITAM signaling via the FcRγ-chain [45, 46] or FcγRIIA [47], but other studies did not

support this model [48]. Another concept proposes GPIb-signaling via the association with 14-3-3ζ [49], *Src family kinases* (SFK) [50, 51] and PI3K [52]. It was further suggested that GPIb-signaling involves the sequential activation of nitric oxide, *cyclic guanosine monophosphate* (cGMP), protein kinase G, p38 and *extracellular-signal-regulated kinase* (ERK) pathways [53, 54].

The fundamental role of the GPIb-vWF interaction for thrombus formation under high shear conditions was demonstrated using transgenic mice with a mutated extracellular domain of GPIbα or mice treated with Fab fragments of the GPIb blocking antibody p0p/B. In both cases, arterial thrombus formation was prevented by the absence of functional GPIb [33, 55]. Moreover, the GPIb-vWF interaction has now also been recognized as a suitable pharmacologic target for prevention and treatment of ischemic stroke, since both prophylactic and therapeutical administration of anti-GPIbα Fab fragments, as well as vWF-deficiency profoundly protected mice from secondary infarct growth in a model of focal cerebral ischemia [56, 57].

1.2.2 GPV

GPV, which contains 16 LRRs, is a special subunit of the GPIb-V-IX complex since it is the only subunit not required for the correct expression of the complex [58]. Consistently, expression of GPV on the surface of transfected cells does not depend on the presence of the other subunits [59]. GPV has been proposed to strengthen the interaction of the GPIb-V-IX complex with vWF under high shear conditions [60]. Furthermore, GPV contains a thrombin cleavage site [61] and was suggested to form a high-affinity binding site for thrombin [62]. Two independent groups generated *Gp5*$^{-/-}$ mice [25, 63], which did not suffer from a BSS-like phenotype and overall displayed grossly normal platelet functionality. Only after activation with threshold doses of thrombin an increased responsiveness was observed [63]. Two suggestions were made to explain this phenotype: (I) absence of the thrombin substrate GPV lowers the effective thrombin concentrations needed to activate platelets [63], or (II) lack of GPV enables the GPIb-thrombin interaction leading to platelet activation independent of thrombin cleavage activity [64]. For one of the two *Gp5*$^{-/-}$ mouse strains reduced tail bleeding times, accelerated thrombus formation and increased embolization were reported [63, 65], whereas analysis of the second mouse line revealed unaltered tail bleeding times and impaired thrombus formation [25, 66]. The latter group ascribed the defective thrombus formation to the role of GPV in collagen signaling, thereby establishing collagen as ligand for GPV [66]. However, the interaction between GPV and collagen is largely neglected in the literature [3, 26].

The latest report on *Gp5*$^{-/-}$ mice used mice backcrossed to the C57Bl/6 background and confirmed the increased thrombin responsiveness as well as slightly reduced adhesion on collagen [67]. Using laser-injury the authors demonstrated that the effect of GPV-deficiency on thrombus formation depends on the severity of the injury and concluded that GPV is only of minor relevance for arterial thrombus formation [67].

1.3 The Platelet Collagen Receptors Integrin α2β1 and GPVI

Besides GPV [see above, 66] several platelet collagen receptors have been identified [3]. Among these are the αIIbβ3 integrin and GPIb which indirectly interact with collagen via vWF [68]. GPVI and α2β1 integrin are considered to be the most important receptors directly interacting with collagen. GPVI is required for collagen-induced platelet activation, while integrin α2β1 contributes to platelet adhesion to collagen and only makes minor contributions to platelet activation [3].

1.3.1 Integrin α2β1

Integrin α2β1 was the first platelet collagen receptor to be identified and serves mainly as an adhesion receptor [69]. Upon stimulation with soluble collagen α2β1 is essential for platelet adhesion and activation and absence of functional α2β1 leads to delayed aggregation after stimulation with fibrillar collagen [reviewed in 3]. Some controversies exist about the relevance of α2β1 for platelet adhesion on fibrillar collagen under flow. Under these conditions, several groups reported impaired adhesion in the absence of functional α2β1 [70-72]. However, this was questioned by others, who reported no effect of α2β1-deficiency [73, 74]. *In vivo*, however, lack of α2β1 had only minor effects on thrombus formation [71, 75] and – with one exception [72] – was reported not to affect hemostasis [70, 74, 76]. Thus, it is generally accepted that α2β1 contributes to adhesion, but that its loss can be compensated [7].

1.3.2 GPVI

GPVI, a 62-kDa type I transmembrane receptor of the *immunoglobulin* (Ig) superfamily and is non-covalently associated with ITAM bearing FcRγ-chain dimers. GPVI is exclusively expressed in platelets and megakaryocytes and the complex serves as the major activating platelet collagen receptor [3]. Crosslinking of GPVI by ligand binding brings the Src family tyrosine kinases Fyn and Lyn into contact with the FcRγ-chain, starting a tyrosine phosphorylation cascade via Syk, the adaptors *linker of activated T cells* (LAT) and SLP-76 (*Src homology domain 2 containing leukocyte protein of 76 kD*). This in turn leads to the activation of effector proteins, most notably PLCγ2, PI3K and small G proteins. These signaling events culminate in calcium mobilization, degranulation, integrin activation and aggregation [3, 4] (see Figure 1-2).

Two patients with compound heterozygous mutations in the *Gp6* gene, leading to a mild bleeding phenotype, have been reported [77, 78]. One of these mutations results in impaired function, while the other prevents expression of GPVI. In addition, a few GPVI-deficient patients have been described who had anti-GPVI antibodies in their blood [79, 80]. This phenomenon can be reproduced in mice by injecting of anti-GPVI antibodies (JAQ1-3) which results in down-regulation of the receptor from the platelet surface and a GPVI knockout-like phenotype for a prolonged time period [81, 82]. As described above, GPVI is crucial for integrin activation and subsequent firm adhesion of platelets on collagen-coated surfaces, or the ECM [3, 83].

Mice lacking the GPVI/FcRγ-chain complex are profoundly protected against experimental arterial thrombosis and ischemic stroke in the *transient middle cerebral artery occlusion* (tMCAO) model [55, 56, 84, 85]. Interestingly, whereas an isolated GPVI-deficiency is not associated with a major hemostatic defect, the concomitant lack of the integrin collagen receptor α2β1 (which by itself has no effect on hemostasis [76]) results in severe bleeding [86], indicating partially redundant functions of these two structurally distinct receptors.

1.4 Phospholipase D in Platelets

Phospholipase D (PLD) is a phosphodiesterase which hydrolyzes *phosphatidylcholine* (PC), one of the most abundant phospholipids in cells, to *phosphatidic acid* (PA) and choline (Figure 1-4A). However, in the presence of a primary alcohol, the alcohol but not water is the preferred substrate leading to the generation of phosphatidyl alcohol instead of PA (Figure 1-4A). This transphosphatidylation is characteristic for PLD and is commonly used in assays measuring the activity of the enzyme [87]. Two mammalian PLD isoforms exist: PLD1 (120 kD) [88] and PLD2 (105 kD) which share about 50% sequence homology [89]. Both PLDs are ubiquitously expressed [90] and both isoforms have been detected in platelets [91]. Both mammalian PLDs contain a *Phox homology* (PX), a *pleckstrin homology* (PH) domain and the PLD motifs I-IV (Figure 1-4B) [92]. Motif II and IV bear the two highly conserved HKD motifs (with the amino acids histidine, lysine and aspartic acid), which are responsible for the catalytic activity of the enzyme [93, 94]. The two PLD isoforms differ in the loop-region, which is only present in PLD1 and supposed to auto-inhibit the basal activity of the enzyme [95]. Binding of PIP_2 to its binding region and *phosphatidylinositol-3,4,5-triphosphate* (PIP_3) to the PX domain are required for the enzymatic activity of PLDs [96]. Apart from these two phospholipids numerous molecules are suggested to regulate PLD, among them PKC and GTPases of the ARF (*ADP ribosylation factor*) and Rho (*Ras homolog gene family*) families [reviewed in 96, 97, 98]. Likewise, many downstream targets of PLD or of its enzymatic product PA have been proposed, thus linking PLD activity to several processes, like cytoskeletal rearrangements, membrane trafficking and exo- and endocytosis [90, 96-99]. However, prior to this study no PLD-deficient mice were reported, but potential downstream targets of PLD were identified mostly by correlation studies (linking PLD activity to simultaneous cellular events) or by inhibiting PA generation with 1-butanol to divert PLD activity. Yet, primary alcohols only partially prevent PA production even at maximal applicable concentrations and 1-butanol and phosphatidylbutanol have off-target effects on cell behaviors that may confound interpretation of the obtained results [100].

Despite these limitations the role of PLD in platelets has been investigated [reviewed in 101]. Thrombin [102], collagen [103] or TxA_2 [104] stimulation or integrin outside-in signaling were reported to result in PLD translocation to the platelet plasma membrane and PLD activation [91]. PLD was suggested to be required for secretion of dense granules [105] and lysosomes [91]. It was further proposed that PLD contributes to Rap1 activation downstream of PAR1 [106, 107]. However, definite proof for the aforementioned roles of PLD in platelets has been missing and the relevance of PLD for thrombosis and hemostasis has remained elusive.

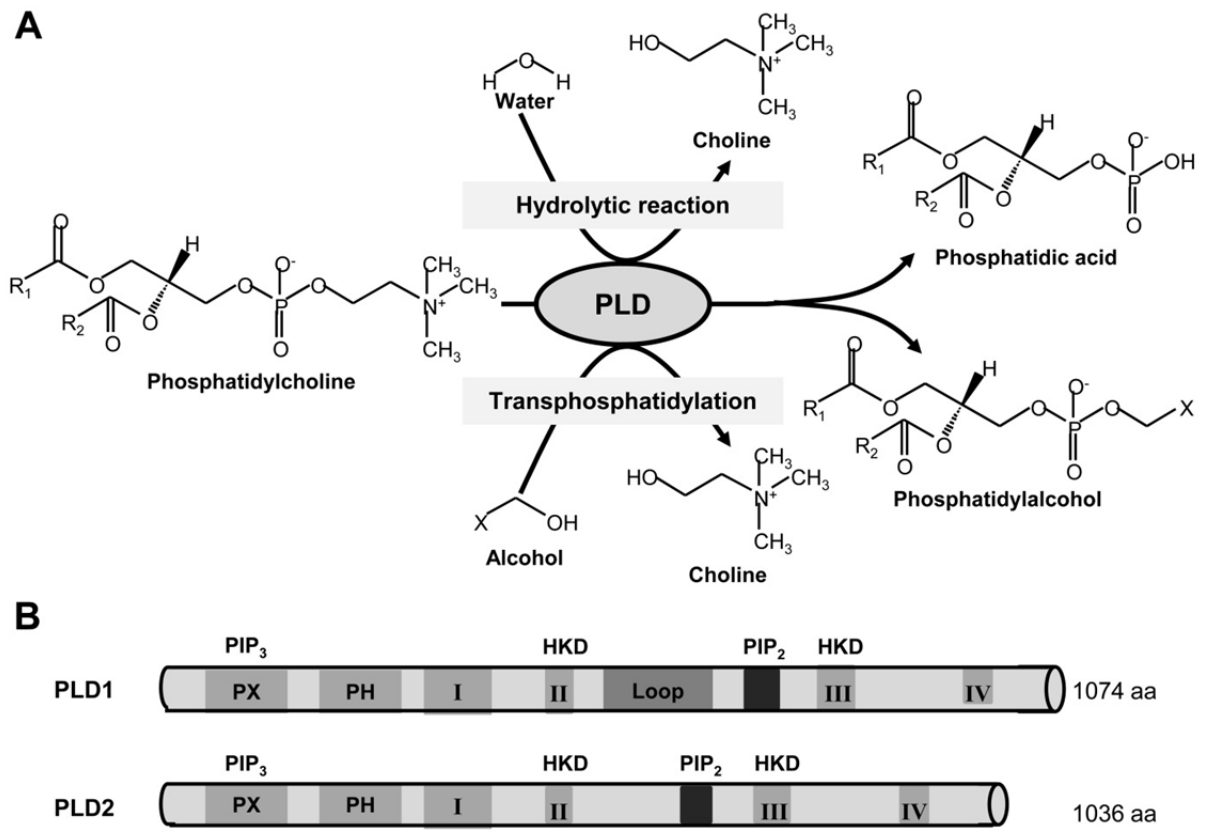

Figure 1-4: Enzymatic reaction (A) and isoforms (B) of mammalian phospholipase D. A) Under physiological conditions, PLD hydrolyses *phosphatidylcholine* (PC) into *phosphatidic acid* (PA) and choline. In the presence of primary alcohols, however, transphosphatidylation is the preferred reaction leading to choline and phosphatidyl-alcohol instead of PA. R_1 and R_2 indicate aliphatic chains and X indicates the remaining part of the primary alcohol (CH_3 in case of butanol, H in case of ethanol). B) The two PLD isoforms contain a *Phox homology* (PX), a *pleckstrin homology* (PH) domain, the PIP_2-binding region and the PLD motifs I-IV with the conserved HKD motifs. The loop region is characteristic for PLD1. aa, *amino acid residues*. Modified from Kanaho *et al.*, 2009 [92].

1.5 Store-Operated Calcium Entry in the Hematopoietic System

Ca^{2+} is a ubiquitous second messenger that regulates a variety of cellular functions [108]. In non-excitable cells, such as platelets [5] and immune cells [109], the main route of Ca^{2+} influx is the so-called SOCE, a process wherein depletion of intracellular stores causes the activation of plasma membrane calcium channels [110]: Ligand binding to receptors (GPCR or ITAM receptors) triggers PLC activation, leading to the hydrolysis of PIP_2 into DAG and IP_3. IP_3 binds to IP_3 receptors in the membrane of the *endoplasmic reticulum* (ER), thereby causing calcium efflux from the ER into the cytosol. The decreased Ca^{2+}-concentration in the ER subsequently opens *Ca^{2+}-release activated Ca^{2+}* (CRAC) channels within the plasma membrane, triggering further influx of Ca^{2+} from the extracellular compartment (Figure 1-5A).

The existence of such a process was proposed already in 1986 [111] and although it was early detected in mast cells [112] and lymphocytes [113, 114], the calcium sensor in the intracellular store and the channel remained elusive for more than 15 years [115].

RNAi screens identified the *stromal interaction molecule 1* (STIM1) as the SOCE-mediating calcium sensor within the ER [116-118]. Furthermore, a second STIM isoform in mammals, STIM2 was identified as a positive regulator of SOCE as well [116]. Both STIM isoforms share 60% homology and contain Ca^{2+}-binding EF-hand motifs and a single *sterile α-motif* (SAM) domain on the luminal side of the ER (Figure 1-5B). The two STIM isoforms differ in their cytoplasmic region, which contains multiple *serine and proline* (S/P) and *lysine* (K) residues. STIM2, but not STIM1, contains a C-terminal ER retention sequence [119].

Shortly after STIM, Orai1 (also termed CRACM1, for *Ca^{2+}-release activated Ca^{2+} modulator 1*) was identified as the pore-forming subunit of CRAC channels [120-122]. Orai1 is a type IV-A plasma membrane protein with four predicted transmembrane segments and a coiled-coil domain at the C-terminus. Mammals possess three different Orai isoforms (Orai1-3) [120], which can all contribute to STIM1-mediated SOCE [123]. However, they differ in their cation selectivity as well as in their pharmacological effects in response to 2-aminoetoxydiphenyl-borate. Cell culture experiments revealed that Orai1 is the Orai isoform which enables the largest currents upon store-depletion [123].

In 2007 our laboratory provided the first *in vivo* study of STIM1, reporting about mice with a constitutive active STIM1 protein due to a mutation within the calcium-binding EF-hand [124]. Thereafter, reports about STIM1- and Orai1-deficient mast cells [125, 126], platelets [127, 128] and T cells followed [126, 129-131]. These studies, together with reports on human patients [120, 132], established the STIM1-Orai1 axis as essential for SOCE in platelets [5], mast cells and T cells [133], albeit the role of Orai1 in mouse T cell signaling remains somewhat controversial [126, 130]. Lack of STIM1 or Orai1 abolishes SOCE downstream of the *T cell antigen receptor* (TCR), FcεRI [119] and platelet receptors [5]. Human patients lacking functional STIM1 or Orai1 suffer from immunodeficiency, resulting from defective T cell activation, congenital myopathy and ectodermal dysplasia [133]. In contrast, the role of STIM2 is less clear. *Stim2* knockdown in cells had no [117] or only a minor [116] effect on SOCE in the initial RNAi screens. STIM2 is able to interact with Orai1 [134] and to partially compensate for STIM1-deficiency in human patients, if overexpressed [132]. Nevertheless, STIM2-deficiency had only a moderate effect on SOCE in T-cells [129] and endogenous STIM2 was not sufficient to restore SOCE in STIM1-deficient T-cells [132]. Brandman *et al.* demonstrated that STIM2 is more sensitive to minor changes in ER Ca^{2+} content than STIM1 and proposed STIM2 to be a regulator of basal calcium levels [135].

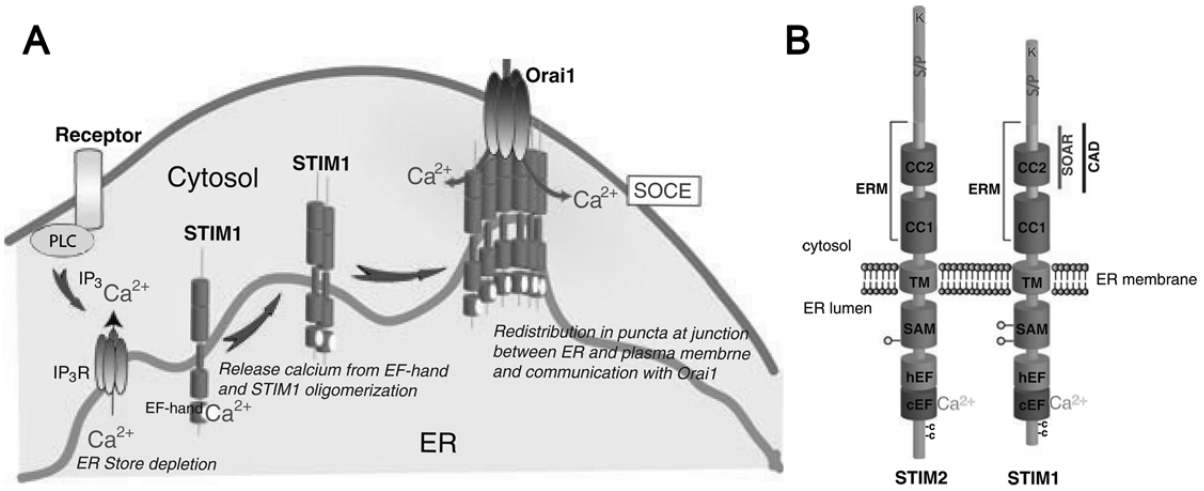

Figure 1-5: Simplified model of coupling STIM1 to Orai1 for SOCE activation (A) and schematic representation of the functional domains of the two STIM isoforms (B). A) Receptor stimulation causes *phospholipase* (PL) C activation and subsequent IP_3 (*inositol-1,4,5-trisphosphate*) generation leading to *IP_3 receptor* (IP_3R)-mediated Ca^{2+}-release from the *endoplasmic reticulum* (ER) Ca^{2+} stores. A decrease in the ER Ca^{2+} level leads to dissociation of Ca^{2+} from the EF-hand motif of STIM1, which triggers its oligomerization. As a result, STIM1 redistributes in *puncta* on the ER membrane in close proximity with the plasma membrane. STIM1 functionally interacts with Orai1 tetramers, resulting in *store-operated calcium entry* (SOCE). B) STIM proteins contain a pair of highly conserved cysteines (C), *canonical* (cEF) and *hidden* (hEF) *EF hands*, *a sterile α-motif* (SAM), N-linked glycosylation sites (indicated by circles), a transmembrane (TM) domain, two coiled-coil regions (CC1 & CC2), an *ezrin-radixin-myosin-like* (ERM) domain and *serine-proline-rich* (S/P) and *lysine-rich* (K) domains. SOAR indicates the *STIM1 Orai1 activating region*, supposed to mediate the Orai1-STIM1 interaction [136]. Modified from Baba *et al.*, 2009 [119].

1.6 Immune Thrombocytopenia and FcγR-Signaling

Immune thrombocytopenia (ITP) is a relatively common acquired autoimmune disease characterized by immunologic destruction of normal platelets, leading to thrombocytopenia (blood platelet count < 100 x 10^9/l) and hence to an increased bleeding risk [137, 138]. In most cases, ITP occurs in isolation in response to an unknown stimulus (primary ITP). Secondary ITP is attributed to coexisting conditions, like viral (e.g. HIV, hepatitis C) or bacterial infections (e.g. *Helicobacter pylori*), other autoimmune diseases (like antiphospholipid antibody syndrome) or certain drugs [137, 138]. Despite numerous established therapies (e.g. corticosteroids, *intravenous immunoglobulin* (IVIG), anti-D treatment and splenectomy) in a considerable number of patients platelet counts remain low [reviewed in 138], underlining the need for new therapeutic options.

The pathophysiology underlying ITP is complex (see Figure 1-6), but autoantibody-mediated platelet destruction is considered to be the primary event in developing ITP [137]. Platelet-reactive T cells [139] and reduced platelet production [140, 141] contribute to this disorder.

However, the latter is most likely caused by anti-platelet antibodies, which have a similar effect on megakaryocytes [141, 142]. Anti-platelet autoantibodies are a diagnostic hallmark of ITP; although they can only be detected in 60% of patients [137]. Antibodies against GPIb/IX lead to Fc-independent platelet destruction, possibly via direct toxicity or via complement fixation [41, 143-146]. However, the most common target of ITP autoantibodies is the platelet integrin αIIbβ3 (GPIIb/IIIa) [147]. Macrophages are key players in the pathology of ITP: 1) Via their *Fcγ receptors* (FcγR) they clear antibody-opsonized platelets from the circulation [137], 2) macrophages serve as *antigen-presenting cells* (APC), thereby promoting the ongoing production of autoimmune antibodies [148] (Figure 1-6).

The central role of macrophages and their Fcγ receptors establishes them as primary targets in research for novel ITP treatment options. Humans express six different Fcγ receptors (RI, RIIA-C, RIIIA-B), while mice express three different activating FcγRs, namely FcγRI, FcγRIII (the orthologoue to FcγRIIIA) and FcγRIV (most closely related to FcγRIIA) and the only inhibitory FcγR – FcγRIIB [149]. All of these four receptors are present on mouse macrophages and monocytes and they differ in their affinity to different IgG-subclasses. FcγRI is a high affinity FcγR which is constantly saturated, making it irrelevant for IgG pathologies. *In vivo*, FcγRIII exclusively binds IgG1, while FcγRIV prefers IgG2a and IgG2b antibodies [149]. All activating murine FcγR need the FcRγ-chain with its ITAM as signal transducing unit and for proper assembly for the entire FcγR. In contrast, FcγRIIb bears an intrinsic *immunoreceptor tyrosine-based inhibitory motif* (ITIM) to induce signaling [149]. While the role of ITAM-phosphorylation in FcγR-mediated signaling is well established (Figure 1-7), the role of Ca^{2+} mobilization in this process is controversially discussed. Early studies suggested that calcium levels are critical for phagocytosis, since reduction or excess of cytosolic Ca^{2+} levels ($[Ca^{2+}]_i$) impaired phagocytic ingestion rates [150, 151]. This could be confirmed by some studies on *in vitro* phagocytosis of murine macrophages [152-154]. In contrast, other studies reported that phagocytosis was Ca^{2+}-independent [155-157]. So far, SOCE in macrophages has just been detected downstream of *Toll-like receptors* (TLR) and other GPCR family members [158-161], a role of SOCE in macrophage ITAM-signaling remains to be demonstrated.

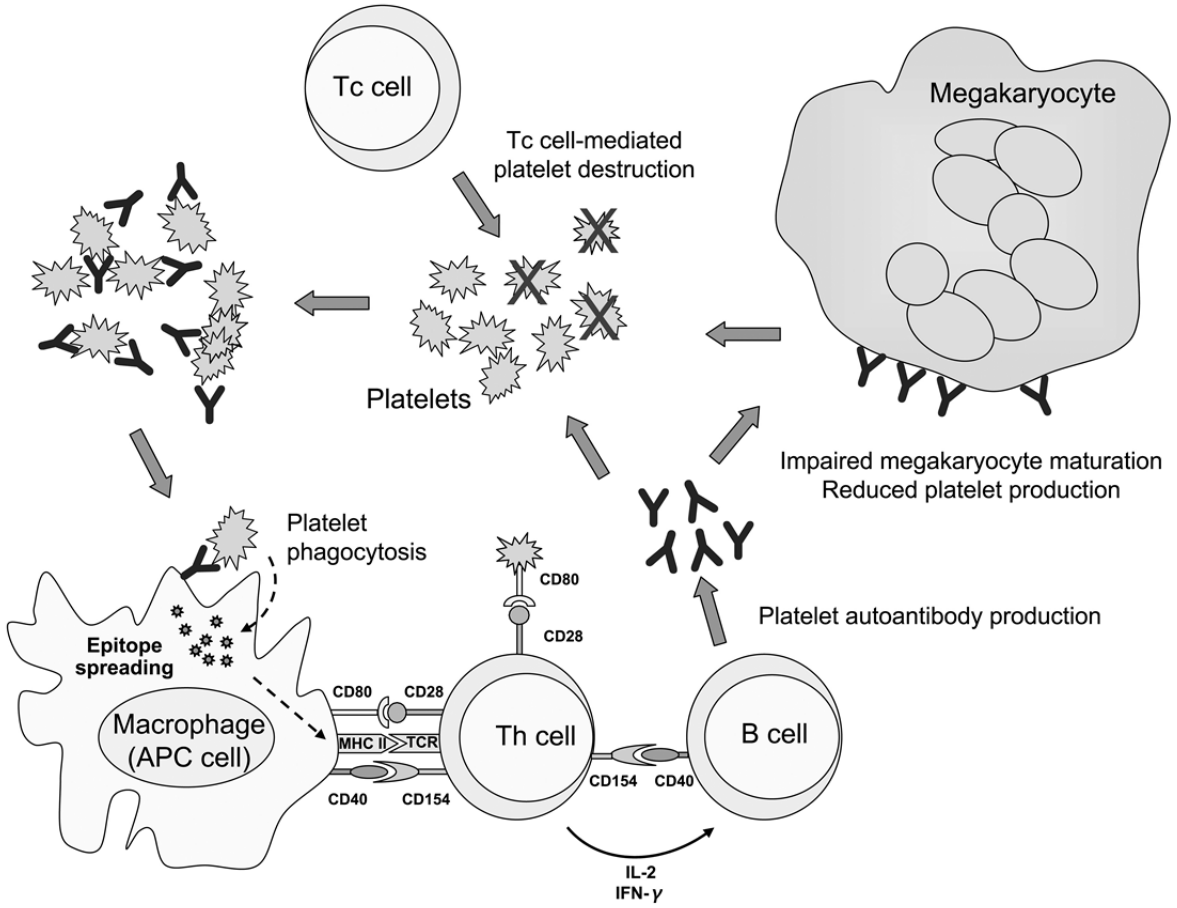

Figure 1-6: Simplified scheme of the pathophysiology of immune thrombocytopenia. The primary mechanism for the loss of tolerance in ITP remains unknown. The occurrence of antiplatelet autoantibodies remains the central pathogenetic mechanism. Autoantibodies opsonize platelets which are phagocytozed and destroyed by macrophages predominantly in the spleen. Platelet glycoproteins are cleaved to peptides by macrophages or another *antigen-presenting cell* (APC) and expressed on the APC cell surface via his *major histocompatibility complex* (MHC) class II molecules. APCs are crucial in generating a number of new or cryptic epitopes ("epitope spreading"). The *T cell receptor* (TCR) of the *helper T* (Th) cell can then bind the peptide-MHC complex which triggers the upregulation of CD154 (CD40 ligand). The interaction between CD154 on the T cells and CD40 on the APC is a synergistic interaction. An additional costimulatory signal can originate from the binding of the CD80 molecule, overexpressed on the cell membrane of ITP platelets, with CD28 expressed on Th cells. The activated Th cell produces cytokines (*interleukin-2*, IL-2 and *interferon-*γ, IFN-γ) that promote B cell differentiation and autoantibody production. Apart from opsonizing platelets these autoantibodies also bind bone marrow megakaryocytes, thereby impairing megakaryocyte maturation and platelet production. An alternative pathway of platelet destruction is caused by autoreactive *cytotoxic T*-cells (Tc), although the relevance of this mechanism *in vivo* is not known. Taken from Stasi *et al.*, 2008 [145].

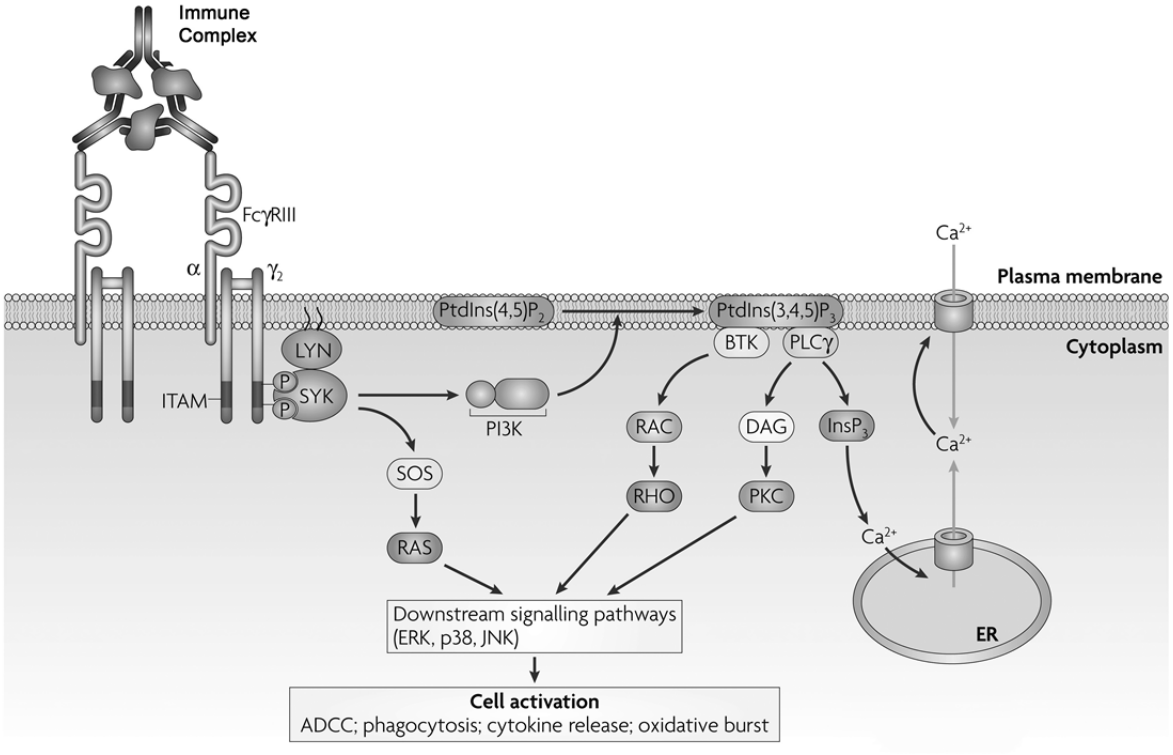

Figure 1-7: Signaling pathways triggered by activating FcγRs. Crosslinking of activating *Fc receptors for IgG* (FcγRs) by immune complexes induces the phosphorylation of receptor-associated γ-chains by SRC kinase family members. This generates *SRC homology 2* (SH2) docking sites for SYK (*spleen tyrosine kinase*), which in turn activates a number of other signal-transduction molecules, such as *phosphoinositide 3-kinase* (PI3K) and son of *sevenless homologue* (SOS) and with this activating Ras. The generation of *phosphatidylinositol-3,4,5-trisphosphate* (PtdIns(3,4,5)P3) recruits *Bruton's tyrosine kinase* (BTK), leading to Rac, Rho and *phospholipase* (PL) Cγ activation, which in turn leads to activation of downstream kinases and the release of calcium from the *endoplasmic reticulum* (ER). Modified from Nimmerjahn and Ravetch, 2008 [149].

1.7 Aim of the Study

The aim of this study was to investigate two different signaling processes in platelets and to understand the relevance of store-operated calcium entry in immune thrombocytopenia: 1) GPV has been reported to contribute to collagen signaling, but it is generally considered that this receptor is of minor relevance for platelet physiology and thrombus formation. This study intended to verify the role of GPV in platelet collagen responses and to clarify the relevance of this receptor during thrombus formation using *Gp5*$^{-/-}$ and different double-deficient mice. 2) Platelets contain the two PLD isoforms, PLD1 and PLD2, both of which presumably become activated upon platelet stimulation. However, the function of PLD in the process of platelet activation and aggregation has not been definitively explored. Thus, one aim of this thesis was to investigate the role of PLD1 in platelet function and signaling.

Therefore, PLD-deficient mice were analyzed. 3) While the central importance of SOCE via the STIM1-Orai1 axis is well established for calcium mobilization downstream of ITAM receptors in mast cells and T cells, the contribution of the second STIM isoform, STIM2 is less clear. Furthermore, the requirement of Ca^{2+}-mobilization in FcγR-signaling is also unclear. Hence, the third aim of this study was to reveal the relevance of SOCE for FcγR activation and immune thrombocytopenia. To address this question, genetically modified mice lacking central molecules of the SOCE machinery were subjected to models of immune thrombocytopenia.

2 Materials and Methods

2.1 Materials

2.1.1 Kits, Reagents and Cell Culture Material

Reagent	Company
^{3}H-myristic acid	Perkin Elmer (Waltham, MA, USA)
Agarose	Roth (Karlsruhe, Germany)
Alexa488-labeled annexin A5	Self-made
AmplexRed PLD assay kit	Molecular Probes/Invitrogen (Karlsruhe, Germany)
Apyrase (grade III)	Sigma-Aldrich (Deisenhofen, Germany)
Aqueous-soluble, cell-permeable phosphatidic acid	Sigma-Aldrich (Deisenhofen, Germany)
Atipamezol	Pfizer (New York, NY, USA)
β-Mercaptoethanol	Roth (Karlsruhe, Germany)
Collagen-related peptide (CRP)	provided by S.P Watson (University of Birmingham, UK)
Convulxin	Axxora (Lörrach, Germany)
Dinitrophenol human serum albumin (DNP-HSA)	Sigma-Aldrich (Deisenhofen, Germany)
Dulbecco's modified Eagle's medium (DMEM)	Gibco (Karlsruhe, Germany)
Enhanced chemiluminescent Western Lightning Plus-ECL	Perkin Elmer (Waltham, MA, USA)
Epinephrine	Sigma-Aldrich (Deisenhofen, Germany)
Fentanyl	Janssen-Cilag (Neuss, Germany)
Fetal calf serum (FCS)	Perbio (Bonn, Germany)
Flumazenil	Delta Select (Pfullingen, Germany)
Fura-2/AM	Molecular Probes/Invitrogen (Karlsruhe, Germany)
Geneticin	Gibco (Karlsruhe, Germany)
Hering sperm DNA	Sigma-Aldrich (Deisenhofen, Germany)

High molecular weight heparin	Sigma-Aldrich (Deisenhofen, Germany)
Histamine ELISA	IBL International (Hamburg, Germany)
Horm Collagen	Nycomed (Munich, Germany)
H-Phe-Pro-Arg chloromethyl ketone (PPACK)	Calbiochem (Bad Soden, Germany)
Human fibrinogen	Sigma-Aldrich (Deisenhofen, Germany)
Human fibrinogen-Alexa488	Molecular Probes/Invitrogen (Karlsruhe, Germany)
Lepirudin	Celgene (Munich, Germany)
LIF (*leukemia inhibitory factor*)	Chemicon (Hampshire, United Kingdom)
Medetomidine	Pfizer (New York, NY, USA)
Midazolam	Roche (Grenzach-Wyhlen, Germany)
Naloxon	Delta Select (Pfullingen, Germany)
Nitrocellulose membrane for Southern Blot (Hybond XL)	GE Healthcare (Freiburg, Germany)
Non-essential amino acids	Gibco (Karlsruhe, Germany)
Nonidet P-40 (NP-40)	Roche Diagnostics (Mannheim, Germany)
OG488-labeled annexin A5	provided by J.W.M. Heemskerk (University of Maastricht, Maastricht, the Netherlands)
Penicillin/streptomycin	PAA Laboratories (Pasching, Austria)
Peptone (pancreatic digested)	Roth (Karlsruhe, Germany)
Phosphate-buffered saline (PBS)	Gibco (Karlsruhe, Germany)
PLD from *Streptomyces chromofuscus*	Sigma-Aldrich (Deisenhofen, Germany)
Pluronic F-127	Molecular Probes/Invitrogen (Karlsruhe, Germany)
Probequant G 50 Microcolumns	GE Healthcare (Freiburg, Germany)
Rediprime DNA Labelling Kit	GE Healthcare (Freiburg, Germany)
Redivue-α^{32}P-dCTP; 250 µCi	GE Healthcare (Freiburg, Germany)
Rhodocytin	provided by J. Eble (Frankfurt University Hospital, Frankfurt, Germany)

RNeasy kit	Qiagen (Hilden, Germany)
Thapsigargin (TG)	Molecular Probes/Invitrogen (Karlsruhe, Germany)
Thrombin	Roche Diagnostics (Mannheim, Germany)
Trypsin	Gibco (Karlsruhe, Germany)
U46619	Alexis Biochemicals (San Diego, USA)
Yeast extract	AppliChem (Darmstadt, Germany)

All enzymes were purchased from Fermentas (St. Leon-Rot, Germany), Invitrogen (Karlsruhe, Germany) or New England Biolabs (NEB, Ipswich, MA, USA). Primers were purchased from Metabion (Planegg-Martinsried, Germany) or MWG-Eurofins (Ebersberg, Germany).

All non-listed standard reagents were purchased by AppliChem (Darmstadt, Germany), Roth (Karlsruhe, Germany) or Sigma-Aldrich (Deisenhofen, Germany).

2.1.2 Antibodies

2.1.2.1 Purchased Primary and Secondary Antibodies

Antibodies	**Source**
Goat anti-Armenian hamster IgG (no. 127-005-160)	Dianova (Hamburg, Germany)
Goat anti-hamster IgG	Jackson ImmunoResearch (West Grove, PA, USA)
Hamster anti-β1 integrin-FITC (SM2210)	Acris (Herford, Germany)
Hamster anti-mouse FcγRIV (clone 9E9)	[162]
Rabbit anti-human STIM2 (no. 4123)	ProSci (Poway, CA, USA)
Rabbit anti-human vWF (A0082)	Dakocytomation (Hamburg, Germany)
Rabbit anti-Ly17.2 (clone K9.361)	[163]
Rabbit anti-PLD1 (no. 3832)	Cell Signaling (Danvers, MA, USA)
Rabbit anti-PLD2 (P6618)	Sigma-Aldrich (Deisenhofen, Germany)
Rabbit anti-rat IgG (no. 312-005-003)	Dianova (Hamburg, Germany)

Rabbit anti-STIM1 (no. 4916)	Cell Signaling (Danvers, MA, USA)
Rat anti-DNP IgE (clone SPE-7, no. D8406)	Sigma-Aldrich (Deisenhofen, Germany)
Rat anti-mouse CD11b-PerCP (no. 350993)	BD Biosciences (San Jose, CA, USA)
Rat anti-mouse CD44-FITC (no. 553133)	BD Biosciences (San Jose, CA, USA)
Rat anti-mouse CD4-PerCP (no. 553052)	BD Biosciences (San Jose, CA, USA)
Rat anti-mouse FcγRI (clone 290322)	R&D Systems (Wiesbaden, Germany)
Rat anti-mouse FcγRIII (clone 275003)	R&D Systems (Wiesbaden, Germany)
Rat anti-mouse STIM1 (clone 5A2, no. H00006786-M01)	Abnova (Heidelberg, Germany)
Rat anti-mouse-tubulin (MAB1864)	Chemicon (Hofheim, Germany)

2.1.2.2 Monoclonal Antibodies from our Laboratory

Antibody	Internal Name	Antigen	Described in
-	12C6	α2 integrin	unpublished
-	25B11	α5 integrin	unpublished
-	96H10	CD9	unpublished
2.4G2	-	FcγRIIb/RIII (CD32/CD16)	Clone HB-197 purchased from ATCC; [164]
DOM1	89H11	GPV	[146]
DOM2	89F12	GPV	[146]
EDL1	99H9	β3 integrin	[146]
hamster anti-CD3	-	CD3	Clone 145-2C11 purchased from ATCC; [165]
INU1	11E9	CLEC-2	[166]
JAQ1	98A3	GPVI	[81]
JON/A	4H5	GPIIb/IIIa	[167]
JON1	6C10	GPIIb/IIIa	[146]
JON3	5D7	GPIIb/IIIa	[146]
p0p/B	57E12	GPIb	[55]

p0p4	15E2	GPIb	[146]
p0p6	56F8	GPIX	[146]
ULF1	97H1	CD9	[146]
WUG1.9	5C8	P-selectin	unpublished

2.1.3 Mice

2.1.3.1 Genetically Modified Mice

Gp5$^{-/-}$ [25] and *Itga2*$^{-/-}$ mice [76] were kindly provided by François Lanza (UMR_S949 Inserm-Université de Strasbourg, Strasbourg, France) and Beate Eckes (Department of Dermatology, University of Cologne, Cologne, Germany), respectively. *F12*$^{-/-}$ [168] were obtained from Thomas Renné (Department of Molecular Medicine and Surgery and Center for Molecular Medicine, Karolinska Institutet, Stockholm, Sweden). The three aforementioned mouse lines were backcrossed to C57Bl/6 background. *Gp5*$^{-/-}$ and *Itga2*$^{-/-}$ mice were intercrossed to obtain double-deficient mice. The wildtype mice originating from these matings were used as controls for the experiments in the GPV part of this study.

Mice lacking PLD1 or PLD2 were generated as described (see Figure 3-12 and Figure 3-22). PLD1 mice were on a mixed Sv129/C56Bl/6 background, while PLD2 mice were on a pure C56Bl/6 background. After the initial intercrossings of heterozygous mice, wildtype and knockout mice were mated separately for both PLD mouse lines.

Stim1$^{-/-}$, *Stim2*$^{-/-}$ and *Orai1*$^{-/-}$ mice were generated in our laboratory as described previously [127, 128, 169]. These mice were on a mixed Sv129/C56Bl/6 background and heterozygous mice were mated to obtain knockout mice and corresponding controls. Mice deficient in the FcRγ-chain (*Fcer1g*$^{-/-}$) or the FcγRIII receptor (*Fcgr3*$^{-/-}$) were purchased from Taconic Farms (Germantown, NY, USA). C56Bl/6J mice were used as controls for the experiments conducted with the FcRγ-chain and FcγRIII, since both mouse lines were on pure C56Bl/6 background.

Animal studies were approved by the district government of Lower Franconia (Bezirksregierung Unterfranken).

2.1.3.2 Bone Marrow Chimeras

Recipient C57Bl/6 mice (or corresponding transgenic mice for criss-cross experiments) of an age between 5-6 weeks were lethally irradiated with 10 Gray. Femur and tibia of mice of which bone marrow should be transplanted were prepared. Bone marrow was flushed with a 22G needle into prewarmed DMEM with 10% FCS and 1% penicillin/streptomycin. 10 µl of cells was diluted 1:100 and counted in a Neubauer chamber under ten times magnification. Four million cells diluted in 150 µl DMEM were intravenously injected into one recipient mouse. Animals received 2 g/l neomycin in water for 6 weeks.

2.1.4 Buffers and Media

All buffers were prepared with double-distilled water.

Acid-citrate-dextrose (ACD) buffer, pH 4.5

Trisodium citrate dehydrate	85 mM
Anhydrous citric acid	65 mM
Anhydrous glucose	110 mM

Blocking solution for immunoblotting

Bovine serum albumin (BSA) or fat-free dry milk	5%
In PBS or washing buffer (see below)	

Blotto B

BSA	2.5%
Fat-free dry milk	2.5%

Blotting buffer A for immunoblotting

TRIS, pH 10.4	0.3 M
Methanol	20%

Blotting buffer B for immunoblotting

TRIS, pH 10.4	25 mM
Methanol	20%

Blotting buffer C for immunoblotting	
ε-amino-n-caproic acid, pH 7.6	4 mM
Methanol	20%
Church buffer (for Southern Blot)	
Phosphate buffer (0.5 M, pH 7.2)	50%
Sodium dodecyl sulfate (SDS) (20%)	33%
EDTA (0.5 M)	0.1%
Hering sperm DNA	1%
BSA	10 g/l
Church wash buffer (for Southern Blot)	
Phosphate buffer (0.5 M, pH 7.2)	4%
SDS (20%)	5%
Coating buffer (ELISA), pH 9.0	
$NaHCO_3$	50 mM
Coomassie staining solution	
Acetic acid	10%
Methanol	40%
Coomassie brilliant blue	0.01%
Coomassie destaining solution	
Acetic acid	10%
Methanol	40%
Coupling buffer, 2x, pH 9.0	
$NaHCO_3$	14 g/l
Na_2CO_3	8.5 g/l
Decalcification buffer, pH 7.2	
EDTA in PBS	10%

Denaturation buffer (for Southern Blot)	
NaCl	1.5 M
NaOH	0.5 M
EF-Medium	
FCS	10%
Dulbecco's modified Eagle's medium (DMEM)	90%
ES-Medium	
FCS	10%
Nonessential amino acids	1%
DMEM	89%
β-mercaptoethanol	3.5 µl
LIF	1000 U/ml
G418	0 or 400 µg/ml
Freezing medium (stem cells)	
FCS	50%
DMEM	40%
Dimethyl sulfoxide (DMSO)	10%
Immunoprecipitation (IP) buffer, pH 8.0	
TRIS / HCl	15 mM
NaCl	155 mM
EDTA	1 mM
NaN_3	0.005%
Laemmli buffer for SDS-PAGE	
TRIS	40 mM
Glycine	0.95 mM
SDS	0.5%

Luria-Bertani (LB) medium

Peptone (pancreatic digested)	10 g/l
Yeast extract	5 g/l
NaCl	10 g/l
Agar (for LB plates, not for solution)	15 g/l

Lysis buffer (for DNA isolation), pH 7.2

TRIS base	100 mM
EDTA	5 mM
NaCl	200 mM
SDS	0.2%
Proteinase K (to be added directly before use)	100 µg/ml

Lysis buffer (for tyrosine phosphorylationassay), pH 7.5

TRIS base	20 mM
EDTA	2 mM
NaCl	300 mM
EGTA	2 mM
Na_3VO_4	2 mM
Igepal CA-630	2%
Add complete mini protease inhibitor	1 tablet / 10 ml

Neutralisation buffer (for Southern Blot), pH 7.2

NaCl	1.5 mM
TRIS/HCl	0.5 M

Phosphate buffered saline (PBS), pH 7.14

NaCl	137 mM
KCl	2.7 mM
KH_2PO_4	1.5 mM
Na_2HPO_4	8 mM

Saline-Sodium citrate (SSC, for Southern Blot) buffer, 10x

NaCl	1.5 M
Sodium citrate	0.25 M

SDS sample buffer, 2x

β-mercaptoethanol (for reducing conditions)	10%
TRIS buffer (1.25 M), pH 6.8	10%
Glycerine	20%
SDS	4%
Bromophenol blue (3',3",5',5"-tetrabromophenolsulfonphthalein)	0.02%

Separating gel buffer (Western Blot), pH 8.8

TRIS/HCl	1.5 M

Stacking gel buffer (Western Blot), pH 6.8

TRIS/HCl	0.5 M

Stripping buffer (Western Blot), pH 6.8

TRIS/HCl	62.5 mM
SDS	2%
β-mercaptoethanol (for reducing conditions)	100 mM

TAE buffer, 50x, pH 8.0

TRIS	0.2 M
Acetic acid	5.7%
EDTA (0.5 M, pH 8.0)	10%

TE buffer, pH 8.0

TRIS base	10 mM
EDTA	1 mM

Tris-buffered saline (TBS), pH 7.3

NaCl	137 mM
TRIS/HCl	20 mM

Tyrode's buffer, pH 7.3

NaCl	137 mM
KCl	2.7 mM
$NaHCO_3$	12 mM
NaH_2PO_4	0.43 mM
$CaCl_2$	0, 1 or 2 mM
$MgCl_2$	1 mM
HEPES (*4-(2-hydroxyethyl)-1-piperazineethanesulfonic acid*)	5 mM
BSA (to be added directly before use)	0.35%
Glucose (to be added directly before use)	1%

Washing buffer (for Western Blot)

Tween 20 in PBS, pH 7.2	0.1%

2.2 Methods

2.2.1 Stem Cell Work

2.2.1.1 Preparation of Feeder Cells

A mouse strain containing a neomycin cassette in the genome was used for the preparation of feeder cells. For this, fertile *collagen 9* knockout mice were time-mated. At day 14.5 mice embryos were excised of the pregnant mouse. Then, the embryos were washed in PBS and subsequently the skeleton muscles and the skin of the embryo were homogenized in a final volume of 10 ml EF-Medium (for a number of 7-9 embryos) with 10% trypsin and incubated in a 37°C waterbath for at least 5 min. This step was repeated once. 1 ml of the homogenized embryos in medium was added to 9 mL EF-Medium in a 10 cm tissue culture dish. After one day of incubation at 37°C and 5% CO_2, the EF-Medium was changed and when the cells were grown confluently, one 10 cm tissue culture dish was split into two 175 cm^2 tissue culture flasks. The densely grown cells were trypsinized, collected and spun down (all cell culture centrifugation steps: 5 min with 900 rpm in a Multifuge 3 S-R from Heraeus). The cells were collected in a final volume of 15 ml EF-Medium. Subsequently, the cells were irradiated with 40 Gray. After spinning down, freezing medium was added to the

pellet and the cells in Freezing-Medium were stored as 1 ml aliquots (cells of an 175 cm^2 tissue culture were frozen in 3 ml freezing medium) in 2 ml cryo-tubes at –80°C. One cryo-tube with cells was used for checking contamination and efficiency of irradiation. Therefore, one tube with feeder cells was added to a 10 cm tissue culture dish with EF-Medium and was monitored under the microscope every day for one week.

2.2.1.2 Culturing of Purchased Stem Cell Clones

Frozen tubes of the purchased stem cell clones were thawed and added to one well of a six well plate containing feeder cells and ES-Medium containing G418. After growing at 37°C and 5% CO_2 to a certain density, the cells were trypsinized and cultured in a 25 cm^2 flask. Two days later, the cells were trypsinized again and added to a 75 cm^2 tissue culturing flask. Finally the cells were trypsinized and a small amount of cells was transferred to one well of a 24 well plate to confirm the presence of the targeted allele (see below, 2.2.1.3) via Southern Blot. The majority of cells were frozen into four aliquots. Three cryo-tubes were stored at –80°C and one tube with ES cells was used for the generation of chimeric mice. Therefore, this tube was sent on dried ice to Michael Bösl (Transgenic Core Facility, MPI, Martinsried) who injected these cells into blastocysts and sent us the chimeric mice.

2.2.1.3 Analysis of Stem Cell DNA

The cells which had been cultured for analysis of the stem cell DNA were cultured in ES-medium containing G418 until a confluent layer was observed and the medium turned yellow. The supernatant was removed and the cells were lysed with lysis buffer supplemented with 100 µg/ml proteinkinase K. 500 µl lysis buffer were added to one well. The cells were lysed for at least 1 day at 37°C and 5% CO_2. Following lysis, DNA of the stem cells was precipitated with 500 µl isopropanol per well. Therefore, sterile conditions were not necessary any more. The samples were agitated on a shaker between 4-6 h at room temperature. In the meantime, 1.5 ml tubes were labeled with the corresponding numbers and filled with 150 µl TE buffer. The precipitated DNA fibers were transferred with a stick into the corresponding 1.5 ml tube. After shaking the samples for a few minutes at 55°C with open lid to remove traces of isopropanol, DNA was incubated with closed lid in a 55°C incubator overnight. Afterwards, the samples were shortly vortexed and ready for analysis.

Genomic DNA was digested for Southern Blotting over night at 37°C. The pipetting scheme was:

20 µl	DNA solution
4 µl	10x restriction buffer of the enzyme
25 u	Restriction enzyme
Add to 40 µl	Water

The digested DNA samples were separated on a 0.7% agarose gel for at least 3-4 hours at 140 kV. Then, a photo was taken from the gel with a ruler to estimate the size of the bands after development. The gel was incubated with denaturation buffer for 20 min twice and subsequently with neutralization buffer for 20 min twice. Afterwards, DNA was blotted from the agarose gel on a nitrocellulose membrane over night at RT. After blotting, gel slots were labeled on the membrane. Then, DNA was UV-crosslinked with the membrane (120,000 µJ/cm^2; HL-2000 HybriLinker from UVP). The membrane was briefly preincubated in Church wash buffer before blocking it 1 h in Church buffer at 68°C. For probe labeling and hybridisation, the following steps were performed in an isotope lab: The external probe (10-100 ng) was diluted in 35 µl TE buffer and incubated for 3 min at 96°C. When the DNA was resuspended in the Rediprime DNA Labeling Kit, 5 µl ^{32}P-CTP was added to one sample and incubated for 20 min at 37°C. In the meantime, the buffer of the Probequant G 50 Microcolumns was removed via centrifugation. The DNA with the radioactive substance was loaded on the column and centrifuged for 1 min at 380 *g*. The flow-through containing the radioactively labeled DNA was incubated for 3 min at 96°C, immediately transferred to -20°C for 3 min and then added to the membrane in the Church buffer. The membrane was shaken in Church buffer over night at 68°C. Then, the membrane was washed twice with Church wash buffer for 20 min at 68°C. Subsequently, a film was put on the membrane and stored at –80°C. The film was developed after 3-5 days depending on the counts per minute detected with a Geiger counter.

2.2.2 Mouse Genotyping

2.2.2.1 Isolation of Genomic DNA from Mouse Ears

One third of one ear was cut and dissolved in 500 µl DNA lysis buffer (see above) by overnight incubation at 56°C under shaking conditions (900 rpm). 500 µl phenol/chloroform were added and, after vigorous shaking, samples were centrifuged at 12,851 *g* (11,000 rpm) for 10 min at room temperature (RT). Approximately 450 µl supernatant were taken,

transferred into a new tube and 400 µl isopropanol were added. After vigorous shaking, samples were centrifuged at full speed for 10 min at 4°C. The resulting DNA pellet was washed with 1 ml of 70% ethanol and centrifuged at full speed for 10 min at 4°C. The DNA pellet was left to dry and finally resuspended in 50-100 µl TE buffer.

2.2.2.2 PCRs

2.2.2.2.1 Standard PCR Protocol and Agarose Gel Electrophoresis

The pipeting scheme shown is representative for 1 sample (final volume: 25 µl) for the below described genotyping PCRs.

1 µl	DNA solution
2.5 µl	10x Taq buffer
2.5 µl	25 mM MgCl2
1 µl	10 mM dNTP
1 µl	10 µM fwd primer
1 µl	10 µM rev primer
0.25 µl	Taq polymerase
15.75 µl	Water

The PCR program shown is representative for the PCR programs used to genotype the mice. T_A indicates the annealing temperature, the corresponding T_A are listed below.

95°C	5:00 min	
95°C	0:30 min	} 35x
T_A	0:30 min	
72°C	0:30-1:00 min (depending on product size)	
72°C	5:00 min	
20°C	∞	

20 µl PCR reaction were separated on agarose gels for analysis.

1.2% Agarose gels were prepared by adding 1.2 g agarose to 100 ml 1x TAE buffer. The agarose in TAE buffer was boiled in a microwave oven. After all agarose was completely dissolved, the TAE-agarose was allowed to cool down to approximately 50°C before 6 µl

ethidium bromide were added and the fluid was poured into a slide with a comb. The sleigh was laid in a chamber filled with 1x TAE buffer. The samples were diluted in 6x loading buffer and loaded into the slots of the gel, a DNA ladder was loaded on each side of the gel to enable size determination of the PCR products. 120 kV were applied for size separation of the DNA and UV light was used to detect the DNA bands after the run.

2.2.2.2.2 Primers and Annealing Temperatures

Genotyping of *F12* mice

For this PCR two different reverse primers had to be added in parallel. Thus, the amount of water used in the PCR mastermix had to be reduced accordingly.

T_A	58°C
Fwd primer	5'– GGC CTC TTG TAT TGA CTG ATG A –3'
Rev primer (WT)	5'– AAC TGC CAT CAT AAC GTT AGC C –3'
Rev primer (KO)	5'– GCA GAG GTT ACG GCA GTT TGT CTC TCC –3'
Resulting band size (WT)	842 bp
Resulting band size (KO)	492 bp

Genotyping of *Pld1* mice

WT allele:

T_A	66°C
Fwd primer	5'– TGT GCA AGT GCG TGT GGG CA –3'
Rev primer	5'– ACA GGG CAC CCA CAG GAG CA –3'
Resulting band size	283 bp

KO allele:

TA	51.4°C
Fwd primer	5'– TTA TCG ATG AGC GTG GTG GTT ATC C –3'
Rev primer	5'– GCG CGT ACA TCG GGC AAA TAA TAT C –3'
Resulting band size	650 bp

Initially the *Pld1* mice were genotyped by Southern Blotting (see below). Southern Blotting was also required for genotyping of the *Pld1* allele in *Pld1*/*Pld2*-double-deficient mice.

Genotyping of *Pld2* mice

WT allele:

T_A	59°C
Fwd primer	5'– AAG CAA CAC CAC ACA TTC CA –3'
Rev primer	5'– CTT CCC GAC TCA CAG CTT TC –3'
Resulting band size	445 bp

KO allele:

TA	55°C
Fwd primer	5'– TCA TTC TCA GTA TTG TTT TGC C –3'
Rev primer	5'– GGA GGA AGA GTG AGA TGA AG –3'
Resulting band size	408 bp

Genotyping of *Stim1* mice

WT allele:

T_A	51.4°C
Fwd primer	5'– GTC ATA GCC TGT AAA CTA GA –3'
Rev primer	5'– GTA GCT GCA GGT AGC ACT AG –3'
Resulting band size	750 bp

KO allele:

TA	51.4°C
Fwd primer	5'– TTA TCG ATG AGC GTG GTG GTT ATC C –3'
Rev primer	5'– GCG CGT ACA TCG GGC AAA TAA TAT C –3'
Resulting band size	650 bp

Genotyping of *Stim2* mice

WT allele:

T_A	59°C
Fwd primer	5'– CCC ATA TGT AGA TGT GTT CAG –3'
Rev primer	5'– GAG TGT TGT TCC CTT CAC AT –3'
Resulting band size	250 bp

KO allele:

TA	51.4°C
Fwd primer	5'– TTA TCG ATG AGC GTG GTG GTT ATC C –3'
Rev primer	5'– GCG CGT ACA TCG GGC AAA TAA TAT C –3'
Resulting band size	650 bp

Initially the *Stim2* mice were genotyped by Southern Blotting (see below).

Genotyping of *Orai1* mice

WT allele:

T_A	56°C
Fwd primer	5'– CTC TTG AGA GGT AAG AAC TT –3'
Rev primer	5'– GAT CCC TAG GAC CCA TGT GG –3'
Resulting band size	900 bp

KO allele:

TA	51.4°C
Fwd primer	5'– TTA TCG ATG AGC GTG GTG GTT ATC C –3'
Rev primer	5'– GCG CGT ACA TCG GGC AAA TAA TAT C –3'
Resulting band size	650 bp

Genotyping of *Fcgr3* mice

For this PCR two different forward primers had to be added in parallel. Thus, the amount of water used in the PCR mastermix had to be reduced accordingly.

T_A	5 cycles with decreasing T_A (1°C intervals, starting with 62°C) => then 30 cycles with 57°C
Fwd primer (WT)	5'– TCC ATC TCT CTA GTC TGG TAC C –3'
Fwd primer (KO)	5'– ACT TGT GTA GCG CCA AGT GCC AA –3'
Rev primer	5'– GCC ATG GTG GAT GGT GGA GGT C –3'
Resulting band size (WT)	572 bp
Resulting band size (KO)	505 bp

2.2.2.3 Southern Blot

For the mouse lines which had to be genotyped by Southern Blot, DNA was purified as described above (2.2.2.1). Then, Southern Blotting was performed as described for stem cell DNA (see 2.2.1.3).

Genotyping of *Pld1* mice

For genotyping the *Pld1* mice by Southern Blotting broad range agarose (Roth; # T846.2) had to be used to separate the digested DNA.

Restriction Enzyme	*Bgl*II
Primers for external probe	Fwd: 5'– GCC TGA CAT GTA GGA CAT A –3' Rev: 5'– CAT GTG GCT GCT GGG CAC TGA –3'
Expected size of bands	WT allele: 9.4 kbp KO allele: 11.0 kbp

Genotyping of *Stim2* mice

Restriction Enzyme	*Bam*HI
Primers for external probe	Fwd: 5'– GTG CTT CAG AGC TTT TCT GT –3' Rev: 5'– CAA GAC TAA CAC CAA ATG AA –3'
Expected size of bands	WT allele: 11.0 kbp KO allele: 6.7 kbp

2.2.2.4 Genotyping by Flow Cytometry

Gp5, *Itga2* and *Fcer1g* mice were genotyped by flow cytometry. Therefore, the expression of GPV, the α2 integrin and GPVI (for the FcRγ-chain mouse, *Fcer1g*) was determined as described below (2.2.4.2).

2.2.3 Molecular Biology and Biochemistry

2.2.3.1 RT-PCR

For platelet RNA isolation $2*10^6$ cells were washed in PBS/EDTA and the pellet was resuspended in 200 µl IP buffer with 1% NP-40. Following addition of 800 µl Trizol reagent, the sample was incubated for 60 min at 4°C. After shaking, 200 µl chloroform was added and incubated for 15 min at 4°C. Sample was centrifuged at 10,621 *g* (10,000 rpm) for 10 min and the upper phase was incubated with three volumes of 70% ethanol and with 10% sodium acetate (pH 5.2) for 1 h at -20°C. After centrifugation at maximal speed for 15 min, the pellet was washed with 70% ethanol, then centrifuged again and pellet was dried at 37°C.

For RNA isolation from was performed using the Qiagen RNeasy kit according to the manufacturers' instructions. 30-40 µl of RNase free water were added and the RNA concentration was determined by absorbance readings at 260 nm, whereas the ratio of absorbance at 260/280 nm and 260/230 nm was used to assess purity. Only samples with 260/280 readings of >1.8 and 260/230 readings of >1.9 were subsequently converted into cDNA. 1-2 µg RNA were incubated with 1 µl Oligo dTP (0.5 µg/µl) in a total volume of 11.9 µl at 70°C for 5 min and afterwards transferred on ice. 2 µl DTT (0.1 M), 1 µl dNTPs (10 mM), 0.5 u RNase inhibitor, 4 µl 5x first strand buffer and 200 u Super Script Reverse Transcriptase were added. The total volume was adjusted to 40 µl by adding RNase-free

water the sample was incubated at 42°C for 1 h. Then, heat inactivation was performed (10 min, 70°C). A gradient PCR was performed with Taq polymerase to determine the correct annealing temperature. Following this, a PCR with the appropriate annealing temperature was performed.

The following primers were used:

Gene	Primer
Actin	5'– CTA AGG CCA ACC GTG AAA AG –3'
	5'– ACC AGA GGC ATA CAG GGA CA –3'
Pld1	5'– GCA TGT CAC TGA AAA GCG AG –3'
	5'– GAA CTG CTC TTC CTG GAT TG –3'
Pld2	5'– GAG TTT GCG GAA GCA CTG TT – 3'
	5'– TCA TCA CAG ACA GGG TCT CG – 3'

2.2.3.2 Immunoblotting

For Western blot analysis $2*10^6$ cells were resuspended in 100 µl IP buffer containing 1% NP-40 and protease inhibitors. After incubation for 20 min at 4°C and centrifugation at 20,817 *g* (14,000 rpm) for 5 min, the supernatant was mixed with an equal amount of 2x SDS sample buffer and boiled at 95°C for 10 min. Samples were separated by 10, 12 or 15% SDS-PAGE and transferred onto a polyvinylidene difluoride membrane. To prevent nonspecific antibody binding, the membrane was incubated in blocking buffer for at least 1 h at RT. Membranes were incubated with the required primary antibody (according to the manufacturers' instructions or with 5 µg/ml) overnight at 4°C with gentle shaking. Afterwards, membranes were washed three times with washing buffer for 15 min at RT under shaking conditions. Next, membranes were incubated with appropriated HRP-labeled secondary antibodies for 1 h at RT. After three washing steps, proteins were visualized by ECL.

2.2.3.3 Histology

2.2.3.3.1 Preparation of Paraffin Sections

Organs from adult mice were washed in PBS and fixed overnight in PBS containing 4% PFA. Afterwards, organs were washed three times with PBS and spleens were directly dehydrated and embedded in paraffin. Fixed femurs were incubated for 3 further weeks in 10 ml decalcification buffer with the buffer being changed twice per week. After decalcification,

femurs were also embedded in paraffin. Organs were cut using a Microm Cool Cut microtom (Thermo Scientific, Braunschweig, Germany) to prepare 3-7 µm thin sections.

2.2.3.3.2 Hematoxylin/Eosin Staining of Paraffin Sections

Sections were deparaffinated by two incubations in Xylol (3 min each). Rehydration was carried out using decreasing ethanol concentrations (100, 96, 90, 80 and 70%) with 2 min incubation time in each solution and a final 2 min incubation in deionized water. Next, sections were stained 2 min with hematoxylin, followed by a 10 min washing step using running tab water and 2 min staining with 0.05% Eosin G. The sections were washed shortly and dehydration was carried out using the same ethanol concentrations and incubation times as described above, but in reversed order. Finally, sections were incubated twice in Xylol for each 3 min, dried and mounted using Eukitt mounting medium. Samples were analyzed using a Leica DHI 4000B inverse microscope equipped with a Leica digital camera (Leica, Wetzlar, Germany).

2.2.3.4 Calcium Measurements

Cells were adjusted to a concentration of $2*10^7$/ml in Ca^{2+}-free Tyrode's buffer. 100 µl of this cell suspension were transferred to a 1.5 ml reaction tube and incubated with 7.5 µM Fura-2-AM and 0.15% pluronic F-127 (in a final volume of 1.5 µl DMSO) for 30 min at 37°C.

For immunoreceptor crosslinking experiments 10 µg/ml 2.4G2 (for macrophages) or CD3e (for T cells) antibodies were added for the last 10 min of Fura labeling. After the labeling, 1 ml Tyrode's buffer without Ca^{2+} was added and cells were washed (5 min, with 639 *g*). The pellet was resuspended and washed once more, before the cells were finally resolved in 500 µl Tyrode's buffer (with or without Ca^2 depending on the intended measurement).

This cell suspension was transferred into a cuvette which had been blocked for 1 h with 1% BSA in water at RT. Fluorescence was measured with a PerkinElmer LS 55 fluorimeter (Perkin Elmer, Waltham, MA, USA). Excitation was alternated between 340 and 380 nm and emission was measured at 509 nm. Basal calcium levels were recorded for 50 s before the indicated reagent, secondary antibody or agonist was added. Each measurement was calibrated using 1% Triton X-100 and EGTA.

2.2.4 *In vitro* Platelet Analyses

2.2.4.1 Platelet Preparation and Washing

Mice were bled under isoflurane anesthesia from the retroorbital plexus. 700 µl blood were collected into a 1.5 ml reaction tube containg either 300 µl heparin in TBS (20 U/ml, pH 7.3) or 300 µl *acid citrate dextrose* (ACD). Blood was centrifuged at 800 rpm (52 *g*; in a Eppendorf Centrifuge 5415C) for 5 min at RT. Supernatant and buffy coat were transferred into a new tube and centrifuged at 800 rpm for 6 min at RT to obtain *platelet rich plasma* (PRP). To prepare washed platelets, PRP was centrifuged at 2800 rpm (639 *g*) for 5 min at RT in the presence of *prostacyclin* (PGI_2) (0.1 µg/ml) and the pellet was resuspended in 1 ml Ca^{2+}-free Tyrode's buffer containing PGI_2 (0.1 µg/ml) and apyrase (0.02 U/ml). After 10 min incubation at 37°C the sample was centrifuged at 2800 rpm for 5 min. After resuspending the platelets once more in 1 ml Ca^{2+}-free Tyrode's buffer, the platelet levels were determined taking a 1:10 dilution of the platelet solution and measuring platelet counts in a Sysmex counter (see below). The pellet was resuspended in the volume of Tyrode's buffer containing apyrase (0.02 U/ml) required to obtain 500,000 platelets/µl and left to incubate for at least 30 min at 37°C before analysis.

For determination of platelet count and size, 50 µl blood were drawn from the retroorbital plexus of anesthetized mice using heparinized microcapillaries and collected into a 1.5 ml reaction tube containing 300 µl heparin in TBS (20 U/ml, pH 7.3). The heparinized blood was diluted with PBS and platelet counts and size were determined using a Sysmex KX-21N automated hematology analyzer (Sysmex Corp., Kobe, Japan).

2.2.4.2 Flow Cytometry

For determination of glycoprotein expression levels, platelets ($1*10^6$) were stained for 10 min at RT with saturating amounts of fluorophore-conjugated antibodies described in section 2.1.2.2 and analyzed directly after addition of 500 µl PBS. For activation studies, platelets were activated with appropriate agonists or reagents for 15 min at RT in the presence of saturating amounts of *phycoerythrin* (PE)-coupled JON/A and *fluorescein isothiocyanate* (FITC)-coupled P-selectin antibodies. Alternatively to JON/A-PE human Alexa 488-labeled fibrinogen (50 mg/ml) was used. Where indicated, washed platelets were first incubated with 1 mM L-α-PA for 5 min at 37°C before stimulation with agonist.

The reaction was stopped by addition of 500 µl PBS and samples were analyzed on a FACSCalibur (Becton Dickinson, Heidelberg, Germany). For a two-color staining, the following settings were used:

Detectors/Amps:

Parameter	Detector	Voltage
P1	FSC	E01
P2	SSC	380
P3	FL1	650
P3	FL2	580
P5	FL3	150

Threshold:

Parameter	Value
FSC-H	253
SSC-H	52
FL1-H	52
FL2-H	52
FL3-H	52

Compensation:

Parameter	Value
FL1	2.4% of FL2
FL2	7.0% of FL1
FL2	0% of FL3
FL3	0% of FL2

2.2.4.3 ATP Release

For determination of ATP release washed platelets were adjusted to a concentration of $0.4x10^6$/µl. Platelets were activated with the indicated agonists for 2 min at 37°C under stirring conditions (1000 rpm). Following activation, EDTA (3 mM final concentration) and formaldehyde (0.1% final concentration) were added and platelets were fixed for 2 h. The platelets were then centrifuged for 1 min at 17,949 *g* (13,000 rpm) and 100 µl supernatant were added to 100 µl absolute ethanol. Samples were stored at -20°C until measuring. Levels of ATP in 12.5 µl sample were quantified using a bioluminescence assay kit according

to the manufacturers´ instructions and a Fluostar Optima luminometer (BMG Lab Technologies, Offenburg, Germany).

2.2.4.4 Aggregation Studies

50 µl washed platelets (with a concentration of $0.5x10^6$ platelets/µl) or heparinized PRP was transferred into a cuvette containing 110 µl Tyrode's buffer (with 2 mM $CaCl_2$). For all measurements with washed platelets, except those with thrombin as agonist, Tyrode's buffer with 100 µg/ml human fibrinogen was used. For determination of aggregation, agonists or reagents (100-fold concentrated) were added and light transmission was recorded over 10 min on an Apact 4-channel optical aggregation system (APACT, Hamburg, Germany). For calibration of each measurement before agonist addition Tyrode's buffer was set as 100% aggregation and washed platelet suspension or PRP was set as 0% aggregation.

2.2.4.5 Spreading on Fibrinogen

Glass coverslips (24 x 60 mm) were coated with 100 µg human fibrinogen overnight at 4°C under humid conditions and blocked for 2 h at RT with 1% BSA in PBS. The coverslips were rinsed with Tyrode´s buffer and 60 µl washed platelets (300,000 cells/µl in Tyrode´s containing calcium) were stimulated with thrombin (0.001 U/ml) and immediately allowed to spread. Platelet spreading was monitored with a Zeiss Axiovert 200 inverted microscope (100x/1.4 oil objective; Zeiss, Jena, Germany) using *differential interference contrast* (DIC) microscopy. Pictures were taken every five seconds for 20 minutes using a CoolSNAP-EZ camera (Visitron, Munich, Germany) and analyzed off-line using MetaMorph software (Spectra Services, Ontario, NY, USA). For statistical analysis bound platelets were fixed with 4% PFA in Tyrode's buffer at the indicated time points and counted.

2.2.4.6 Adhesion Under Flow Conditions

2.2.4.6.1 Flow Chamber on Collagen

Coverslips (24 x 60 mm) were coated with 200 µg/ml fibrillar type-I collagen (Horm) over night at 37°C and blocked for 1 h with 1% BSA. Blood (700 µl) was collected into 300 µl TBS (pH 7.3) containing 20 U/ml heparin and platelets were labeled with a Dylight-488 conjugated anti-GPIX Ig derivative (0.2 µg/ml) for 5 min at 37°C. Two parts of blood were diluted with one part Tyrode´s buffer and filled into a 1 ml syringe. Transparent flow chambers with a slit

depth of 50 µm, equipped with the coated coverslips, were connected to the syringe filled with diluted whole blood. Perfusion was performed using a pulse-free pump under high or low shear stress equivalent to a wall shear rate of 150, 1000 or 1700 s^{-1} (10 min at 150 s^{-1}, otherwise 4 min). During the perfusion platelet adhesion was monitored with a Zeiss Axiovert 200 inverted microscope (40x/0.75 air objective) and pictures were taken every second using a CoolSNAP-EZ camera. Thereafter, coverslips were washed with Tyrode's buffer at the same shear rate for half the blood perfusion period and phase-contrast and fluorescent images were recorded from at least five different microscope fields (40x objective). Image analysis was performed off-line using MetaMorph software. Thrombus formation was depicted as the mean percentage of total area covered by thrombi and as the mean integrated fluorescence intensity per mm^2.

2.2.4.6.2 Flow Chamber on vWF

Glass cover slips were coated with a polyclonal rabbit anti-human vWF antibody (1:500-diluted in coating buffer) over night at 4°C under humid conditions. The coverslips were blocked for 1 h at RT with 1% BSA in PBS. Blocked coverslips were incubated with murine plasma for 2 h at 37°C to allow binding of vWF to immobilized antibody against vWF. Perfusion experiments were performed as described above. For shear rates higher than 1700 s^{-1} a 2 ml-syringe was used.

2.2.4.6.3 Procoagulant Activity Measurements

For the measurement of procoagulant activity flow adhesion experiments were essentially performed as described above (2.2.4.6.1), but with either additional 5 U/ml heparin in the Tyrode's buffer used or with 20 µM PPACK and 0.5 U/ml fragmin to prevent coagulation. After the blood perfusion period, 250 µl 0.5 µg/ml fluorescently labeled annexin A5 in Tyrode's buffer containing calcium was rinsed over the adherent platelets. Thereafter, coverslips were washed with Tyrode's buffer at the same shear rate for 4 min. Phase-contrast and fluorescent images were taken from at least 10 different collagen-containing microscopic fields, which were randomly chosen.

2.2.4.7 PLD Activity Measurements

PLD-mediated PA production was analyzed with a fluorescent *in vitro* assay according to the manufacturers' instruction. In this enzymatically coupled assay, PLD hydrolyzes

phosphatidylcholine in the presence of PIP_2 to PA and choline, which is then oxidized by choline oxidase to betaine and H_2O_2. In the presence of horseradish peroxidase, H_2O_2 oxidizes Amplex red in a 1:1 stoichiometry to generate fluorescent resorufin (7-Hydroxy-3*H*-phenoxazin-3-one). In brief, washed platelets were adjusted to a concentration of $1x10^6$/ml. Platelets were activated with different agonists for the indicated time points at 37°C under shaking conditions (350 rpm) and lysed subsequently. Lysate samples (100 µl) were mixed with 100 µl of the Amplex red reaction buffer. The PLD activity was determined in duplicate for each sample by measuring fluorescence activity after a 1 h incubation at 37°C in the dark with a Fluostar Optima luminometer. A standard curve was performed with purified PLD from *Streptomyces chromofuscus* at concentrations ranging from 0 to 250 mU/ml.

2.2.4.8 Tyrosine Phosphorylation

For tyrosine phosphorylation studies, $0.7x10^6$ platelets/µl were activated with 1-2.5 µg/ml convulxin under constant stirring conditions (1,000 rpm) at 37°C. Stimulation was stopped by the addition of an equal volume ice-cold lysis buffer after the indicated time points. For whole-cell tyrosine-phosphorylation, 4x NuPage sample buffer (Invitrogen, Karlsruhe) was added; samples were incubated at 70°C for 10 min and separated by SDS-PAGE on 4-12% NuPage Bis-Tris gradient gels (Invitrogen, Karlsruhe) under reducing conditions followed by transfer onto a PVDF membrane. Membranes were blocked for 1 h at RT in 5% BSA in PBS and then incubated with primary anti-phosphotyrosine antibody 4G10 over night at 4°C. The membranes were then washed four times for 15 min in washing buffer before incubation with secondary anti-mouse horseradish peroxidase-conjugated antibody in washing buffer (1:2,000). Following extensive washing, proteins were visualized by (ECL).

2.2.5 *In vivo* Analyses of Platelet Function

2.2.5.1 Determination of Platelet Lifespan

Mice were injected intravenously with 5 µg of a Dylight-488 conjugated anti-GPIX Ig derivative. At 1 h after injection (day 0), as well as at the other indicated time points, 50 µl blood were collected and the percentage of GPIX-positive platelets was determined by flow cytometry (see 2.2.4.2).

2.2.5.2 Collagen/Epinephrine-Triggered Model of Thromboembolism

Mice were anesthetized by intraperitoneal injection of triple anesthesia (dormitor, dormicum and fentanyl). Anesthetized mice received a mixture of collagen (0.7 mg/kg) and epinephrine (60 µg/kg) injected into the retroorbital plexus. Prior to the experiment and 3 min after the injection of collagen/epinephrine platelet counts were determined.

2.2.5.3 Intravital Microscopy of Thrombus Formation in $FeCl_3$-Injured Mesenteric Arterioles

Mice (4-5 weeks of age) were anesthetized with Avertin (2,2,2-tribromoethanolin 2-methyl-2-butanol) and the mesentery was exteriorized through a midline abdominal incision. Arterioles (35-60 µm diameter) were visualized with a Zeiss Axiovert 200 inverted microscope (10x/0.25 air objective) equipped with a 100-W HBO fluorescent lamp source and a CoolSNAP-EZ camera. Digital images were recorded and analyzed off-line using MetaMorph software. Injury was induced by topical application of a 3 mm^2 filter paper saturated with *ferric chloride* ($FeCl_3$; 20%) for about 10 s. Adhesion and aggregation of fluorescently labeled platelets (Dylight-488 conjugated anti-GPIX Ig derivative) in arterioles was monitored for 40 min or until complete occlusion occurred (blood flow stopped for >1 min). All $FeCl_3$-injury experiments presented in this study were performed by Ina Hagedorn from our working group.

2.2.5.4 Mechanical-Injury of the Abdominal Aorta

To open the abdominal cavity of Avertin-anesthetized mice (10-16 weeks of age), a longitudinal midline incision was performed and the abdominal aorta was exposed. A Doppler ultrasonic flow probe (Transonic Systems, Maastricht, Netherlands) was placed around the aorta and thrombosis was induced by mechanical injury with a single firm compression (5 s) of a forceps upstream of the flow probe. Blood flow was monitored until complete occlusion occurred or 30 min had elapsed. Ina Hagedorn performed all aorta injury models presented in this study.

2.2.5.5 $FeCl_3$-Induced Injury of the Carotis

Mice (10-16 weeks of age) were anesthetized with Avertin and the right carotid artery was exposed through a vertical midline incision in the neck. Injury was induced by topical application of a 0.5 mm by 1 mm filter paper saturated with 15% ferric chloride for 3 min.

Blood flow was monitored with an ultrasonic flow probe (Transonic Systems, Maastricht, Netherlands) until full occlusion of the vessel occurred or 30 min. These experiments were performed by Ina Hagedorn.

2.2.5.6 Transient Middle Cerebral Artery Occlusion (tMCAO)

Experiments were conducted on 8-12 week-old mice by members of the working group of Prof. Dr. G. Stoll (Department of Neurology, University of Würzburg) according to the recommendations for research in mechanism-driven basic stroke studies [170]. Briefly, mice were anesthetized with 2% isoflurane in a 70% N_2/30% O_2 mixture. A servo-controlled heating blanket was used to maintain core body temperature close to 37°C throughout surgery. After a midline neck incision was made, a standardized silicon rubber–coated 6.0 nylon monofilament (6021PK10, Doccol, Redlands, CA, USA) was inserted into the right common carotid artery and advanced via the internal carotid artery to occlude the origin of the middle cerebral artery (MCA). After 30 or 60 min, mice were reanesthetized and the occluding filament was removed to allow reperfusion the filament was withdrawn to allow reperfusion. For measurements of ischemic brain volume animals were killed 24 h after induction of tMCAO and brain sections were stained with 2% *2,3,5-triphenyl tetrazolium chloride* (TTC, Sigma-Aldrich). Planimetric measurements (ImageJ software, National Institutes of Health, Bethesda, MD, USA) were performed by researchers blinded to the treatment group and were used to calculate lesion volumes, which were corrected for brain edema as described [171]. Global neurological status was scored according to Bederson *et al.* [172]. Motor function and coordination were graded with the grip test [173] by two independent and blinded investigators 24 h after tMACO. *Magnetic resonance imaging* (MRI) was performed 24 hours and 7 days after transient ischemia on a 1.5 T unit (Vision; Siemens, Munich, Germany) under inhalation anesthesia. A custom-made dual-channel surface coil was used for all measurements (A063HACG; Rapid Biomedical, Rimpar, Germany). The MR protocol included a coronal T2-weighted sequence (slice thickness, 2 mm) and a coronal T2-weighted gradient-echo *constructed interference in steady state* (CISS) sequence (slice thickness, 1 mm). MR images were transferred to an external workstation (Leonardo; Siemens) for data processing. The visual analysis of infarct morphology and the search for eventual intracerebral hemorrhage were performed in a blinded manner. Infarct volumes were calculated by planimetry of hyperintense areas on high-resolution CISS images.

2.2.5.7 Bleeding Time Assay

Mice were anesthetized by intraperitoneal injection of triple anesthesia and a 2-mm segment of the tail tip was removed with a scalpel. Tail bleeding was monitored by gently absorbing blood with filter paper at 20 s intervals without directly contacting the wound site. When no blood was observed on the paper, bleeding was determined to have ceased. The experiment was manually stopped after 20 min by cauterization.

2.2.6 Isolation and Analyses of Immune Cells

2.2.6.1 Isolation of Immune Cells

2.2.6.1.1 Isolation of CD4-Positive T Cells

Mice were sacrificed by CO_2 inhalation or via cerebral dislocation and spleen and lymph nodes were extracted. The cells were homogenized and CD4 positive cells were isolated using a $CD4^+$ T cell isolation kit (No. 130-090-860, Miltenyi Biotec, Bergisch Gladbach, Germany) and LS columns (Miltenyi) according to the manufacturers' instructions.

2.2.6.1.2 Isolation of Peritoneal Macrophages

Mice were sacrificed by CO_2 inhalation and longitudinal midline incision of the fur was performed. The peritoneum was flashed out twice with ice-cold 1% BSA in PBS and cells were harvested by 10 min centrifugation with 480 *g* (1,500 rpm). The pellet was resuspended in 5 ml 1% BSA in PBS and cells were counted in a Sysmex cell counter. After a washing step (7 min, 1,500 rpm) the cells were resuspended in Tyrode's buffer to obtain the desired concentration for the experiments.

2.2.6.2 Flow Cytometric Analysis of Macrophages

For determination of FcγR expression levels, peritoneal macrophages ($1*10^5$) were stained for 15 min at RT with saturating amounts of fluorophore-conjugated antibodies against FcγR (see 2.1.2.1) and F4/80-PE as gating antibody. The macrophages were analyzed directly after addition of 500 µl PBS.

The following settings were used:

Detectors/Amps:

Parameter	Detector	Voltage
P1	FSC	E01
P2	SSC	282
P3	FL1	650
P3	FL2	580
P5	FL3	150
P6	FL3-A	-
P7	FL4	508

2.2.6.3 Immune Thrombocytopenia

Initial platelet counts were assessed as described above for each mouse (see 2.2.4.1). These values were considered 100% and subsequent counts were normalized to these values. Mice were intravenously injected with the indicated amounts (4, 7 or 11 µg per mouse) of anti-GPIIb/IIIa antibodies (JON1 and JON3) to induce FcγR-mediated thrombocytopenia. After injection, platelet counts were assessed every 24 h.

Fc-independent thrombocytopenia was induced by intraperitoneal injection of 100 µg p0p/B.

2.2.6.4 Anaphylaxis Experiments

2.2.6.4.1 IgG-Mediated Anaphylaxis

FcγR-mediated hypothermia was induced by intraperitoneal injection of 100 µg anti-GPIIb/IIIa antibodies (JON1 or JON3). Body temperature was measured with a rectal probe directly before the injection and every 30 min for 3 h.

2.2.6.4.2 IgE-Mediated Anaphylaxis

For the FcεR-mediated anaphylactic response mice were primed by intravenous injection of 30 µg anti-*dinitrophenol* (DNP) IgE per mouse 24 h before the experiment. After measuring the initial body temperature anaphylaxis was induced by i.v. injection of 250 µg DNP

conjugated to human serum albumin (HSA). Body temperature was measured with a rectal probe directly before the injection and every 10 min for 1.5 h. For the histamine ELISA blood was taken from the retro-orbital plexus 20 min after the injection of DNP-HAS and plasma was analyzed by ELISA according to the manufacturers' instructions.

2.2.7 Statistical Analysis

Results are shown as mean ± SD from at least three individual experiments per group. When applicable Fisher's exact test was used for statistical analysis. Otherwise, the Welch's *t* test was performed for statistical analysis. *P*-values <0.05 were considered statistically significant.

3 Results

3.1 Glycoprotein V Limits Thrombus Formation

GPV has been reported to be a collagen receptor [66], but its importance relative to GPVI and the collagen-binding integrin α2β1 is considered to be rather small [3]. One aim of this study was to clarify the importance of GPV in collagen signaling and to reveal potential functional redundancies between GPV and α2β1. Therefore, *Gp5*$^{-/-}$ mice [25] were intercrossed with mice lacking the α-subunit of the integrin α2β1 (*Itga2*$^{-/-}$ mice) [76] to obtain double-deficient mice (termed DKO in all figures). These mice were compared with the two single-deficient mouse lines and wildtype controls. An additional aim of this study was to clarify the controversial role of GPV in thrombosis [65-67]. This part of the study was conducted together with Ina Hagedorn, who performed the arterial thrombosis models.

3.1.1 GPV Reduces Thrombin-Responsiveness and Contributes to Aggregation Responses upon Collagen-Stimulation

To rule out any general defects in platelet formation due to the combined deficiency of GPV and α2β1, platelet count and platelet lifespan as well as abundance of major platelet glycoproteins were determined. Deletion of the *Gp5* gene resulted in slightly increased platelet size, independent of the expression of *Itga2*, without affecting the platelet count or platelet lifespan (Table 3-1 and data not shown). Platelet lifespan was assessed using a fluorescently labeled anti-GPIX derivative which was intravenously injected into mice and the percentage of fluorescently labeled platelets was determined over time (not shown). Targeting of *Gp5* or *Itga2* resulted in complete absence of the respective proteins on the platelet surface, but also some other glycoproteins were affected (Table 3-1). Most notably, β1 integrin expression was reduced in mice lacking the α2-subunit even though α5-expression was upregulated in these animals. The reduced β1-levels were less pronounced in double-deficient mice, since β1-levels were slightly higher in *Gp5*$^{-/-}$ mice. All knockout mice displayed increased expression of CLEC-2 and CD9 and in mice lacking GPV (independent of the presence of α2) anti-GPIX signals were slightly but significantly higher. This indicated that the expression of GPV somehow influences the expression of CLEC-2 and CD9 via undefined mechanisms. The increased GPIX-signals could also be a result of higher accessibility of GPIX for the anti-GPIX antibodies in the absence of GPV.

To assess platelet function, the cells were stimulated with different agonists and integrin activation (using JON/A-PE, an antibody which preferably binds the activated conformation of

αIIbβ3 [167]) as well as exposure of P-selectin, which is expressed in α-granules and serves as a marker for degranulation, were measured by flow cytometry (Figure 3-1). *Itga2*$^{-/-}$ platelets displayed overall unaltered agonist-induced integrin activation and P-selectin exposure (Figure 3-1) upon activation with all tested agonists at all concentrations. Independent of the expression of *Itga2*, the absence of GPV resulted in slightly increased responses towards low and intermediate thrombin concentrations, as revealed by increased integrin activation and P-selectin exposure (Figure 3-1) thereby confirming earlier studies [63].

	WT	***Itga2*$^{-/-}$**	***Gp5*$^{-/-}$**	**DKO**
Count [10^5/µl]	1003 ± 296	1084 ± 221	924 ± 244	927 ± 232
Size [fl]	5.6 ± 0.2	5.7 ± 0.2	6.0 ± 0.2 ***	6.1 ± 0.2 ***
α-GPIb [MFI]	414 ± 39	428 ± 81	396 ± 28	404 ± 32
α-GPV [MFI]	376 ± 24	378 ± 28	9 ± 9 ***	7 ± 7 ***
α-GPIX [MFI]	502 ± 56	521 ± 28	533 ± 29 *	535 ± 33 *
α-GPVI [MFI]	56 ± 9	54 ± 6	54 ± 7	60 ± 7
α-β3 [MFI]	82 ± 15	77 ± 18	83 ± 16	87 ± 12
α-αIIbβ3 [MFI]	685 ± 71	600 ± 160	667 ± 187	711 ± 84
α-β1 [MFI]	169 ± 20	128 ± 20 ***	186 ± 16 **	152 ± 16 **
α-α2 [MFI]	96 ± 22	8 ± 5 ***	105 ± 27	9 ± 6 ***
α-α5 [MFI]	37 ± 3	50 ± 3 ***	38 ± 3	56 ± 2 ***
α-CLEC-2 [MFI]	186 ± 16	204 ± 21 *	209 ± 9 ***	218 ± 29 **
α-CD9 [MFI]	1459 ± 69	1410 ± 67 *	1557 ± 95 ***	1529 ± 74 **

Table 3-1: Platelet count, size and platelet surface receptor expression in wildtype, *Itga2*$^{-/-}$, *Gp5*$^{-/-}$, and double-deficient mice. Mean platelet size and platelet counts were determined using a Sysmex cell counter. Surface expression of prominent platelet glycoproteins was determined by flow cytometry. Diluted whole blood from the indicated mice was incubated with FITC-labeled antibodies at saturating conditions for 15 min at *room temperature* (RT) and platelets were analyzed directly in a FACSCalibur. Results are expressed as mean values ± SD for at least 8 mice per group. MFI, *mean fluorescence intensity*. * P<0.05; ** P<0.01; *** P<0.001 as compared to wildtype (WT) values.

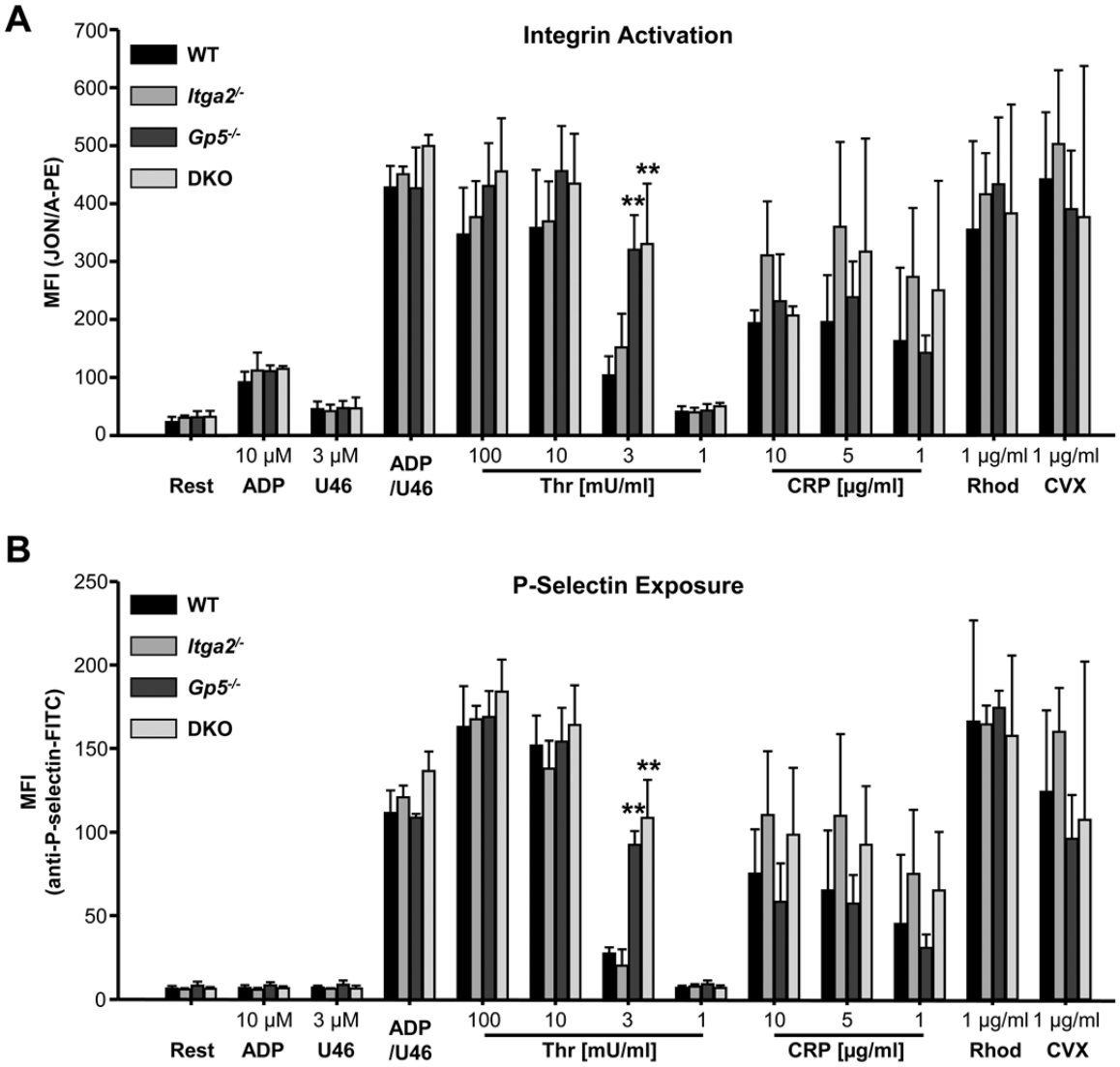

Figure 3-1: Increased thrombin responsiveness of *Gp5*$^{-/-}$ platelets. Washed blood was incubated for 15 min with the indicated agonists in the presence of JON/A-PE (A) or FITC-conjugated antibody against mouse P-selectin (B). The cells were gated *by forward and sideward scatter characteristics* (FSC and SSC). Data shown are mean fluorescence intensities (MFI) ± SD (n=4 mice per group; the data are representative of three independent experiments). * P<0.05; ** P<0.01; *** P<0.001 as compared to wildtype (WT) values.

Next, it was investigated whether the absence of both receptors causes additional defects in platelet aggregation. *Gp5*$^{-/-}$ platelets displayed unaltered aggregation responses to all tested agonists, except for threshold concentrations of thrombin at which they showed higher activation responses (Figure 3-2 and not shown). This coincides with the results obtained by flow cytometry. *Itga2*$^{-/-}$ platelets consistently responded delayed upon stimulation with all tested concentrations of collagen, even though maximal aggregation was similar to wildtype (WT) platelets. This delayed response was most pronounced at low collagen concentrations and was significantly increased in DKOs lacking GPV and α2 (Figure 3-2). For all other

agonists tested no differences could be observed between the aggregation responses between WT and *Itga2*$^{-/-}$ platelets (Figure 3-2 and not shown).

These results demonstrate that GPV is dispensable for collagen-triggered platelet aggregation as long as $\alpha 2\beta 1$ is present. The concomitant absence of both receptors, however, results in dramatically delayed shape change and platelet aggregation. This indicated that GPV and $\alpha 2\beta 1$ have overlapping functions in collagen-triggered platelet aggregation and confirmed the proposed role of GPV in collagen signaling [66].

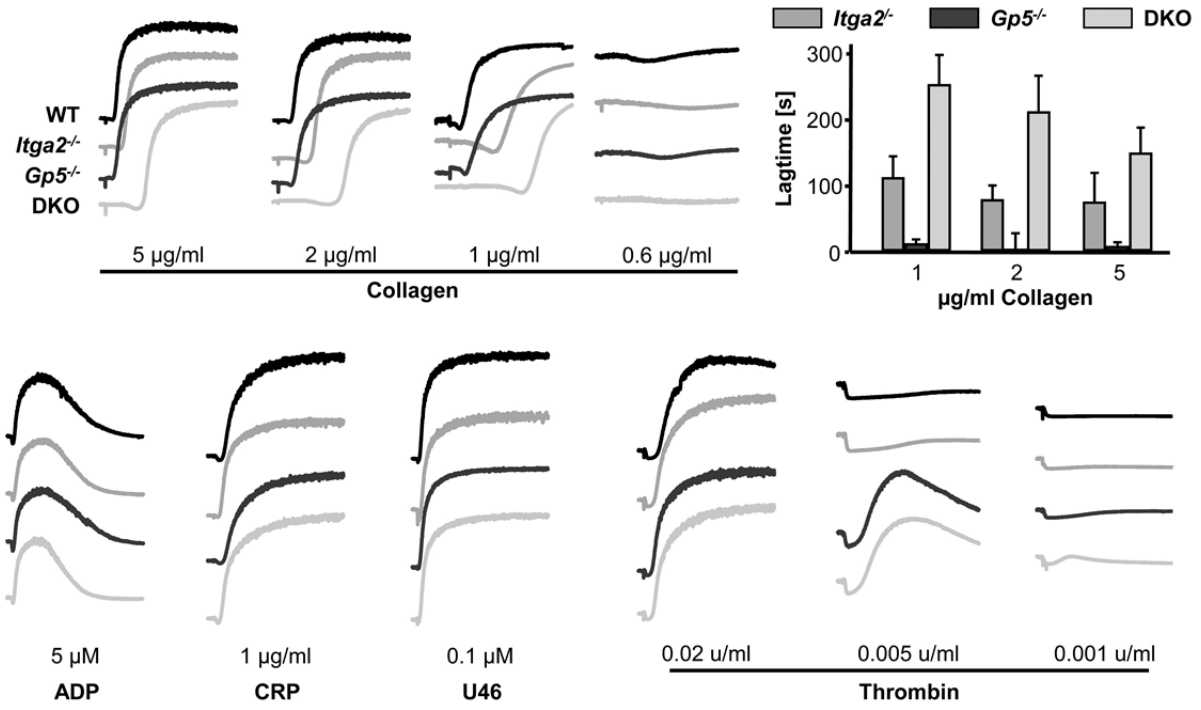

Figure 3-2: GPV-deficiency increases the lag time observed in platelets lacking the α-subunit of α2β1 integrin upon stimulation with collagen. Washed platelets (in case of ADP stimulation, platelet-rich plasma was used) were activated with the indicated agonists. Light transmission was recorded on an Apact four-channel aggregometer over 10 min and was calculated as arbitrary units with 100% transmission adjusted with buffer. The results shown are representative of at least four individual experiments. The bar graphs depict the lag time (time from addition of collagen to maximal aggregation) after subtraction of WT values as mean ± SD.

3.1.2 GPV is Dispensable for Adhesion and Aggregation on Collagen or vWF Under Flow

In vivo, platelet activation on exposed collagen occurs in flowing blood. Therefore, flow adhesion experiments were performed to test the effect of GPV and $\alpha 2\beta 1$ double-deficiency under more physiological conditions. Anticoagulated blood was rinsed at different shear rates over a collagen coated surface (200 µg/ml coating) and platelet surface coverage was determined at the end of each perfusion experiment. At all shear rates tested only very few *Itga2*$^{-/-}$ platelets adhered and formed only small aggregates (Figure 3-3; for 1000 s^{-1}: surface coverage of 48.48 ± 4.79% with WT vs. 12.22 ± 8.02% with *Itga2*$^{-/-}$ blood; $P<0.001$). In contrast to the aggregation studies no additional defects could be observed in double-deficient platelets, lacking GPV and $\alpha 2\beta 1$. Aggregates formed by *Gp5*$^{-/-}$ single-deficient platelets were indistinguishable from WT platelets in flow adhesion experiments on collagen (Figure 3-3; for 1000 s^{-1}: surface coverage of 47.09 ± 9.85% with *Gp5*$^{-/-}$ vs. 11.68 ± 10.86% with DKO blood; $P<0.001$ compared to WT, $P>0.05$ as compared to *Itga2*$^{-/-}$ blood). This indicated that GPV is dispensable for platelet-collagen interactions under flow conditions.

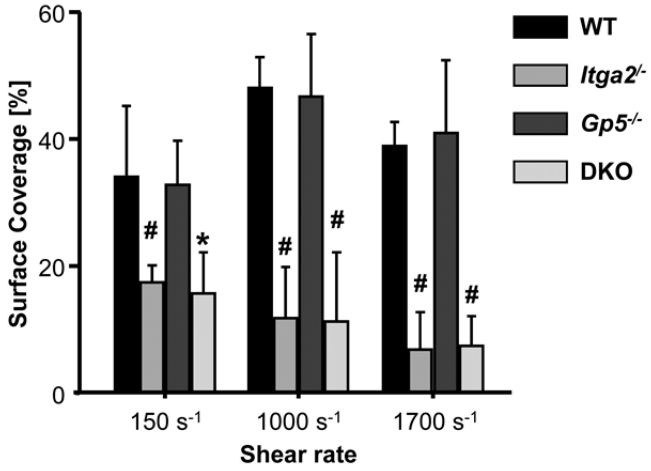

Figure 3-3: Impaired adhesion and defective aggregate formation of *Itga2*$^{-/-}$ platelets on collagen. Whole blood was perfused over a collagen-coated (0.2 mg/ml) surface at the indicated shear rates and then washed with Tyrode's buffer for a period equal to half of the perfusion time. Perfusion times were 10 min (150 s^{-1}) or 4 min (1000 and 1700 s^{-1}). The bar graphs display the mean surface coverage ± SD (n≥4 mice each). * $P<0.01$; # $P<0.001$ as compared to WT values.

To investigate whether GPV-deficiency influences the interaction between vWF and GPIb, blood was perfused over murine von Willebrand factor with a wall shear rate of 1700 s^{-1}. Consistent with previous reports [25, 66] the number of firmly adhered platelets on vWF was independent of GPV expression (data not shown). This suggested that the GPIb-vWF interaction is not affected by the absence of GPV.

3.1.3 GPV Decelerates Thrombus Formation Independent of the Expression of Other Collagen Receptors

So far the role of GPV in thrombosis has been controversial: Some studies reported increased thrombus formation [64, 65], albeit with increased embolization [65], while others observed decreased thrombus formation in mice lacking GPV [66]. Here, the aim was to clarify the role of GPV in arterial thrombus formation, since this receptor is generally considered to be of minor relevance *in vivo* (see 1.2.2), despite the functional redundancy between GPV and $\alpha 2\beta 1$ observed *in vitro* (see Figure 3-2). Therefore, platelet accumulation at sites of *ferric chloride* ($FeCl_3$)-induced mesenteric arteriole injury was determined using intravital fluorescence microscopy (Figure 3-4). Remarkably, the beginning of thrombus formation started earlier in mice lacking GPV (7.4 ± 1.6 min in WT and 5.6 ± 0.8 min in *Gp5*$^{-/-}$ mice, $P<0.001$) and this was independent of the expression of $\alpha 2$ (8.2 ± 2.7 min in *Itga2*$^{-/-}$, n.s. as compared to WT and 5.3 ± 0.8 min in double-deficient mice, $P<0.001$ compared to WT and $P<0.01$ compared to *Itga2*$^{-/-}$ mice). Consequently, the time to occlusion was also significantly reduced in mice lacking GPV (17.7 ± 3.0 min in WT and 11.1 ± 2.4 min in *Gp5*$^{-/-}$ mice, $P<0.001$). Again this was independent of the presence of $\alpha 2$ (18.5 ± 3.8 min in *Itga2*$^{-/-}$, n.s. compared to WT and 10.4 ± 2.6 min in DKO, $P<0.001$ compared to WT or *Itga2*$^{-/-}$ mice) (Figure 3-4). These surprising results indicated that GPV counter-regulates thrombus formation.

Our flow adhesion experiments had not revealed any effect of GPV-deficiency *ex vivo* (Figure 3-3) and were somewhat contradictory to the observed phenotype of *Gp5*$^{-/-}$ mice *in vivo* (Figure 3-4). Since GPV is a platelet-specific receptor, the accelerated thrombus formation in *Gp5*$^{-/-}$ mice has to be a platelet-based effect. Blood coagulation is crucial for thrombus formation and activated platelets promote coagulation by exposing PS on their surface [9, 10]. Therefore, a possible role for GPV in the procoagulant activity of platelets was investigated. Whole blood from WT and *Gp5*$^{-/-}$ mice was anticoagulated with heparin, thereby maintaining physiological Ca^{2+} and Mg^{2+} concentrations and perfused over collagen at shear rates of 1000 or 1700 s^{-1}. After each run Alexa488-annexin A5, which specifically binds to PS exposed by procoagulant platelets, was rinsed over the adhered platelets. Surface coverage and the percentage of annexin A5 positive platelets, which contribute to coagulation, was determined. However, no differences were revealed between WT and *Gp5*$^{-/-}$ platelets (Figure 3-5), a finding which was reported by others recently [174]. Thus, it can be concluded that GPV is dispensable for platelet procoagulant activity.

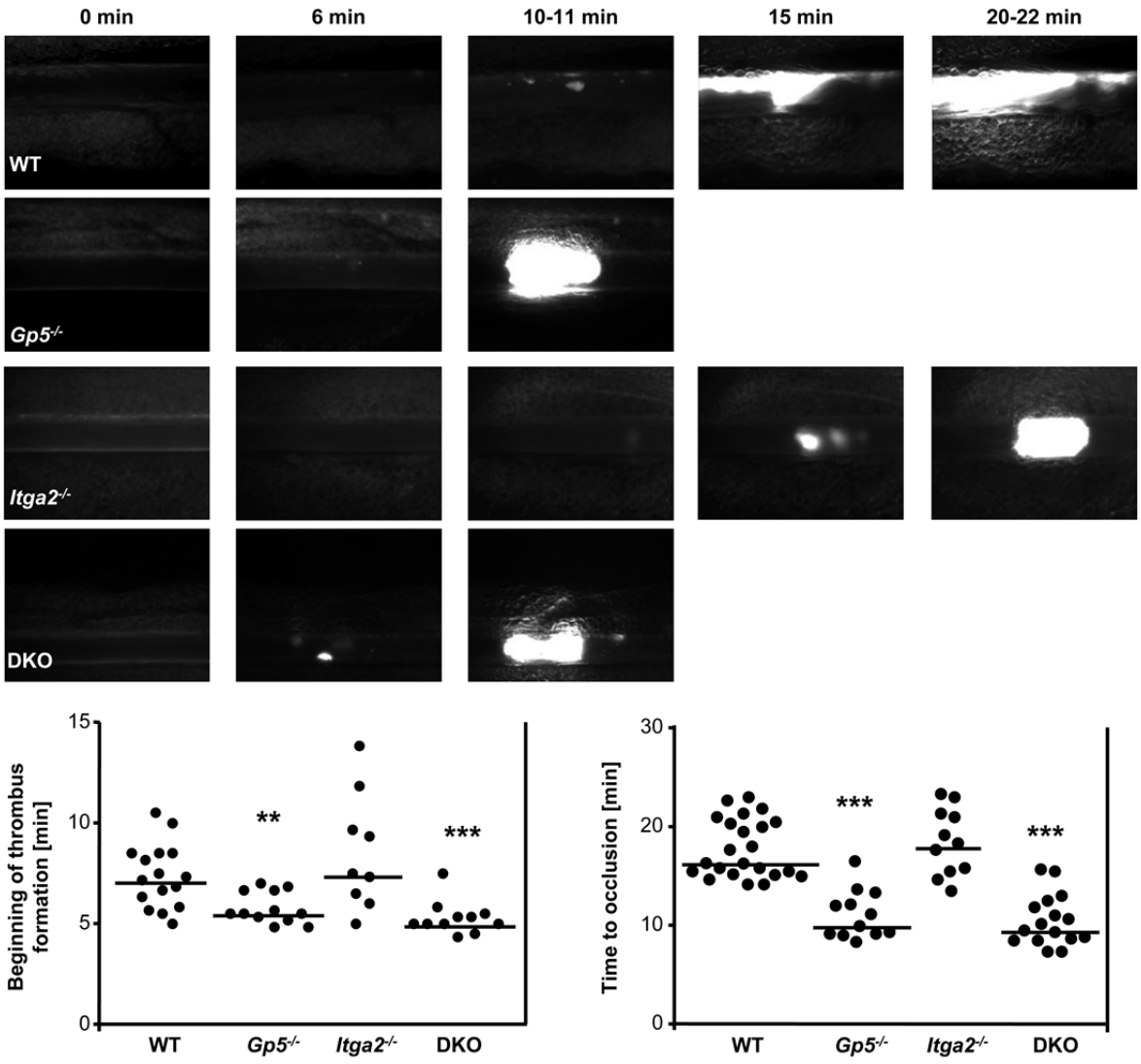

Figure 3-4: Accelerated thrombus formation in *Gp5*$^{-/-}$ mice independent of the expression of α2β1. Mesenteric arterioles were injured with 20% $FeCl_3$ and adhesion and thrombus formation of fluorescently-labeled platelets was monitored by intravital microscopy. Each dot represents one vessel, horizontal lines indicate the median. * P<0.05; ** P<0.01; *** P<0.001 as compared to WT values.

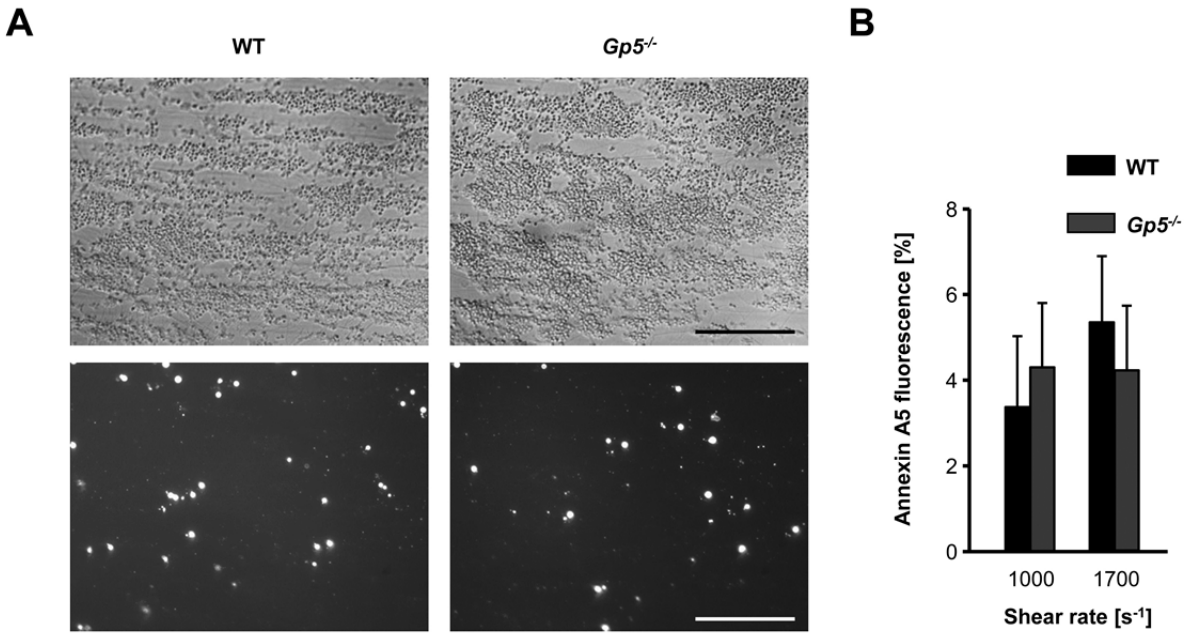

Figure 3-5: GPV-deficiency does not alter platelet procoagulant activity. Whole blood was perfused over a collagen-coated (0.2 mg/ml) surface at a shear rate of 1000 or 1700 s^{-1} for 4 min. Adherent platelets were stained with Alexa488–annexin A5 (0.25 mg/ml). A) Representative phase contrast (top) and fluorescence images (bottom) of the experiments performed at a shear rate of 1000 s^{-1}. Scale bar 100 µm. B) Mean relative amount of annexin A5 positive platelets ± SD (n≥5 mice) for the indicated shear rates. *P*>0.05 for both tested flow rates.

In contrast to the aggregation studies (Figure 3-2), no effect of α2-deficiency on thrombus formation could be observed in *Gp5*$^{-/-}$ mice (Figure 3-4). To reveal potential functional redundancies of the different collagen receptors *in vivo*, the effect of GPVI-deficiency was assessed in the different mouse lines. Therefore, the anti-GPVI antibody JAQ1 was injected into mice, since it results in complete absence of the GPVI receptor from the platelet surface for several days [81]. However, this antibody causes also a mild transient thrombocytopenia, with platelet levels returning to normal levels within 3 days. Thus, *Gp5*$^{-/-}$, *Itga2*$^{-/-}$ and DKO mice were subjected to the chemical injury model on day 5 after injection of 100 µg JAQ1 *i.p.*. At this time point platelet counts were normal and platelets still lacked GPVI. The efficiency of the JAQ1 treatment was confirmed by flow cytometry prior to each experiment. Lack of the principal platelet activating collagen GPVI led to slightly delayed thrombus formation (7.8 ± 0.8 min in untreated and 9.7 ± 2.8 min in JAQ1-treated mice, *P*<0.05) and only 7 out of 15 vessels occluded within the observation period (Figure 3-6; with time to occlusion of the remaining vessels of 27.8 ± 8.3 min compared to 17.4 ± 3.9 min in untreated WT mice, *P*<0.05). This was in line with previous studies [55].

Remarkably, even if GPVI was absent, GPV-deficiency still caused a slightly earlier beginning of thrombus formation (6.6 ± 1.7 min in JAQ1-treated *Gp5*$^{-/-}$ mice, *P*>0.05 compared to untreated WT mice and *P*<0.05 as compared to JAQ1-treated WT mice). This

resulted in faster vessel occlusion in *Gp5*$^{-/-}$ mice (12.0 ± 2.9 min in JAQ1-treated *Gp5*$^{-/-}$ mice, *P*<0.001 compared to JAQ1-treated WT mice) even if compared with untreated WT mice (*P*<0.01, Figure 3-6). Again, these findings were independent of the presence of $\alpha 2\beta 1$ (beginning of thrombus formation: 7.9 ± 1.1 min in JAQ1-treated *Itga2*$^{-/-}$ and 5.1 ± 08 min in JAQ1-treated DKO mice, *P*<0.001; 6 out of 21 vessels remained open in *Itga2*$^{-/-}$ mice, while all vessels occluded within 20 min in DKOs; Figure 3-6). These results indicated that GPV-deficiency can compensate for the absence of GPVI in arterial thrombus formation.

To test whether this finding can be reproduced *ex vivo,* GPVI-depleted blood of WT and *Gp5*$^{-/-}$ mice was rinsed over collagen in a blood perfusion chamber. However, platelet adhesion on fibrillar collagen was almost completely abolished after GPVI-depletion, independent of the expression of GPV (not shown).

The relevance of collagen-GPVI signaling in the ferric chloride model of arterial thrombosis has recently been questioned [175]. In contrast, GPVI-signaling is considered to be the predominant trigger of thrombus formation after mechanical injury of the abdominal aorta [176]. Therefore, the effect of GPV- and GPVI-deficiency was assessed in this model, were blood flow after vascular injury is monitored by an ultrasonic flow probe (Figure 3-7). Within 10 min after the aortic injury no blood flow was detectable in WT and *Gp5*$^{-/-}$ mice (n=8 mice per group). Depletion of GPVI protected WT mice (7 out of 8 vessels remained open), but astonishingly not *Gp5*$^{-/-}$ mice (all 7 tested mice displayed firm thrombi within 10 min), indicating that GPV-deficiency fully compensates for the lack of GPVI in this collagen-driven model of arterial thrombosis (Figure 3-7).

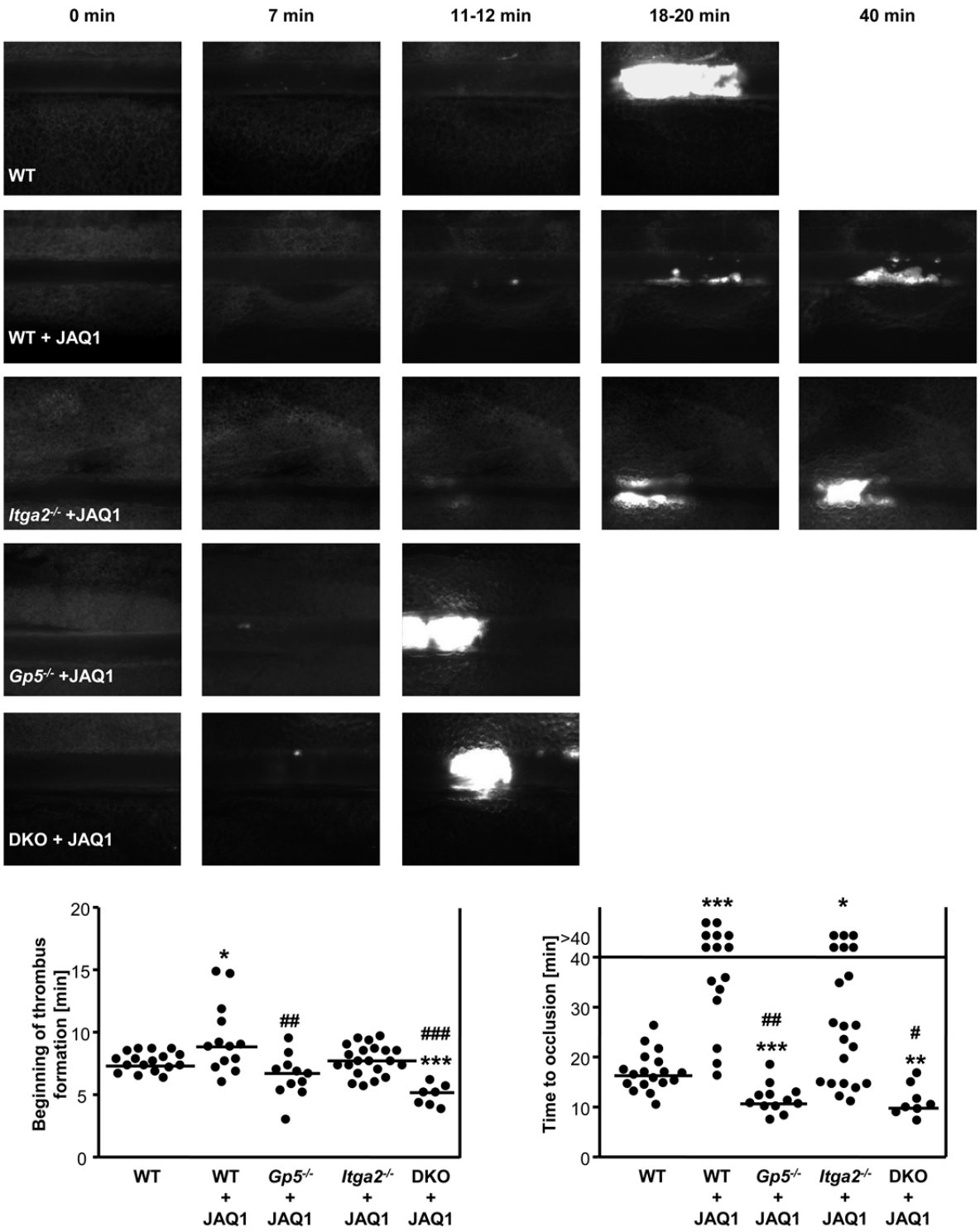

Figure 3-6: Accelerated thrombus formation in *Gp5*$^{-/-}$ mice despite the lack of GPVI. Mesenteric arterioles were injured with 20% $FeCl_3$ and adhesion and thrombus formation of fluorescently-labeled platelets was monitored by intravital microscopy. Each dot represents one vessel, horizontal lines indicate the median. * P<0.05; ** P<0.01; *** P<0.001 as compared to untreated WT mice. $^{\#}$ P<0.05; $^{\#\#}$ P<0.01; $^{\#\#\#}$ P<0.001 as compared to JAQ1-treated WT mice.

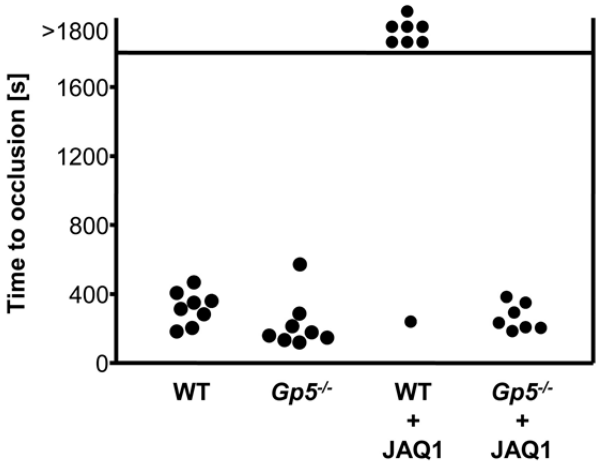

Figure 3-7: GPV-deficiency compensates for the lack of GPVI in an aortic injury model. The abdominal aorta was mechanically injured by a single firm compression with forceps and blood flow was monitored with a Doppler flowmeter. Time to final occlusion is shown. Each symbol represents one individual mouse.

The fact that GPV-deficiency counterbalanced the absence of GPVI raised the possibility that GPV serves as a general negative regulator of platelet activation. Therefore, we investigated whether the lack of GPV could compensate for the absence of further activating receptors. We had shown that CLEC-2 is required for stable thrombus formation and signals via a hemITAM motif and utilizes the same signaling cascade as GPVI. Hence, CLEC-2 was chosen as next receptor to test a potential compensatory effect of GPV-deficiency. The injection of the monoclonal anti-CLEC-2 antibody, INU1, leads to a transient depletion of the receptor, similar to GPVI after JAQ1-treatment [166]. Consequently, WT and *Gp5*$^{-/-}$ mice received 100 µg INU1 *i.p.* 5-6 days prior to the chemical injury. Platelet count and CLEC-2 expression were tested by flow cytometry before the *in vivo* experiments. In line with previous results, lack of CLEC-2 did not affect beginning of thrombus formation in WT mice (8.1 ± 1.2 min vs. 8.9 ± 2.6 min in INU1-treated WT mice; $P>0.05$). However, measurement of the time to occlusion revealed that 9 out of 20 vessels remained open ($P<0.01$) and the time to occlusion was delayed in the vessels which formed stable thrombi (16.1 ± 3.3 min vs. 24.9 ± 5.4 min in INU1-treated WT mice; $P<0.001$; Figure 3-8). Thrombus formation started earlier in INU1-treated *Gp5*$^{-/-}$ mice (7.0 ± 1.8 min, $P<0.05$ compared to INU1-treated or untreated WT mice), but nevertheless 11 out of 18 vessels remained open ($P<0.001$ compared to untreated, but not significant compared to INU1-treated WT mice, Figure 3-8). However, the analysis of the subpopulation of mice, which formed stable thrombi revealed an effect of GPV-deficiency. In these cases, the time to occlusion in INU1-treated *Gp5*$^{-/-}$ mice was comparable to untreated WT mice (16.5 ± 3.7 min, $P>0.05$ compared to untreated and $P<0.01$ compared to INU1-treated WT mice). These results indicate that the impaired thrombus formation upon CLEC-2 depletion is only slightly affected by GPV.

The interaction between GPIb and vWF is crucial for the formation of stable thrombi [2, 33, 55]. To test whether GPV modulates this aspect, the GPIb-vWF interaction was blocked with p0p/B Fab fragments, which bind to the vWF binding site on GPIb and prevent GPIb-vWF

interactions [55]. 100 µg Fab fragments were injected *i.v.* in WT and *Gp5*$^{-/-}$ mice prior to the chemical injury and thrombus formation was monitored using intravital microscopy (Figure 3-8). P0p/B-treated mice were unable to form occlusive thrombi, since a small channel remained open. This resembled the phenotype of *vWF*$^{-/-}$ mice [177], which was independent of the presence of GPV on the platelet surface (Figure 3-8). However, one notable difference between p0p/B-treated *Gp5*$^{-/-}$ and WT mice was the accelerated beginning of thrombus formation in p0p/B-treated *Gp5*$^{-/-}$ mice (10.6 ± 2.1 min in p0p/B-treated WT and 7.6 ± 1.6 min in p0p/B-treated *Gp5*$^{-/-}$ mice, $P<0.05$) which was similar to untreated WT mice (8.7 ± 1.5 min, $P>0.05$) (Figure 3-8). Likewise, no difference could be observed upon mechanical injury of the aorta in p0p/B-treated mice, since all vessels remained open in WT and *Gp5*$^{-/-}$ mice (n=7 mice per group; not shown).

Thrombin is the most potent soluble platelet agonist and of particular interest in the context of GPV-deficiency, since *Gp5*$^{-/-}$ platelets are hyper-reactive towards low doses of this agonist. To investigate whether lack of GPV has any effect in the absence of active thrombin, thrombin was completely inhibited by injecting 5 mg/kg of the direct thrombin inhibitor Lepirudin *i.v.* prior to the topical injury of the mesenterial arterioles. This treatment dramatically delayed thrombus formation and completely prevented the formation of occlusive thrombi independent of GPV expression (data not shown).

However, the lack of an observable effect of GPV-deficiency after ablation of the entire thrombin-signaling pathway did not exclude a role for GPV in thrombin-triggered thrombus formation. Therefore, a more subtle approach was chosen to test whether the increased responsiveness of *Gp5*$^{-/-}$ platelets towards thrombin *in vitro* is the main trigger of the observed *in vivo* phenotypes. Mice deficient in FXII have a defect in the contact activation (or intrinsic) coagulation pathway and as a consequence the mice should have less thrombin at sites of vascular injury. Therefore *Gp5*$^{-/-}$ mice were crossed with *F12*$^{-/-}$ mice [168] to obtain double-deficient mice. These mice were then subjected to $FeCl_3$-injury of the mesenteric arterioles and compared with the respective single-deficient mice (Figure 3-9). Absence of FXII dramatically delayed beginning of thrombus formation independent of GPV expression (WT mice: 8.0 ± 1.2 min; *F12*$^{-/-}$ mice 18.4 ± 9.3 min, $P<0.05$; *Gp5*$^{-/-}$/*F12*$^{-/-}$ mice 15.5 ± 6.2 min, $P<0.05$, compared to *F12*$^{-/-}$ mice: $P>0.05$). In line with previous results [178, 179] thrombus formation was abolished in mice lacking FXII, again no effect of GPV-deficiency could be observed (Figure 3-9).

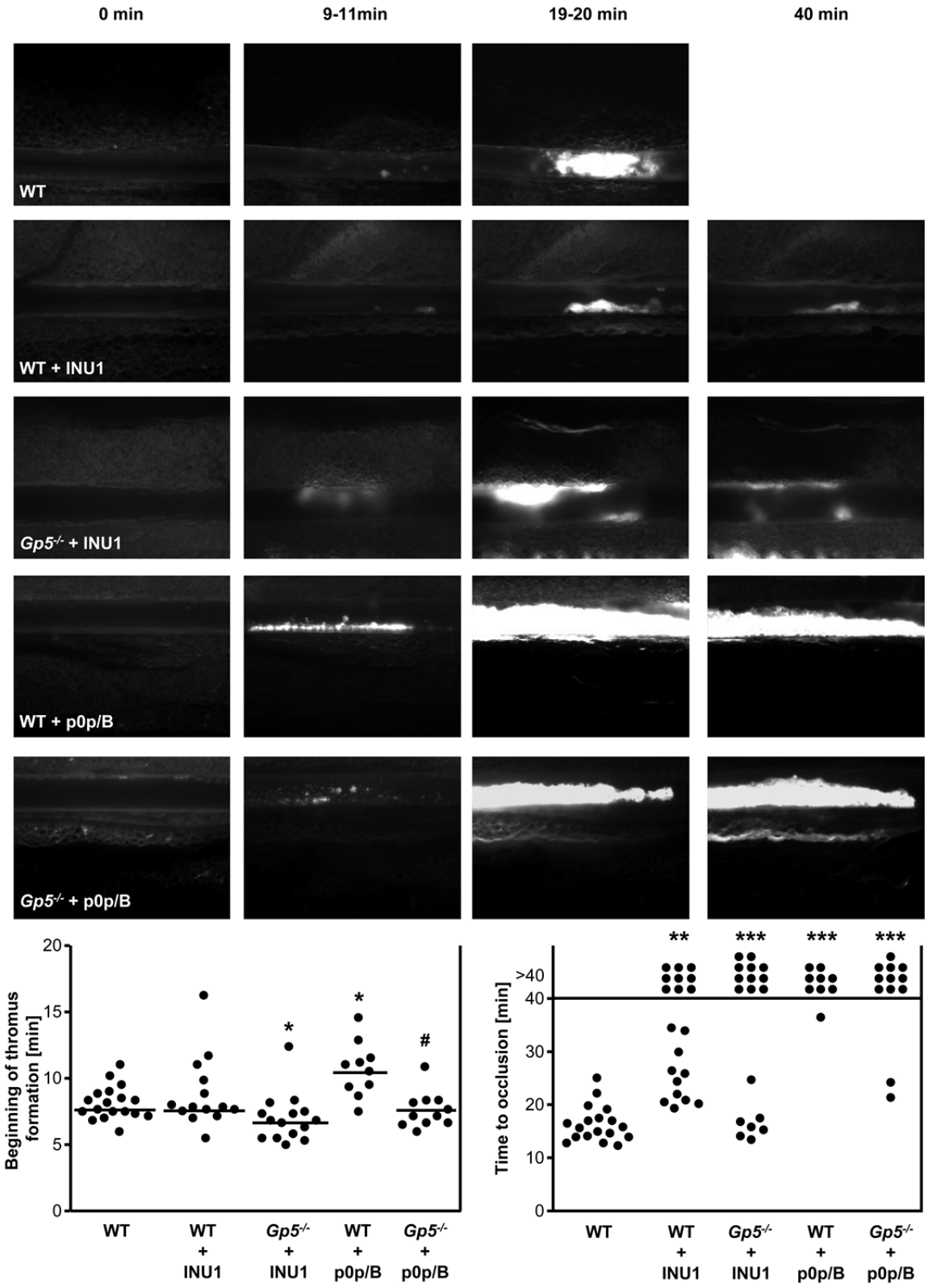

Figure 3-8: GPV-deficiency cannot compensate for the lack of CLEC-2 or functional GPIb. Mesenteric arterioles were injured with 20% $FeCl_3$ and adhesion and thrombus formation of fluorescently-labeled platelets was monitored by intravital microscopy. Each dot represents one vessel, horizontal lines indicate the median. * P<0.05; ** P<0.01; *** P<0.001 as compared to untreated WT values. # P<0.05 as compared to p0p/B-treated WT mice.

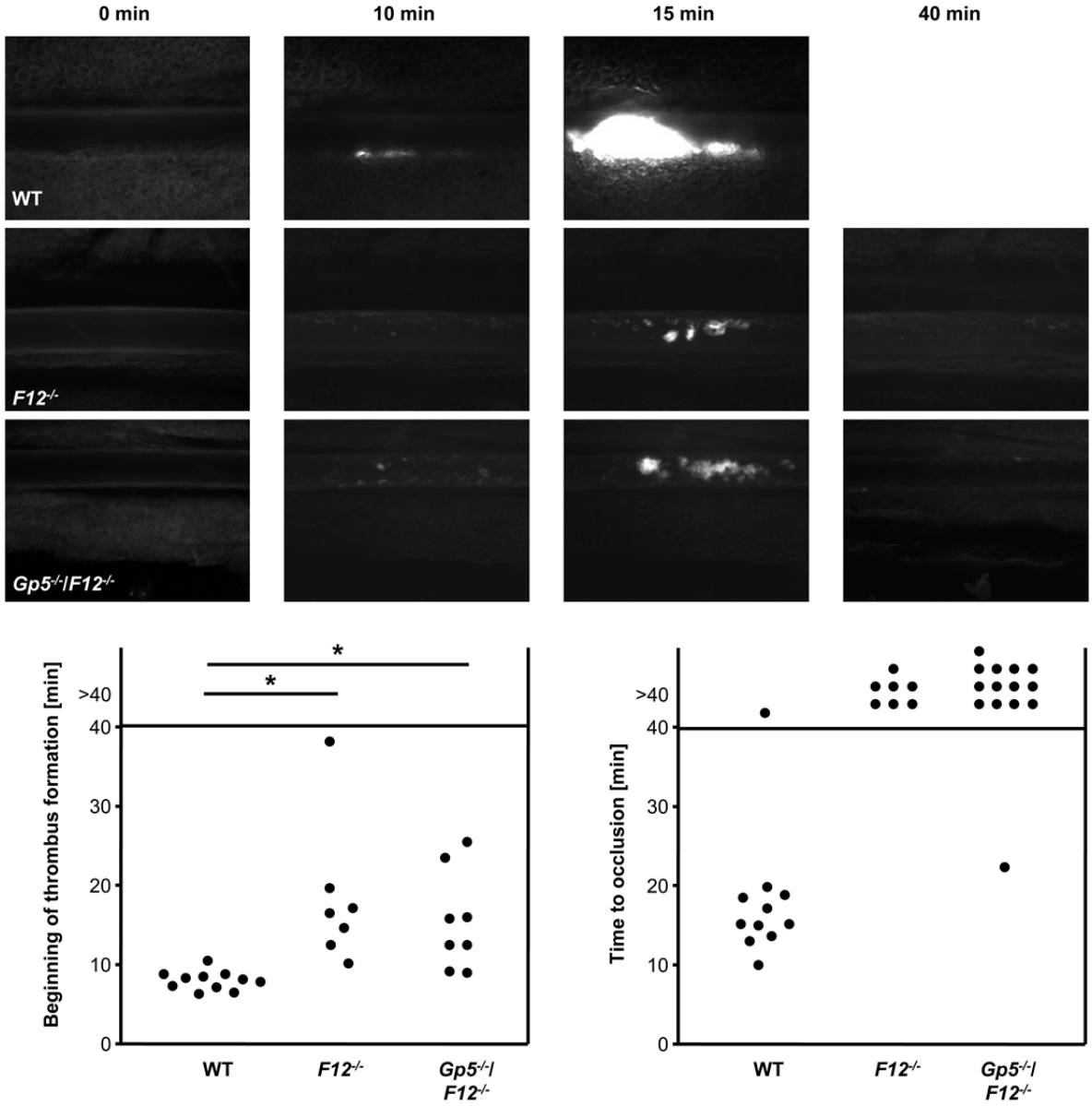

Figure 3-9: GPV-deficiency does not compensate for the lack of FXII. Mesenteric arterioles were injured with 20% $FeCl_3$ and adhesion and thrombus formation of fluorescently-labeled platelets was monitored by intravital microscopy. Each dot represents one vessel.* *P*<0.05.

In summary, the data of the arterial thrombosis models indicated that GPV lessens thrombus formation. Further, it was revealed that GPV-deficiency fully compensates for the lack of GPVI and/or $\alpha 2\beta 1$ in thrombus formation. However, lack of GPV did not counterbalance the lack of CLEC-2, thrombin signaling, GPIb-vWF interactions or FXII.

3.1.4 GPV is Required for JAQ1-Mediated Protection from Ischemic Stroke

Ischemic stroke is the third leading cause of death and disability in industrialized countries [180]. Infarct development during experimental ischemic stroke is largely dependent on GPIb- and GPVI-mediated platelet adhesion and activation [56]. The fact that GPV limits thrombus formation and that i is required for the protective effect of GPVI-deficiency in arterial thrombosis prompted us to investigate the role of GPV in a model of focal cerebral ischemia in collaboration with Prof. Dr. Guido Stoll (Department of Neurology, University of Würzburg). To initiate cerebral ischemia, a thread was advanced through the carotid artery into the middle cerebral artery to reduce the regional cerebral flow by >90%. After 30 or 60 min the thread was removed to allow reperfusion [56]. *2,3,5-triphenyltetrazolium chloride* (TTC) staining, which differentiates between metabolically active and inactive tissues, was used to determine infarct volumes 24 hours after reperfusion (Figure 3-10A, D). Infarct volumes were indistinguishable between WT (for 60 min tMCAO: 78.7 ± 32.8 mm^3) and *Gp5*$^{-/-}$ mice (87.0 ± 25.3 mm^3, P>0.05) independent of the occlusion time tested (Figure 3-10A). Consequently, no differences could be observed in the Bederson score assessing global neurological damage or the grip test, which specifically measures motor function and coordination (Figure 3-10B-C). For the case that the phenotype of GPV-deficiency is hidden in otherwise “normal” mice, a potential role of GPV in ischemic stroke was tested in mice pre-treated with p0p/B (not shown), to block GPIb-vWF interaction, or JAQ1 (Figure 3-10), to deplete GPVI. Both treatments have been shown to reduce the ischemic damage [56] and should consequently shift the threshold so that a potential effect of GPV-deficiency could be observable. In line with the results obtained in the thrombosis models, GPV-deficiency did not have an effect in p0p/B-treated mice (data not shown). Absence of GPVI decreased the infarct size of WT mice (42.2 ± 24.4 mm^3, P<0.05 compared with untreated WT mice), but not of *Gp5*$^{-/-}$ mice (88.7 ± 29.5 mm^3, P<0.01 compared with JAQ1-treated WT; P>0.05 compared with untreated WT; Figure 3-10A, D). The reduced infarct size was accompanied by an increase in the Bederson score (1.67 ± 1.32 in JAQ1-treated WT and 2.89 ± 0.93 in JAQ1-treated *Gp5*$^{-/-}$ mice, P<0.01) and a deterioration of the grip test (3.67 ± 0.87 in JAQ1-treated WT and 1.56 ± 1.51 in *Gp5*$^{-/-}$ mice, P<0.01) indicating that it was functionally relevant.

These data indicated that GPV does not affect the outcome after ischemic stroke *per se*, though is essential for the protective effect of GPVI-depletion.

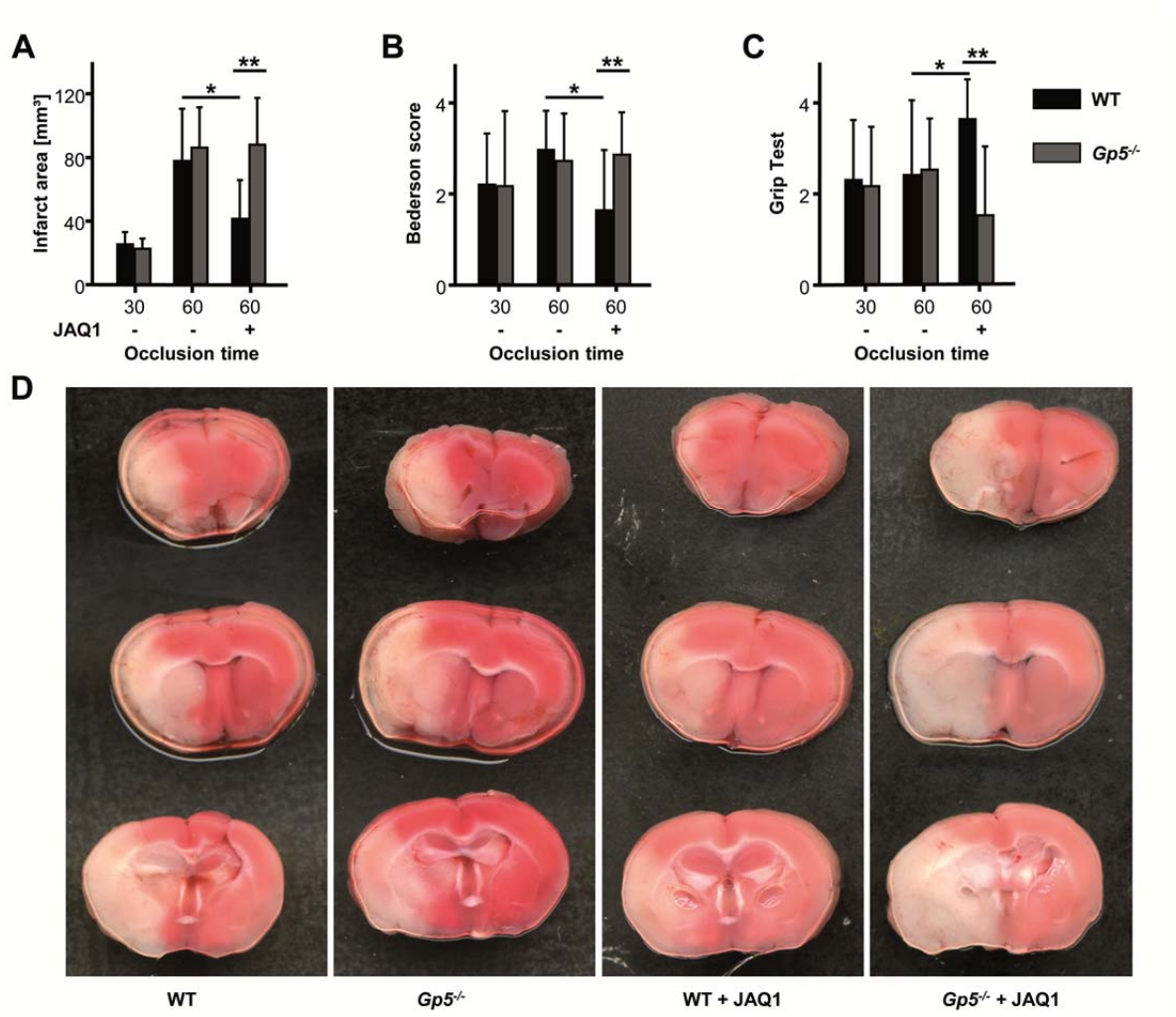

Figure 3-10: GPV-deficiency prevents the protective effect of GPVI-depletion in cerebral ischemia. A) Brain infarct volumes of the indicated mice after 30 min or 60 min occlusion. B & C) Neurological Bederson score (B) and grip test (C) assessed at day 1 after tMACO of the indicated mice. D) Representative images of three corresponding coronal sections from the indicated mice after 60 min occlusion stained with TTC 24 hours after tMCAO. Data are mean ± SD (n≥8 mice per group). * P<0.05, ** P<0.01, *** P<0.001.

3.1.5 GPV-Deficiency Compensates for the Hemostatic Defect Caused by the Absence of CLEC-2 and GPVI

After assessing the relevance of GPV in thrombotic processes it was tested whether GPV is equally important for hemostasis. Thus, 2 mm fragments from the tail tip of mice were cut and time until bleeding arrested was determined. The ability of mice to arrest bleeding at the site of a defined tail wound serves as an indicator of physiological blood clotting [181].

GPV-deficiency led to slightly decreased tail bleeding times (572 ± 132 s in WT and 454 ± 97 s in *Gp5*$^{-/-}$ mice, P<0.05; Figure 3-11), which indicates that GPV dampens hemostasis. This *Gp5*$^{-/-}$ phenotype was independent of the expression of $\alpha 2\beta 1$ (548 ± 97 s in

Itga2$^{-/-}$ mice, *P*>0.05 compared to WT and 402 ± 68 s in DKO, *P*<0.01 compared to WT and compared to *Itga2*$^{-/-}$ mice; Figure 3-11). A previous study demonstrated that the combined deficiency of $\alpha 2\beta 1$ and GPVI leads to severe hemostatic defects [86]. Therefore, the effect of additional GPV-deficiency was tested using JAQ1-treated mice (Figure 3-11). Lack of GPVI prolonged tail bleeding times in WT mice (742 ± 221 s, *P*<0.05 compared to untreated mice) and led to a severe bleeding phenotype in *Itga2*$^{-/-}$ mice (9 out of 15 mice did not stop bleeding within the 20 min observation period, *P*<0.01; none of the mice stopped bleeding after less than 900 s). In contrast, JAQ1 treatment did not alter the tail bleeding times of *Gp5*$^{-/-}$ mice significantly independent of α2β1 expression (480 ± 166 s for JAQ1-treated *Gp5*$^{-/-}$ mice, *P*<0.01 compared to JAQ1-treated WT and 500 ± 163 s for JAQ1-treated DKO mice, *P*<0.01; Figure 3-11).

This indicated that GPV-deficiency compensates for the lack of GPVI and $\alpha 2\beta 1$ in hemostasis, which resembled the observations from the arterial thrombosis models. The effect of GPV-deficiency on thrombus formation in a CLEC-2-deficient background was somewhat ambiguous (Figure 3-8). Therefore, it was tested whether GPV-deficiency could counterbalance the loss of CLEC-2 in hemostasis (Figure 3-11). Mice received 200 µg INU1 *i.p.* 5-6 days prior to the experiments. Absence of CLEC-2 increased the tail bleeding time of WT mice, thereby confirming previous results [166]. In contrast, tail bleeding times of *Gp5*$^{-/-}$ mice were not affected (589 ± 313 s for INU1-treated WT, 290 ± 184 s for INU1-treated *Gp5*$^{-/-}$ mice, *P*<0.01). These results showed that GPV-deficiency can compensate for the lack of CLEC-2 in hemostasis, indicating that the relevance of GPV might be higher in hemostasis than in thrombosis.

The surprising effect of GPV-deficiency on tail bleeding times of CLEC-2-depleted mice raised the question whether lack of GPV could make up for the combined absence of GPVI and CLEC-2. Combined treatment with JAQ1 and INU1 depleted both ITAM receptors as confirmed by flow cytometry (not shown). Concomitant absence of GPVI and CLEC-2 dramatically increased tail bleeding times in WT mice (only half of the mice were able to arrest bleeding, tail bleeding time of the other mice increased to 950 ± 141 s, *P*<0.001 compared to untreated controls; Figure 3-11). In *Gp5*$^{-/-}$ mice the loss of both ITAM receptors did not alter tail bleeding times significantly (440 ± 155 s, *P*>0.05 as compared to controls, but *P*<0.001 compared with double-depleted WT mice; Figure 3-11). These data establish GPV as important mediator in hemostasis, since lack of GPV can fully compensate for the combined absence of the two platelet activating ITAM receptors, GPVI and CLEC-2.

To assess a potential effect of GPV-deficiency on hemostasis of mice lacking functional GPIb, the GPIb-vWF interaction was blocked in WT and *Gp5*$^{-/-}$ mice using p0p/B Fab fragments and tail bleeding times were determined. Blockade of GPIb caused a hemostatic

defect in WT (*P*<0.001 compared with untreated mice), since only three out of ten mice were able to arrest bleeding within the observation period (Figure 3-11). Similar results were obtained with *Gp5*$^{-/-}$ (3 out of 9 mice were able to arrest bleeding; Figure 3-11), indicating that the lack of GPV cannot counterbalance non-functional GPIb.

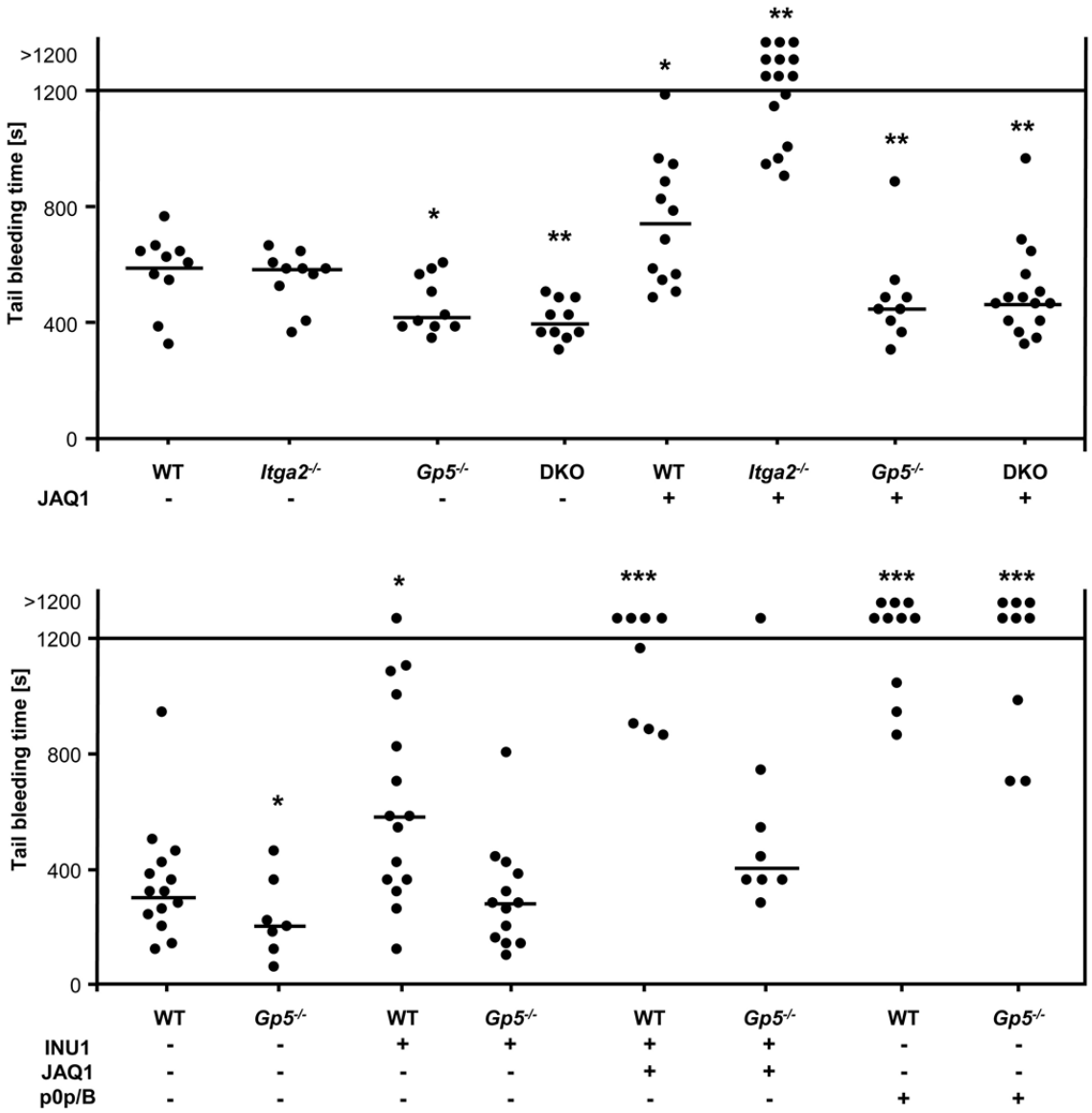

Figure 3-11: GPV-deficiency can compensate for the loss of ITAM-receptors in hemostasis. Displayed are tail bleeding times of the indicated mouse lines. Each symbol represents one animal, horizontal lines indicate the median (not depicted if the median would have been above 1200 s). * *P*<0.05; ** *P*<0.01; *** *P*<0.001, compared to untreated WT mice in the corresponding panel. In cases were mice were unable to arrest bleeding Fisher's exact test was used to calculate *P*-values.

Collectively, these data demonstrated that GPV-deficiency can compensate for the isolated or combined lack of $\alpha 2\beta 1$, GPVI and CLEC-2. Isolated lack of GPV resulted in decreased tail bleeding times, while absence of GPV did not prevent the hemostatic effect caused by impaired GPIb-vWF interactions.

3.2 Phospholipase D1 is an Essential Mediator of GPIb-Dependent Integrin Activation

Platelets express the two phospholipase D isoforms PLD1 and PLD2, but their role in platelet signaling is virtually unknown. To investigate the potential role of PLD1 in platelet physiology *Pld1*$^{-/-}$ mice, which had been generated in our laboratory by Dr. Attila Braun, see construct in Figure 3-12A, were analyzed together with Dr. Margitta Elvers.

Intercrossing of *Pld1*$^{+/-}$ mice yielded *Pld1*$^{-/-}$ mice, as confirmed by Southern Blotting (Figure 3-12B), in the expected Mendelian ratio. PLD1-deficient mice showed normal growth, were fertile and appeared healthy (data not shown), indicating that PLD1 is not required for mouse development. The absence of PLD1 in *Pld1*$^{-/-}$ mice was confirmed by RT-PCR and Western Blotting, which also demonstrated that the expression of PLD2 was not altered (Figure 3-12C, D). This argued against a compensatory up-regulation of the second PLD isoform.

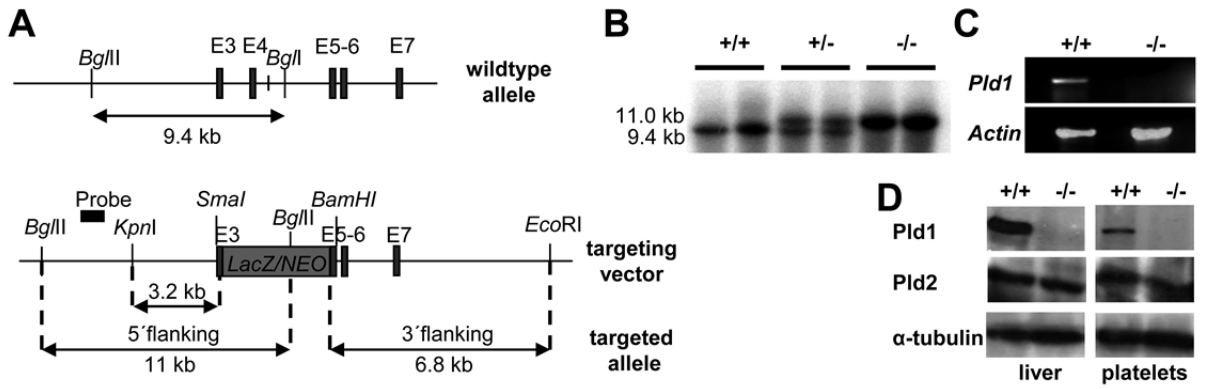

Figure 3-12: Generation of *Pld1*$^{-/-}$ mice. A) Targeting strategy: Exons 3 to 5 were targeted for heterologous recombination. Neo-LacZ: neomycin resistance and *LacZ* cDNA. B) Southern Blot of *Bgl*II-digested genomic DNA of wildtype (+/+), heterozygous (+/-), or homozygous (-/-) mice labeled with the external probe indicated in A. C) RT-PCR of platelet cDNA from wildtype (+/+) and *Pld1*$^{-/-}$ (-/-) platelets. D) Protein lysates of the indicated organs immunoblotted using anti-PLD1, PLD2 antibodies. Tubulin was used as loading control.

3.2.1 Lack of PLD1 Abolishes the Inducible PLD Activity in Platelets

To study consequences of PLD1-deficiency on the hematopoietic system, blood cell counts were determined in *Pld1*$^{-/-}$ mice. Blood cell counts were not altered but the mean platelet volume of PLD1-deficient platelets was slightly increased. Associated with this was a small increase in surface expression of most platelet surface receptors, including GPV, CD9 and β1 and β3 integrins (Table 3-2).

To test the possibility that the lack of PLD1 affects platelet turnover, the *in vivo* life span of the cells was determined as described previously (see 3.1.1). The lifespan of *Pld1*$^{-/-}$ platelets

was slightly decreased compared to WT platelets (Figure 3-13A). This could indicate a defect in platelet formation. Low platelet counts result in increased platelet production, thus defects in platelet production should become more obvious under thrombocytopenic conditions. Anti-GPIb antibodies trigger platelet agglutination *in vitro* and cause thrombocytopenia *in vivo* via an ill-defined Fc-independent mechanism [146, 182]. Therefore, 2.5 µg/mouse of an anti-GPIbα antibody were injected intravenously and platelet counts were monitored the following days. Independent of the expression of PLD1, platelet counts decreased to about 30% of normal levels and recovered within 3 days (data not shown). These findings indicated that megakaryopoiesis and platelet formation is not dramatically affected in PLD1-deficient mice.

	WT	***Pld1*$^{-/-}$**		**WT**	***Pld1*$^{-/-}$**
PLT [10^5/µl]	849 ± 257	889 ± 322	**α-GPIX [MFI]**	521 ± 16	542 ± 22
MPV [fl]	5.1 ± 0.3	5.6 ± 0.2	**α-GPVI [MFI]**	40 ± 4	49 ± 8
RBC [10^6/µl]	9.53 ± 1.53	9.14 ± 1.88	**α-αIIbβ3 [MFI]**	658 ± 24	691 ± 25
WBC [10^6/µl]	7.98 ± 2.76	6.93 ± 1.99	**α-β1 [MFI]**	144 ± 3	176 ± 2
HCT [%]	48.9 ± 7.5	45.8 ± 9.3	**α-α2 [MFI]**	99 ± 5	105 ± 2
α-GPIb [MFI]	367 ± 7	373 ± 30	**α-CD9 [MFI]**	1491 ± 109	1710 ± 54
α-GPV [MFI]	335 ± 7	358 ± 9			

Table 3-2: Blood cell counts and surface expression of platelet glycoproteins in *Pld1*$^{-/-}$ mice. Mean blood cell counts, platelet size and hematocrit levels were determined using a Sysmex cell counter. Surface expression of prominent platelet glycoproteins was determined by flow cytometry. Diluted whole blood from the indicated mice was incubated with FITC-labeled antibodies at saturating conditions for 15 min at RT and platelets were analyzed directly in a FACSCalibur. Results are expressed as mean values ± SD for at least 9 mice per group. PLT*, platelet count*; MPV, *mean platelet volume*; RBC, *red blood cell count*; WBC, *white blood cell count*; MFI, *mean fluorescence intensity*.

To confirm that the absence of PLD1 is accompanied by an altered PLD activity, PLD activity was measured in platelets from WT and *Pld1*$^{-/-}$ mice. Platelets were stimulated with thrombin and *collagen-related peptide* (CRP) as representative agonists for GPCR (thrombin) and ITAM-signaling (CRP). PLD activity was assessed using a nonradioactive enzymatically coupled assay that measures choline (one of the two products of PLD activity) release. While the basal PLD activity was unaltered, the inducible PLD activity was abolished in *Pld1*$^{-/-}$ platelets (Figure 3-13B), supporting the current concept that PLD1 is the main regulatory PLD isoform [90].

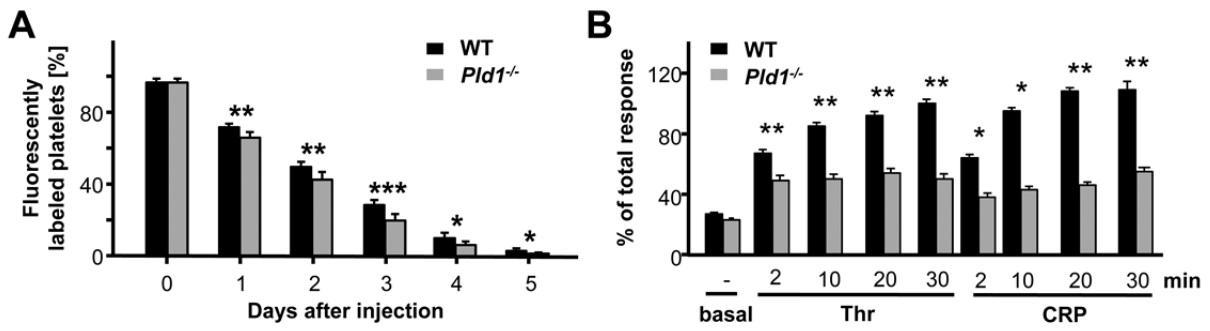

Figure 3-13: Lack of PLD1 abolishes inducible PLD activity in platelets. A) *Pld1*$^{-/-}$ platelets have a slightly reduced life span. Mice were injected intravenously with a Dylight-488 conjugated anti GPIX Ig derivative and the population of fluorescently labeled platelets was monitored over 5 days using flow cytometry. B) PLD activity of wildtype and *Pld1*$^{-/-}$ platelets was measured using a non-radioactive, choline-detecting assay under resting conditions (basal) or upon stimulation with *thrombin* (Thr) or CRP. PLD activity of wildtype platelets upon thrombin stimulation was set as 100%. * *P*<0.05; ** *P*<0.01; *** *P*<0.001.

3.2.2 PLD1-Deficiency Does not Affect Degranulation but Impairs Integrin Activation

To assess whether the lack of the inducible PLD activity had any functional consequences on platelet activation, flow cytometry analyses were performed. Platelets were stimulated with different agonists inducing ITAM- or GPCR signaling and integrin activation (using the conformation-specific JON/A-PE antibody) as well as exposure of P-selectin were determined, as described above (see 3.1.1). P-selectin exposure of PLD1-deficient platelets was unaltered in response to all tested agonists (Figure 3-14A and data not shown). Lack of PLD1 resulted in slightly reduced integrin activation in response to low and intermediate concentrations of thrombin and CRP (Figure 3-14B). To investigate in more detail whether the decreased integrin activation in *Pld1*$^{-/-}$ platelets was physiologically relevant, the ability of αIIbβ3 to bind its main ligand fibrinogen was assessed by flow cytometry (Figure 3-14C). In these measurements, PAR4 activating peptide (abbreviated PAR-4 from now on) was used instead of thrombin, because thrombin cleaves fibrinogen, which would have confounded the measurements. These measurements confirmed the phenotype for low and intermediate concentrations of CRP and PAR-4 (Figure 3-14C). Pre-incubation with exogenous aqueous-soluble cell-permeable *phosphatidic acid* (PA), the bioactive cleavage product of PLD activity, "rescued" the phenotype of *Pld1*$^{-/-}$ platelets in integrin activation, while basal levels were unaltered (Figure 3-14D). This indicated that the enzymatic activity of PLD1 is responsible for proper integrin activation (and not a scaffolding role of the protein).

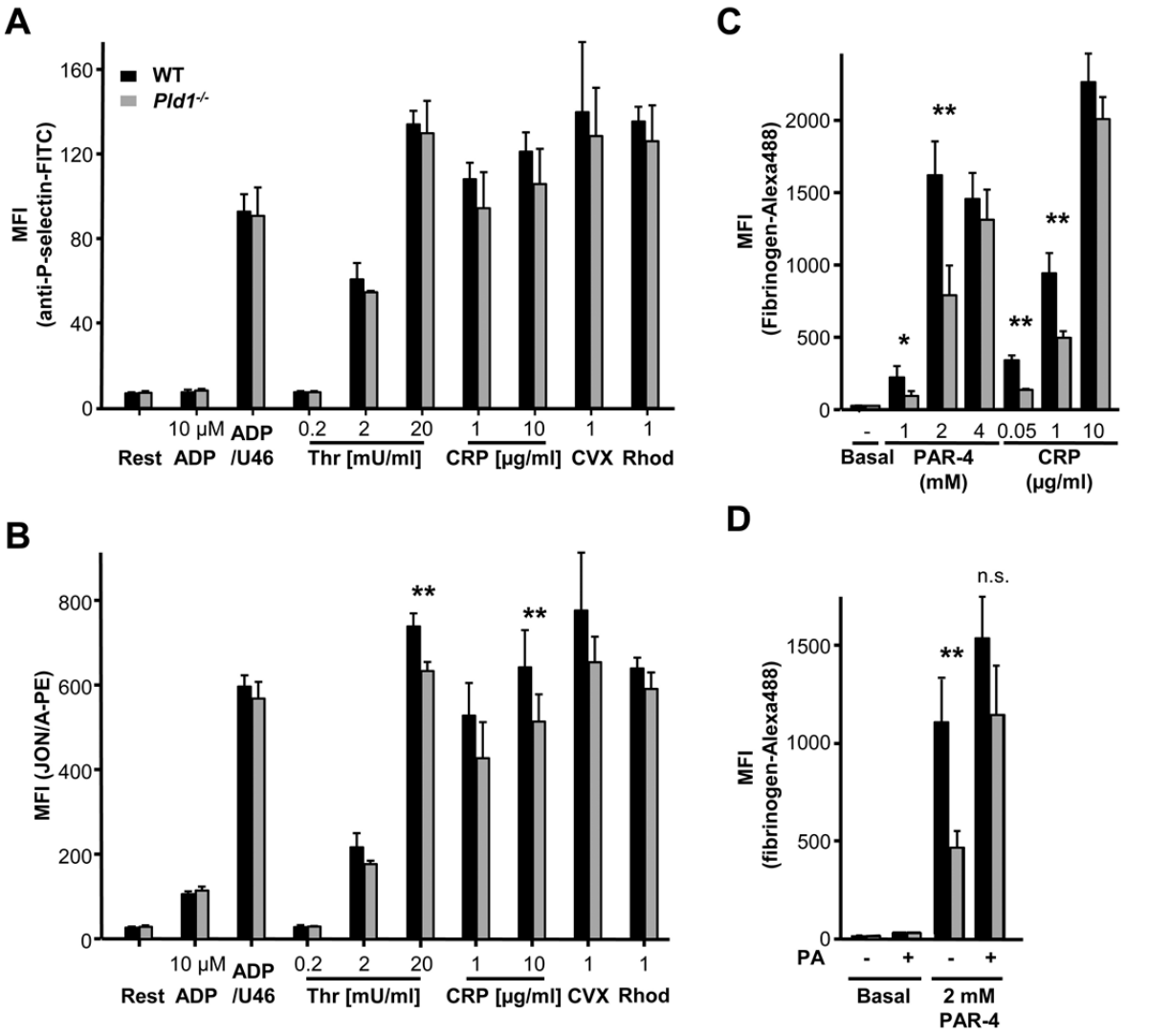

Figure 3-14: PLD1-deficiency leads to impaired αIIbβ3 integrin activation at threshold concentrations. Washed blood from wildtype and *Pld1*$^{-/-}$ mice was incubated for 15 min with the indicated agonists in the presence of FITC-conjugated antibody against P-selectin (A), JON/A-PE (B) or 50 mg/ml Alexa488-labeled fibrinogen (C & D). For the *phosphatidic acid* (PA) rescue experiment (D) platelets were incubated 5 min at 37°C with vehicle or 1 mM L-α-PA. Results shown as *mean fluorescence intensity* ± SD of one representative experiment (with n≥4 per group). * *P*<0.05; ** *P*<0.01; *** *P*<0.001. Rest, *resting*; ADP, *Adenosine-diphosphate*; U46, U46619 (thromboxane analog; 3 µM); Thr, *thrombin*; CRP, *collagen-related peptide*; CVX, *convulxin* (1 µg/ml); Rhod, *rhodocytin* (1 µg/ml); PAR-4, *Protease-activated receptor 4 activating peptide*; PA, *phosphatidic acid*; n.s., not significant.

According to the literature, it was expected that PLD1 should be involved in degranulation processes [reviewed in 97]. To investigate this, ATP release, which serves as a marker for dense granule secretion, was measured. Washed platelets of both genotypes were stimulated with thrombin or CRP for 2 min at 37°C under stirring conditions and subsequently fixed. ATP concentrations in the supernatant were measured with a bioluminescence assay kit. However, consistent with the results for P-selectin exposure (for α-granules), no difference in ATP release between WT and *Pld1*$^{-/-}$ platelets was evident (not shown).

To investigate whether the defect in inside-out integrin activation observed in flow cytometry results in impaired aggregation capacity of *Pld1*$^{-/-}$ platelets, the same agonists were tested at different concentrations. None of the tested conditions revealed any differences in aggregation responses between WT and PLD1-deficient platelets (Figure 3-15A and data not shown).

To test whether PLD1-deficiency impairs outside-in signaling of platelet integrins, WT and *Pld1*$^{-/-}$ platelets were allowed to spread on human fibrinogen upon thrombin co-stimulation (Figure 3-15B). Neither platelet adherence nor the kinetics of filopodia or lamellipodia formation were affected by the lack of PLD1. Another important process mediated by αIIbβ3 outside-in signaling is clot retraction. Thus, platelet rich plasma (PRP) of control and *Pld1*$^{-/-}$ mice was stimulated with 5 U/ml thrombin in the presence of 20 mM $CaCl_2$ to induce clotting. The subsequent retraction of the clot was monitored for 5 h. Consistent with the results of the spreading assay, clot retraction was indistinguishable between the two groups (not shown). This indicated that PLD1 is dispensable for outside-in signaling through the αIIbβ3 integrin.

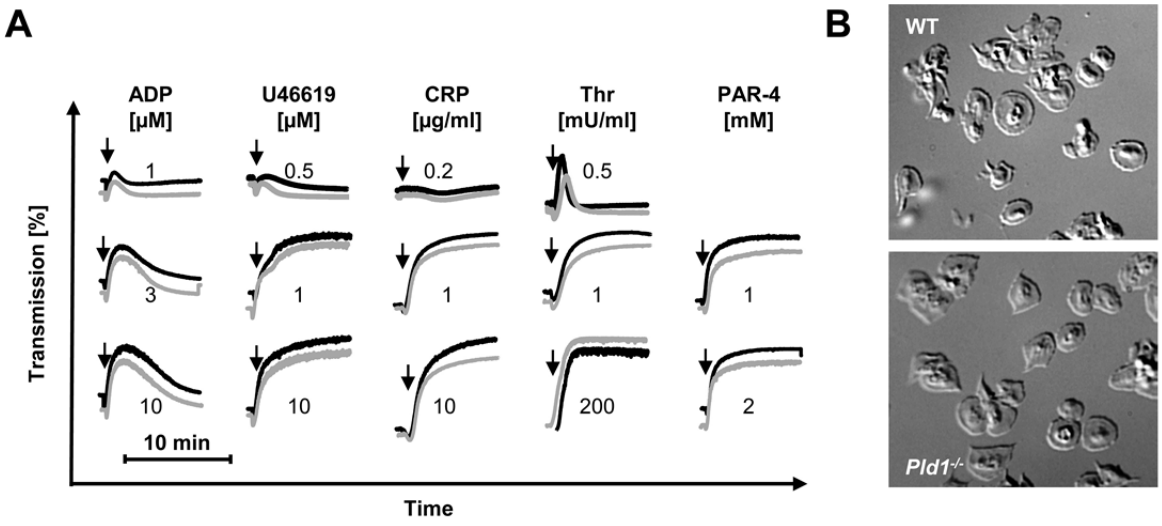

Figure 3-15: Neither aggregation nor spreading on fibrinogen is impaired in PLD1-deficient platelets. A) Washed platelets from wildtype (black line) and *Pld1*$^{-/-}$ (gray line) mice were activated with the indicated agonists. Light transmission was recorded on an Apact four-channel aggregometer over 10 min and was calculated as arbitrary units with 100% transmission adjusted with plasma. The results shown are representative of at least three individual experiments. The arrows indicate the time point of agonist addition. B) Washed platelets from wildtype or *Pld1*$^{-/-}$ mice were allowed to adhere and spread on immobilized human fibrinogen upon thrombin activation. *Differential interference contrast* (DIC) images were taken after 30 min, and are representative of 4 individual experiments.

3.2.3 *Pld1*$^{-/-}$ Platelets Fail to Firmly Adhere to vWF Under Flow

To test the functional consequences of the altered integrin activation under more physiological conditions, platelet adhesion and thrombus formation on a collagen-coated surface under flow were analyzed in a whole-blood perfusion system (described in 0). Under low and intermediate shear rates (150 and 1000 s^{-1}, respectively), which model flow conditions in venules or large arteries, respectively, no significant differences in adhesion or stable platelet aggregate formation were detected between WT and *Pld1*$^{-/-}$ blood (Figure 3-16). However, under high shear rates (1700 s^{-1}), which model flow conditions in arterioles [183], PLD1-deficiency reduced thrombus stability: Both, WT and *Pld1*$^{-/-}$ platelets, adhered to the collagen matrix and initiated the formation of aggregates, but in contrast to WT platelets, the platelet aggregates in *Pld1*$^{-/-}$ blood were often unstable and embolized. As a result, after rinsing the chamber virtually no aggregates were detectable; instead, the surface was covered primarily by a single layer of platelets (Figure 3-16A). These findings suggested that the formation and stabilization of platelet thrombi requires PLD1 under high shear conditions, but not under low or intermediate shear conditions. Since platelet adhesion under high shear conditions strictly depends on GPIb (see 1.2.1), these data indicated that the interaction between GPIb and collagen-bound vWF might be impaired in the absence of PLD1.

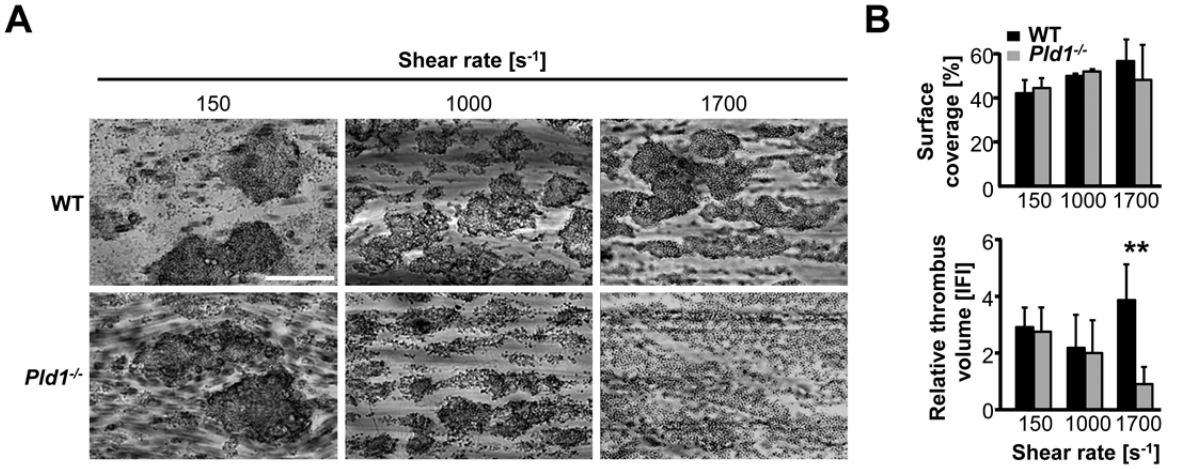

Figure 3-16: Defective aggregate formation of *Pld1*$^{-/-}$ platelets on collagen at high shear. Whole blood was perfused over a collagen-coated surface (0.2 mg/ml) at the indicated shear rates and then washed with Tyrode's buffer for a period equal to the perfusion time. Perfusion times were 10 min (150 s^{-1}) or 4 min (1000 and 1700 s^{-1}). A) Representative phase-contrast images at the end of the perfusion period. Scale bar, 100 µm. B) Mean surface coverage (upper panel) and relative platelet deposition as measured by integrated fluorescence intensity (IFI) per visual field (lower panel). All bar graphs depict mean values ± SD (n≥3 mice each). * P<0.05; ** P<0.01; *** P<0.001.

To directly investigate the potential role of PLD1 in GPIb-dependent platelet-vWF interactions, platelet adhesion to immobilized vWF under flow at high shear was tested. In this assay, thrombogenic collagens are absent, therefore, the induction of integrin αIIbβ3 activation and transition to stable adhesion strictly depends on signals generated by GPIb-

vWF interactions. To test a possible role for PLD1 in this process, WT and *Pld1*$^{-/-}$ blood was perfused over immobilized murine vWF at different shear rates. At all shear rates tested, most of the WT platelets that initially attached to the vWF matrix underwent stable adhesion (Figure 3-17). In contrast, although the initial tethering of *Pld1*$^{-/-}$ platelets was indistinguishable from WT platelets (Figure 3-17B), the transition to firm adhesion was impaired (Figure 3-17C), resulting in reduced numbers of adherent *Pld1*$^{-/-}$ platelets at the end of the experiment. This defect became more apparent at very high shear rates (3400 or 6800 s^{-1}), which model flow conditions in small arterioles and stenosed arteries [183], where the adhesion is entirely GPIb-dependent [2]. These data suggested that the absence of PLD1 affected GPIb-dependent αIIbβ3 integrin activation and stable binding to vWF under flow.

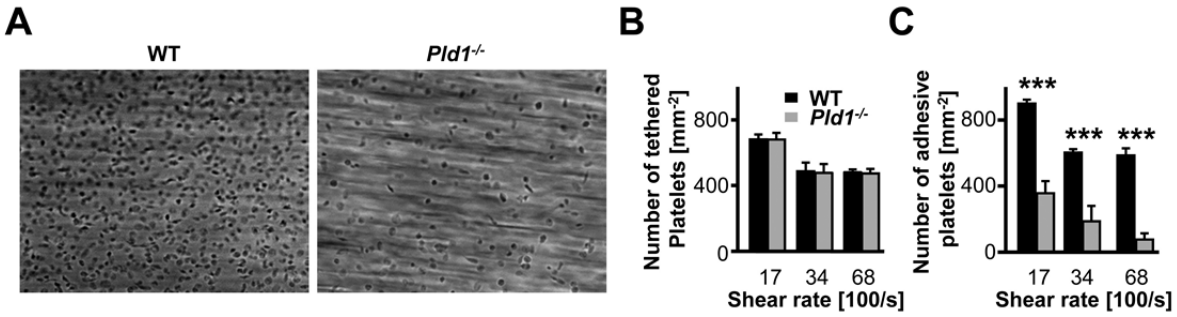

Figure 3-17: *Pld1*$^{-/-}$ platelets fail to firmly adhere to vWF under flow. Whole blood was perfused over immobilized murine vWF with the indicated shear rates and then washed with Tyrode's buffer for a period equal to the perfusion time. A) Representative pictures taken after the washing step, reflecting firmly adherent platelets. B & C) Adhered platelets on the vWF-coated surface were counted after 100 s of blood perfusion B) or at the end of the 4 min blood perfusion and washing step, reflecting firmly adhered platelets C). Bar graphs depict mean values ± SD (n≥3 mice each). * P<0.05; ** P<0.01; *** P<0.001.

3.2.4 Procoagulant Activity of *Pld1*$^{-/-}$ Platelets is Reduced

Activated αIIbβ3 integrin has been implicated in the coagulant activity of platelets [184, 185]. To determine a possible role for PLD1 in this process, anticoagulated whole blood from WT and *Pld1*$^{-/-}$ mice was perfused over fibrillar collagen at shear rates of 1000 or 1700 s^{-1}. At these shear rates GPIb-vWF interactions contribute to collagen-induced procoagulant activity [186]. During and after perfusion, fluorescence microscopic images were taken. In line with the previous experiments, surface coverage was unaltered. However, staining with FITC–annexin A5, which specifically binds to platelets exposing phosphatidylserine at their outer surface, was reduced in PLD1-deficient platelets (P<0.001; Figure 3-18). Phosphatidylserine-exposing platelets contribute to coagulation [186]. The reduced percentage of annexin A5-

positive platelets in *Pld1*$^{-/-}$ blood indicates that PLD1 contributes to platelet procoagulant activity.

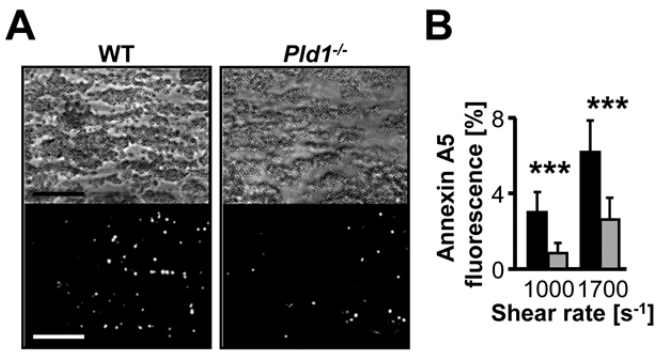

Figure 3-18: PLD1-deficiency reduces procoagulant activity of platelets. Whole blood was perfused over a collagen-coated (0.2 mg/ml) surface at shear rates of 1000 or 1700 s^{-1} for 4 min. Adherent platelets were stained with OG488–annexin A5 (0.25 mg/ml). A) Representative phase contrast (top) and fluorescence images (bottom) of the experiments performed at a shear rate of 1000 s^{-1}. Scale bar 100 µm. B) Mean relative amount of annexin A5 positive platelets ± SD (n≥3 mice) for the indicated shear rates. * P<0.05; ** P<0.01; *** P<0.001.

3.2.5 Reduced Thrombus Stability, but Normal Hemostasis in *Pld1*$^{-/-}$ Mice

To assess the function of PLD1 in platelet activation *in vivo*, the animals were challenged in a thromboembolism model. Mice were intravenously injected with a mixture of collagen (0.7 mg/kg body weight) and epinephrine (60 µg/kg body weight), two platelet-activating agents that in combination cause lethal pulmonary thromboembolism [187]. 40% of the wildtype mice survived the challenge, whereas 93% of the *Pld1*$^{-/-}$ mice survived (P<0.01; Figure 3-19A). In line with this, the number of obstructed vessels in the lungs was significantly decreased in the mutant animals (Figure 3-19A). These results demonstrate that PLD1-deficiency protects mice from thrombotic responses *in vivo*. However, at higher collagen doses all wildtype and mutant mice (n=8 mice per group) died within 5 min and had platelet counts below 5% of control, showing that intravascular aggregate formation in this model can occur independently of PLD1 at sufficiently high agonist doses (not shown).

To investigate the role of PLD1 in shear-dependent arterial thrombus formation *in vivo*, two arterial thrombosis models were used. In the first model, the right carotid artery was injured by topical application of ferric chloride (15%) and blood flow was subsequently monitored with an ultrasonic flow probe. Full occlusion occurred within 14 min in the vessels of all WT mice (n=8; mean time to occlusion, 539 ± 256 s) and persisted in 87.5% of all animals but one until the end of the 30 min observation period (data not shown). In contrast, occlusion was observed in only two of the seven PLD1-deficient mice (28.6%) and occlusion was transient in these two animals. Consequently, all *Pld1*$^{-/-}$ mice displayed normal blood flow through the injured carotid artery at the end of the observation period (P<0.001; not shown). In the second model, thrombosis was induced mechanically in the aorta and blood flow was

again monitored with an ultrasonic flow probe [127, 176]. After a transient increase directly after injury (minutes 0 to 1 in the examples shown; Figure 3-19C), blood flow progressively decreased for several minutes in all animals (minutes 5 to 10). In all of the wildtype mice examined, the decrease progressed to complete and irreversible occlusion of the vessel (mean occlusion time, 444 ± 174 s) (Figure 3-19B, D). In contrast, only 20% of the *Pld1*$^{-/-}$ mice occluded irreversibly within the observation period of 30 min (P<0.001) (Figure 3-19B, D). In 30% of *Pld1*$^{-/-}$ mice no occlusion occurred, whereas in 50% of the *Pld1*$^{-/-}$ mice, the vessels occluded for <1 min and then recanalized and remained open for the remainder of the observation period (Figure 3-19D, E). These results demonstrate that PLD1 is required for occlusive arterial thrombus formation *in vivo*.

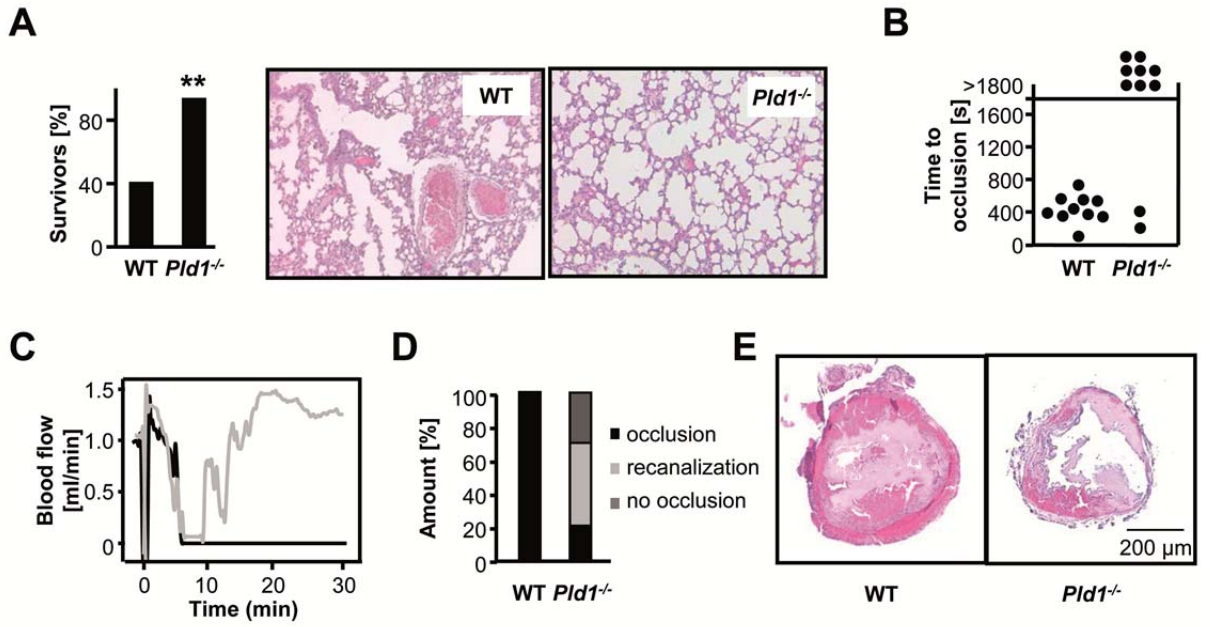

Figure 3-19: Reduced thrombus stability of *Pld1*$^{-/-}$ platelets *in vivo*. A) Lethal pulmonary embolization after injection of collagen and epinephrine in anesthetized wildtype and *Pld1*$^{-/-}$ mice. Survivor rate upon injection of 700 mg collagen and 60 mg epinephrine per kg bodyweight (left). Representative pictures of lung sections (right). Note the large number of obstructed vessels in the wildtype lung section. B-E) Mechanical injury of the abdominal aorta of wildtype and *Pld1*$^{-/-}$ mice was performed and blood flow was monitored with a Doppler flowmeter. The graph depicts time to final occlusion, each symbol represents one individual mouse (B). Representative time course of blood flow in wildtype (black line) or *Pld1*$^{-/-}$ (gray line) aortas (C). Overall outcome for aortic injury. Percent distribution of irreversible occlusion (black), instable occlusion (light gray) and no occlusion (dark gray) (D). Representative cross-sections of the aorta 30 min after injury (E). Scale bar, 200 µm. ** P<0.01.

The thrombus instability observed in *Pld1*$^{-/-}$mice prompted us to investigate the role of PLD1 in a model of focal cerebral ischemia in which infarct development is largely dependent on GPIb-vWF–mediated platelet adhesion and activation [56, 57]. In this model, development of neuronal damage is assessed after tMCAO. A thread was advanced through the carotid artery into the MCA, reducing regional cerebral flow by >90% and inducing cerebral ischemia. The thread was removed after 1 hour to allow reperfusion [56]. Infarct volumes

were assessed 24 hours after reperfusion by TTC staining to differentiate between metabolically active and inactive tissues. In *Pld1*$^{-/-}$ mice, infarct volumes were reduced by 80% in comparison to the infarct volumes of WT mice (WT, 89.9 ± 43.5 mm^3; *Pld1*$^{-/-}$, 18.03 ± 3.43 mm^3; *P*<0.001) (Figure 3-20A, B). Reduction of infarct size was functionally relevant because the Bederson score assessing global neurological damage (Figure 3-20C) was significantly reduced in mutant animals. Likewise, the grip test which specifically measures motor function and coordination, was significantly better in *Pld1*$^{-/-}$ mice compared to WT mice (Figure 3-20D). Serial magnetic resonance imaging of living mice confirmed the protective effect of PLD1-deficiency on infarct development (Figure 3-20E). Infarct volume did not increase between day 1 and day 5, suggesting a sustained protective effect of PLD1-deficiency. Furthermore, no intracranial hemorrhage was detected (Figure 3-20E), indicating that PLD1-deficiency is not associated with an increase in bleeding complications in the brain.

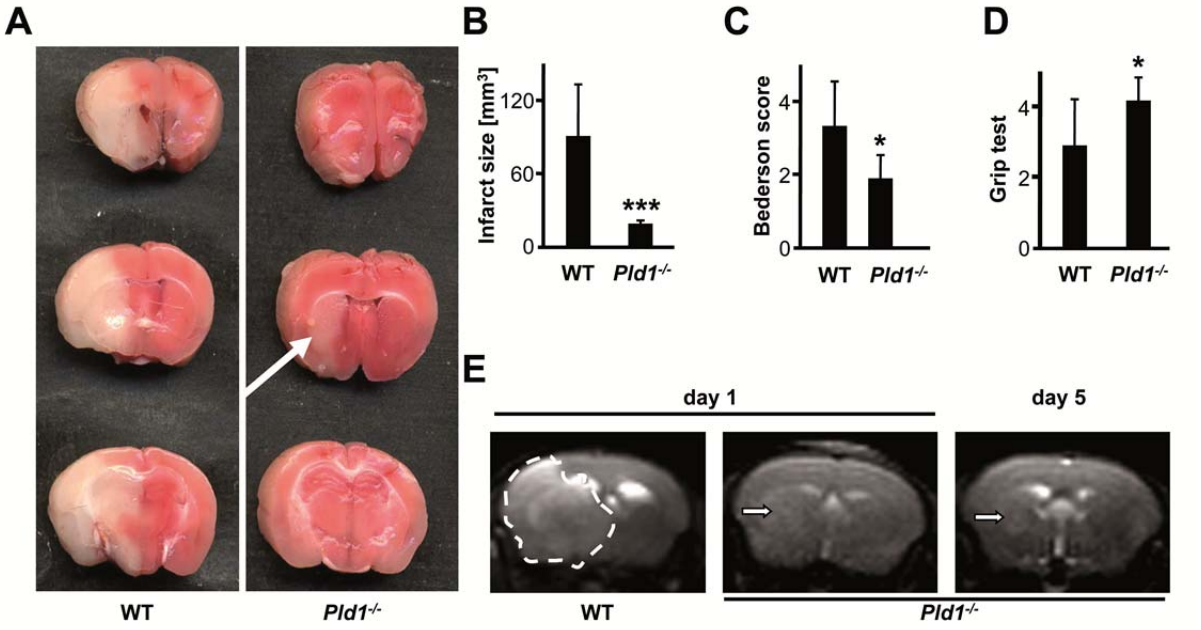

Figure 3-20: *Pld1*$^{-/-}$ mice are protected against cerebral ischemia. A) Representative images of three corresponding coronal sections from WT and *Pld1*$^{-/-}$ mice stained with TTC 24 hours after tMCAO. B) Brain infarct volumes. C & D) Neurological Bederson score and grip test assessed at day 1 after tMACO of the mice mentioned in (A). E) Coronal T2-weighted MR brain imaging shows a large hyperintense ischemic lesion at day 1 after tMCAO in a wildtype mouse (left panel, demarcated by dotted line), but only a small infarct in a *Pld1*$^{-/-}$ mouse (middle panel, white arrow) and the T2 hyperintensity decreases by day 5 subsequent to infarct maturation (right panel, white arrow). Hypointense areas indicating intracerebral hemorrhage were not seen in *Pld1*$^{-/-}$ mice, demonstrating that PLD1-deficiency does not increase the risk of hemorrhagic transformation, even at advanced stages of infarct development. Data are mean ± SD (n=10 mice per group). * *P*<0.05, *** *P*<0.001.

To test whether the defective thrombus stability in *Pld1*$^{-/-}$ mice impaired normal hemostasis, tail bleeding time assays were performed. In this model, the ability of mice to arrest bleeding at the site of a defined tail wound serves as an indicator of physiological blood clotting [181].

Bleeding times did not significantly differ between WT and *Pld1*$^{-/-}$ mice (6.1 ± 4.0 min versus 5.6 ± 3.0 min; *P*>0.05; Figure 3-21), indicating – together with the MRI results after tMCAO (Figure 3-20E) – that PLD1 is not required for normal hemostasis.

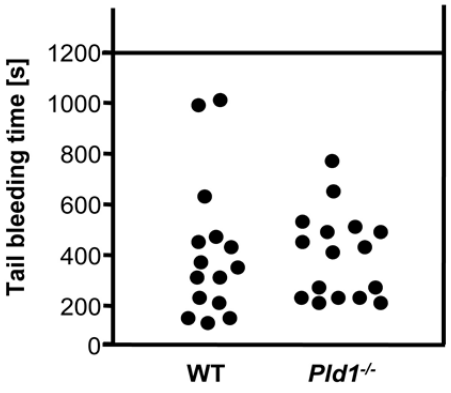

Figure 3-21: PLD1-deficiency does not impair hemostasis. Tail bleeding times for wildtype and *Pld1*$^{-/-}$ mice. Each symbol represents one animal.

3.2.6 Generation of Mice Lacking Phospholipase D2

The PLD activity assay revealed that PLD1-deficiency abolishes the inducible PLD activity, while the basal activity remained unaltered (Figure 3-13). Basal PLD activity is supposed to be mainly mediated by PLD2 [90]. To address the relevance of the basal PLD activity for platelet physiology, *Pld2*$^{-/-}$ mice were generated. To this end, two VGB6 mouse embryonic stem cell clones from KOMP (knockout mouse project) repository were ordered carrying one targeted PLD2 allele (*Pld2*$^{tm1(KOMP)Vlcg}$), leading to a complete deletion of the *Pld2* gene (Figure 3-22A) on this allele.

The identity of the two stem cell clones, AA11 and BD1, was confirmed via PCR genotyping (not shown) and the clones were injected into mouse blastocyst by Michael Bösl (Transgenic Core Facility, MPI Martinsried). Three highly chimeric mice resulted from the blastocyst injection of BD1, while one 60% chimeric male resulted from the AA11 clone. Only two of the BD1 chimeras were fertile and gave rise to heterozygous offspring. Mice heterozygous for the *Pld2*-null mutation, as well as PLD2-deficient (*Pld2*$^{-/-}$) mice, were born at the expected Mendelian ratio. *Pld2*$^{-/-}$ mice displayed unaltered growth, were fertile and exhibited behavior indistinguishable from that of wildtype littermates. The animals appeared healthy and did not exhibit spontaneous bleeding. The polyclonal anti-PLD2 antibody used for the Western Blot depicted in Figure 3-12D is not available anymore and all other tested commercial anti-PLD2 antibodies turned out to be unspecific. Therefore, RT-PCR was used to confirm that the deletion of the *Pld2* gene ablates *Pld2* expression (Figure 3-22B).

Initial analyses indicate that the blood cell count and platelet size as well as the surface expression of major platelet glycoproteins does not differ between wildtype and *Pld2*$^{-/-}$ mice (Table 3-3). A detailed analysis of *Pld2*$^{-/-}$ platelets as well as intercrossing of *Pld2*$^{-/-}$ and *Pld1*$^{-/-}$ mice, to obtain mice lacking both PLD isoforms, is currently performed.

	WT	***Pld2*$^{-/-}$**		**WT**	***Pld2*$^{-/-}$**
PLT [10^5/µl]	885 ± 143	897 ± 190	**α-GPIX [MFI]**	553 ± 15	533 ± 21
MPV [fl]	5.5 ± 0.1	5.5 ± 0.3	**α-GPVI [MFI]**	52 ± 3	53 ± 5
RBC [10^6/µl]	6.75 ± 1.31	5.88 ± 1.19	**α-αIIbβ3 [MFI]**	708 ± 26	729 ± 28
WBC [10^6/µl]	8.31 ± 1.92	7.08 ± 1.50	**α-β1 [MFI]**	173 ± 18	178 ± 3
HCT [%]	49.3 ± 7.9	44.1 ± 6.7	**α-α2 [MFI]**	65 ± 3	65 ± 2
α-GPIb [MFI]	433 ± 19	400 ± 21	**α-CLEC-2 [MFI]**	143 ± 8	141 ± 10
α-GPV [MFI]	317 ± 31	325 ± 33	**α-CD9 [MFI]**	1341 ± 40	1360 ± 40

Table 3-3: Blood cell counts and surface expression of platelet glycoproteins in *Pld2*$^{-/-}$ mice. Mean blood cell counts, platelet size and hematocrit levels were determined using a Sysmex cell counter. Surface expression of prominent platelet glycoproteins was determined by flow cytometry. Diluted whole blood from the indicated mice was incubated with FITC-labeled antibodies at saturating conditions for 15 min at RT and platelets were analyzed directly in a FACSCalibur. Results are expressed as mean values ± SD for at least 9 mice per group. PLT, *platelet count*; MPV, *mean platelet volume*; RBC, *red blood cell count*; WBC, *white blood cell count*; MFI, *mean fluorescence intensity*.

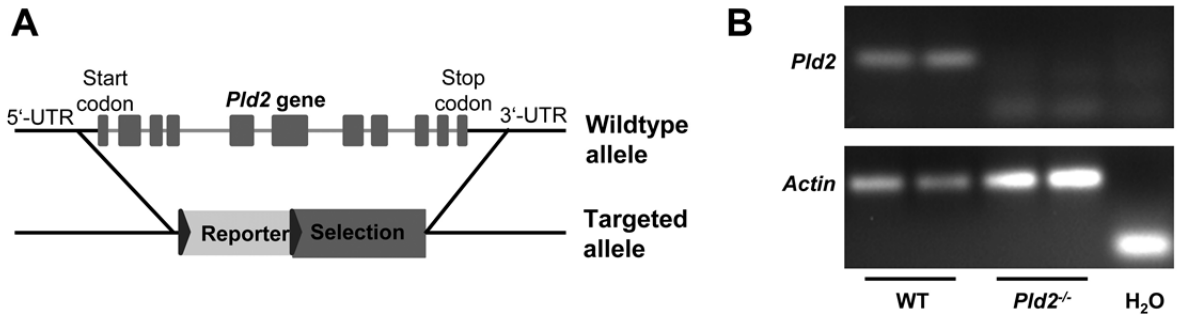

Figure 3-22: Generation of PLD2-deficient mice. A) Simplified targeting strategy, the Velocigene approach leads to a deletion of the entire *Pld2* gene, which is replaced by the ZEN-Ub1 selection cassette containing *LacZ* as reporter and *neomycin* cDNA under the control of the *ubiquitin* promoter as selection marker. B) RT-PCR of cDNA from WT and *Pld2*$^{-/-}$ macrophages.

3.3 Both STIM Isoforms Contribute to Store-Operated Calcium Entry Downstream of T Cell and Fcγ-Receptor Activation

Store-operated calcium entry (SOCE) has been established as central pathway of calcium entry in T cells since two decades [113]. Numerous studies in recent years demonstrated that STIM1 is the central mediator of SOCE in T cells [reviewed in 119]. The role of STIM2, however, is only poorly understood. To address this issue, calcium mobilization in STIM2-deficient T cells was analyzed. The relevance of Ca^{2+}-entry (mostly via SOCE) is well established for cellular responses following mast cell FcεR- or T cell receptor-stimulation. This is not the case for FcγR-signaling, since for this ITAM-receptor the relevance of calcium mobilization remained controversial. One aim of this study was to investigate the importance of Ca^{2+}-mobilization in FcγR activation. Therefore, calcium fluxes in macrophages deficient in STIM1, STIM2 or Orai1 were analyzed. To understand whether SOCE is required for phagocytosis *in vivo* corresponding mice were subjected to a model of experimental immune thrombocytopenia.

STIM1- or Orai1-deficiency is associated with approximately 70% perinatal lethality, probably related to a cardiopulmonary defect. The surviving animals display pronounced growth retardation and a maximal life span of 4 to 6 weeks [127, 128]. Therefore and to restrict the deficiency to the hematopoietic system, bone marrow from *Stim1*$^{-/-}$, *Orai1*$^{-/-}$ or wildtype control mice was transplanted into lethally irradiated wildtype mice. The transplanted mice were analyzed after 10 weeks and will be further referred to as *Stim1*$^{-/-}$ and *Orai1*$^{-/-}$. In contrast to STIM1-deficient mice, STIM2-deficient mice were viable, albeit sudden death of *Stim2*$^{-/-}$ mice was observed starting 8 weeks after birth and only 10% of the animals reached the age of 7 months [169]. Nevertheless constitutive *Stim2*$^{-/-}$ mice were used for all experiments. The analysis of the *Stim2*$^{-/-}$ mice was performed together with Dr. Alejandro Berna-Erro.

3.3.1 Both STIM Isoforms act as Calcium Sensors in T Cells

Several studies established a role for STIM1 in SOCE following *T cell antigen receptor* (TCR) activation in mice [129, 131] and human patients [132]. However, the contribution of STIM2 to this process was less clear [129]. Hence, it was investigated whether STIM2 plays a role in calcium responses upon TCR stimulation and compared with the role of STIM1. Since it was initially reported that Orai1 is not relevant for TCR signaling in mice [126] the role of Orai1 in TCR-mediated calcium responses was not addressed.

Western blot analysis revealed the presence of both STIM isoforms in naïve wildtype T cells (Figure 3-23A, inlay), which stands in contrast to the report of Oh-Hora and colleagues [129].

Genetic ablation of either *Stim* isoform resulted in the absence of the corresponding protein in T cells (Figure 3-23A, inlay).

To assess the relevance of the two STIM isoforms for SOCE the *Sarco/endoplasmic reticulum Ca^{2+}-ATPase* (SERCA) pump inhibitor *thapsigargin* (TG) was used. TG passively depletes the intracellular Ca^{2+}-stores and thereby triggers SOCE independently of receptor stimulation. Fura-2 loaded CD4-positive T cells were stimulated with TG for 10 min in the absence of extracellular calcium. Basal calcium levels were unaffected by the lack of either STIM isoform (24.0 ± 11.5 nM in WT, 27.5 ± 7.7 nM in *Stim1*$^{-/-}$ and 34.8 ± 24.9 nM in *Stim2*$^{-/-}$ T cells) and TG induced a small increase in intracellular calcium concentrations ($[Ca^{2+}]_i$) which was slightly, though yet significantly, reduced in *Stim1*$^{-/-}$, but not in *Stim2*$^{-/-}$ T cells ($\Delta[Ca^{2+}]_i$ 28.9 ± 16.3 nM in WT, 12.3 ± 2.6 nM in *Stim1*$^{-/-}$, $P<0.05$ and 38.3 ± 29.1 nM in *Stim2*$^{-/-}$ T cells, $P>0.05$; Figure 3-23A, B). Upon addition of 1 mM extracellular calcium, a dramatic calcium influx was measurable in Fura-2 labeled WT but not in *Stim1*$^{-/-}$ T cells ($\Delta[Ca^{2+}]_i$ 565.0 ± 185.4 nM in WT vs. 19.3 ± 6.8 nM in *Stim1*$^{-/-}$ T cells, $P<0.001$; see Figure 3-23). In *Stim2*$^{-/-}$ T cells, the calcium influx was reduced by 47% ($\Delta[Ca^{2+}]_i$ 297.8 ± 200.8 nM, $P<0.05$, Figure 3-23 A, B).

Since the use of TG is a purely pharmacological approach, calcium mobilization was also tested upon receptor stimulation. Therefore, Fura-2 loaded T cells were pre-incubated with anti-CD3 antibodies, which were subsequently cross-linked using secondary antibodies to trigger T cell activation (Figure 3-23C, D). CD3 cross-linking led to small increase in $[Ca^{2+}]_i$, followed by a considerable SOCE upon addition of extracellular Ca^{2+} in WT mice ($\Delta[Ca^{2+}]_i$ 29.1 ± 15.3 nM in the absence of extracellular Ca^{2+}, 327.4 ± 165.5 nM upon addition of $CaCl_2$). T cells lacking STIM2 showed a slightly, but non-significantly, reduced store-release ($\Delta[Ca^{2+}]_i$ 15.2 ± 10.0 nM, $P>0.05$) and subsequent SOCE was reduced by 57% ($\Delta[Ca^{2+}]_i$ 142.0 ± 65.9 nM, $P<0.05$). *Stim1*$^{-/-}$ T cells displayed a dramatically reduced store-release ($\Delta[Ca^{2+}]_i$ 2.1 ± 1.3 nM, $P<0.01$), and the SOCE was virtually abolished ($\Delta[Ca^{2+}]_i$ 12.5 ± 5.1 nM, $P<0.01$; Figure 3-23C, D).

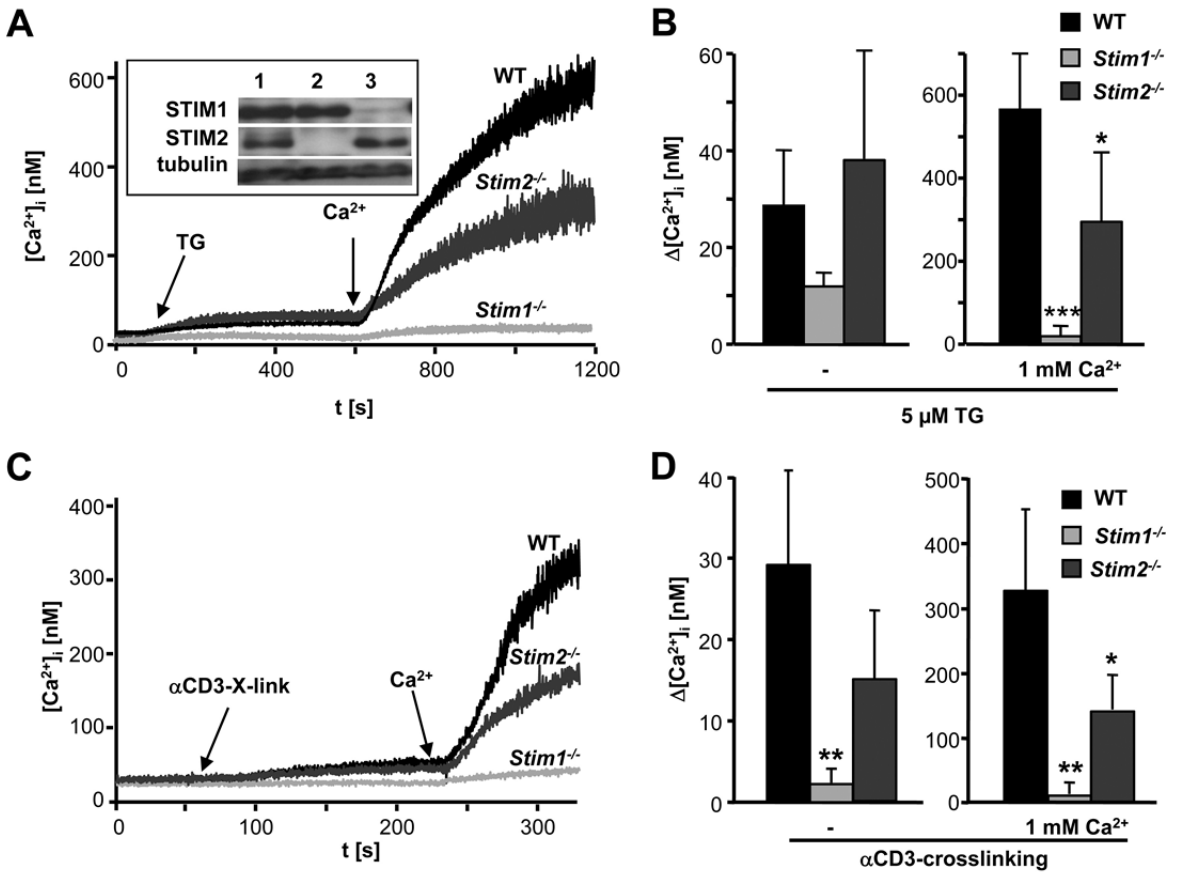

Figure 3-23: Defective calcium-mobilization in STIM-deficient T cells. A-D) Fluorometric Ca^{2+}-measurements of CD4+ T cells isolated by *magnetic-activated cell sorting* (MACS) from WT, *Stim1*$^{-/-}$ and *Stim2*$^{-/-}$ mice. The lack of the corresponding STIM isoform was confirmed with Western Blotting of corresponding T cells from wildtype (1), *Stim2*$^{-/-}$ (2) and *Stim1*$^{-/-}$ (3) mice (A, inlay). A) Fura-2–loaded CD4+ T cells were stimulated with 5 µM TG for 10 min or C) CD3-crosslinking for 3 min, followed by the addition of 1 mM extracellular $CaCl_2$ and monitoring of [Ca2+]i. B, D) Maximal increase in intracellular Ca^{2+} concentrations compared with baseline levels [Ca^{2+}]i ± SD (n≥4 mice per group) before and after addition of 1 mM Ca^{2+} (right) are shown. * *P*<0.05; ** *P*<0.01; *** *P*<0.001.

These results, which established STIM2 as a co-regulator of SOCE downstream of TCR stimulation initiated a fruitful cooperation with the group of Sven Meuth (Department of Neurology, University of Würzburg, now Department of Neurology, University Münster) about the role of both STIM isoforms in myelin-oligodendrocyte glycoprotein ($MOG_{35–55}$)-induced *experimental autoimmune encephalomyelitis* (EAE), a model for multiple sclerosis [188]. These studies revealed that STIM1-deficiency results in complete protection from EAE due to reduced Th1/Th17 responses. Mice lacking STIM2 developed EAE, but the disease course was ameliorated, probably due to an overall reduced proliferative capacity of lymphocytes and a reduction of IFN-γ/IL-17 production by neuroantigen-specific T cells. Meanwhile a second group has confirmed these findings [189].

3.3.2 FcγR Stimulation Induces SOCE in Macrophages

It is well established that Ca^{2+}-mobilization is crucial for many cellular events which follow the stimulation of mast cell or T cell ITAM-receptors. However, this is not true for the FcγR expressed in macrophages. Here, the requirement for Ca^{2+}-mobilization in FcγR-mediated phagocytosis has been controversially discussed [152, 156, 157]. To address this issue, peritoneal macrophages were labeled with Fura-2 and stimulated with TG to provoke store-depletion and subsequent calcium influx (see 3.3.1). The measured calcium traces in WT macrophages revealed that SOCE is indeed functional in macrophages (Figure 3-24A, B). Basal calcium levels were unaltered in *Stim1*$^{-/-}$ and *Stim2*$^{-/-}$ macrophages (not shown). TG-induced store-release was slightly reduced in *Stim1*$^{-/-}$ macrophages ($\Delta[Ca^{2+}]_i$ 27.8 ± 8.3 nM in WT, 16.8 ± 1.6 nM in *Stim1*$^{-/-}$ macrophages, $P<0.01$). In contrast, it was slightly increased in *Stim2*$^{-/-}$ macrophages (42.8 ± 18.5 nM, $P<0.05$), whereas it was unaltered in *Orai1*$^{-/-}$ macrophages (20.4 ± 9.0 nM, $P>0.05$). Upon addition of 1 mM extracellular calcium a robust calcium influx was measurable in Fura-2 labeled WT or *Stim2*$^{-/-}$ cells ($\Delta[Ca^{2+}]_i$ 148.1 ± 185.4 nM in WT, 151.5 ± 50.5 nM in *Stim2*$^{-/-}$ macrophages), but not in macrophages lacking STIM1 or Orai1 (37.0 ± 8.2 nM in *Stim1*$^{-/-}$, $P<0.001$ and 36.8 ± 12.1 nM in *Orai1*$^{-/-}$ macrophages, $P<0.001$; see Figure 3-24A, B). This indicated that SOCE is functional in macrophages and that STIM1 and Orai1 are essential for this process.

The more physiological approach of activating FcγRs via crosslinking of the 2.4G2 antibody (which binds to FcγRIII and FcγRIIb) using anti-rat IgG antibodies, revealed that STIM1 is the main calcium sensor for SOCE in macrophages, since calcium influx in *Stim1*$^{-/-}$ macrophages was basically abolished ($\Delta[Ca^{2+}]_i$ 118.5 ± 59.8 nM in wildtype, vs. 43.2 ± 11.1 nM in *Stim1*$^{-/-}$, $P<0.01$, see Figure 3-24C, D). Again, macrophages lacking *Stim2*$^{-/-}$ displayed unaltered calcium responses ($\Delta[Ca^{2+}]_i$ = 83.0 ± 44.8 nM in *Stim2*$^{-/-}$ macrophages). *Orai1*$^{-/-}$ macrophages will soon be tested in this experimental setting.

In a first attempt to identify potential consequences of the STIM-deficiency, the FcγR expression of *Stim1*$^{-/-}$ and *Stim2*$^{-/-}$ macrophages was determined using flow cytometry. The lack of either STIM isoform results in significant alterations in the FcγR surface expression (Figure 3-25). In case of *Stim1*$^{-/-}$ macrophages the expression of FcγRIII was reduced to 51% of WT levels, while the expression of FcγRIV was increased to 226% of WT levels. In macrophages lacking STIM2, the expression of FcγRIII and FcγRIV was increased by about 40% each (Figure 3-25). This indicated that both STIM isoforms contribute to the proper expression of FcγR in macrophages.

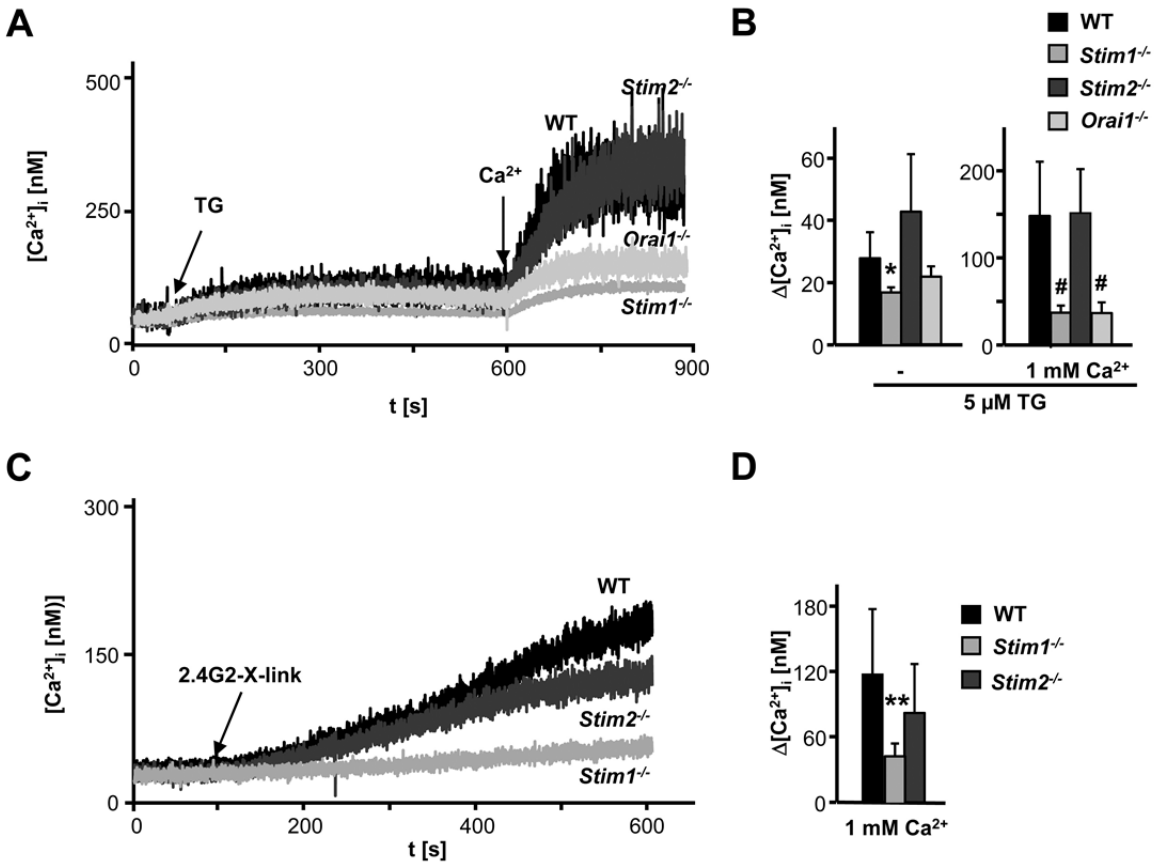

Figure 3-24: Impaired SOCE in *Stim1*$^{-/-}$ macrophages. Fura-2–loaded peritoneal macrophages were stimulated with 5 µM thapsigargin (A-C) for 10 min followed by addition of extracellular 1 mM $CaCl_2$ or with 2.4G2-crosslinking in the presence of extracellular Ca^{2+} (D & E). Intracellular Ca^{2+} concentrations ($[Ca^{2+}]_i$) were monitored online. Representative measurements (A, D) and maximal $[Ca^{2+}]_i$ before (B) and after (C, E) addition of extracellular Ca^{2+} ± SD (n≥5 per group). * P<0.05; ** P<0.01; $^{\#}P$<0.001.

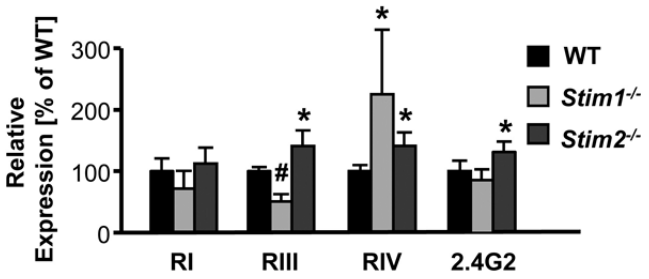

Figure 3-25: Lack of STIM proteins alters FcγR expression. Peritoneal macrophages of the indicated mice were stained with Alexa647–conjugated FcγRI, FcγRIII and FcγRIV-specific mAbs in combination with PE-F4/80 and analyzed by *fluorescence-activated cell sorting* (FACS). Data shown are normalized mean fluorescence intensities (WT was set as 100%) ± SD; n=4, * P<0.05; $^{\#}P$<0.001.

3.3.3 SOCE is Essential for Immune Thrombocytopenia and Systemic Anaphylaxis

FcγR-mediated phagocytosis is critical in the pathology of *immune thrombocytopenia* (ITP) (see 1.6). Thus, this model was chosen to assess the *in vivo* relevance of SOCE for macrophage phagocytosis. In human ITP, platelet surface GPIIb/IIIa (αIIbβ3 integrin) is the most common antigenic target with approximately 70% to 80% of patients displaying autoantibodies to this receptor complex [190-192]. Therefore, 7 µg α-GPIIb/IIIa (JON) antibodies were injected into mice and for the following three days platelet counts were monitored. It has been shown previously that JON3 (rat IgG1)-induced pathologies are predominantly mediated through FcγRIII, whereas JON1 (rat IgG2b)–induced pathologies depend on FcγRIV [146, 149]. Both JON3 and JON1 induced profound thrombocytopenia in WT mice with a maximal reduction of platelet counts of 66.3% (± 9.3) and 77.0% (± 5.4%) after 24 hours, respectively (Figure 3-26), confirming previous results [146]. In contrast, thrombocytopenia was significantly ameliorated in *Stim1*$^{-/-}$ mice with a maximal reduction in platelet counts of 21.3 ± 9.7% for JON3 and 30.0 ± 16.0% for JON1, respectively (P<0.001 in both cases; Figure 3-26). These results were similar to the results obtained with mice lacking the FcRγ-chain (*Fcer1g*$^{-/-}$ mice) [data not shown and 193, 194] and demonstrate that STIM1-dependent processes are crucial for the destruction of IgG-opsonized platelets.

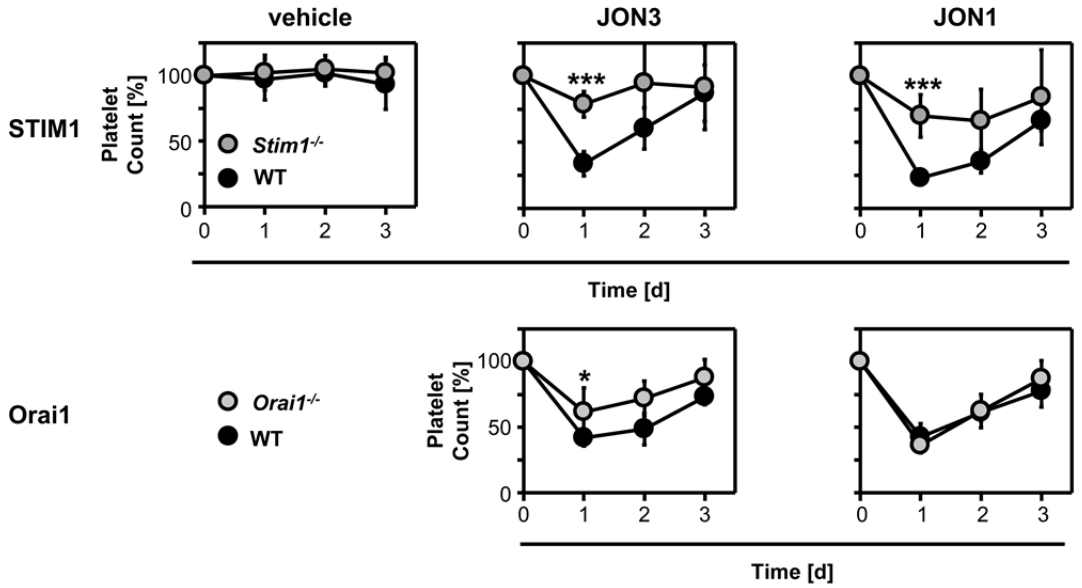

Figure 3-26: STIM1-deficiency protects from antiplatelet IgG-induced thrombocytopenia. *Stim1*$^{-/-}$ (A) or *Orai1*$^{-/-}$ mice (B) and corresponding controls received 7 µg JON3 (rat IgG1) or JON1 (rat IgG2b; both directed against GPIIb/IIIa) or vehicle i.v. and platelet counts were monitored. The results shown are mean normalized platelet counts ± SD of at least 4 mice per group. * P<0.05; ** P<0.01; *** P<0.001 compared to corresponding controls.

Based on these results, a collaboration with Prof. Dr. J. Engelbert Gessner (Molecular Immunology Research Unit, Clinic for Immunology and Rheumatology, Hanover Medical School) was established to investigate the role of STIM1 in FcγR activation [195]. This study confirmed abolished phagocytosis capacity of *Stim1*$^{-/-}$ macrophages *in vitro*. As a direct consequence, STIM1-deficiency resulted in resistance to autoimmune hemolytic anemia, a model were IgG-opsonized red blood cells are phagocytozed, similar to platelets in ITP. Further, an essential role of STIM1 in FcRγ-induced generation of complement component C5a was established. The latter resulted in a protection of *Stim1*$^{-/-}$ mice in a model of acute pneumonitis [195].

The comparison of *Orai1*$^{-/-}$ and WT mice displayed only a minor protection from JON3-induced thrombocytopenia (remaining platelet count of 41.9 ± 6.3% in wildtype vs. 61.7 ± 18.4% in *Orai1*$^{-/-}$ mice on day 1, $P<0.05$) and no effect of Orai1-deficiency on JON1-induced ITP (42.6 ± 10.0 vs. 36.2 ± 5.8% on day 1, see Figure 3-26). This indicated that STIM1 is more important for ITP than Orai1.

Surprisingly, also lack of STIM2 turned out to be protective in this model of IgG-induced thrombocytopenia, although to a lesser extent than the lack of STIM1 (Figure 3-27). Intravenous injection of 7 µg JON1 or JON3 induced thrombocytopenia in both groups, but STIM2-deficient mice were slightly protected (remaining platelet counts on day 1 in WT mice 60.5 ± 10.8% vs. 81.8 ± 10.6% in *Stim2*$^{-/-}$ mice, $P<0.01$, for JON1; JON3-treatment: 43.2 ± 11.2% vs. 69.3 ± 24.1%, $P<0.01$). To further investigate the effect of STIM2-deficiency on GPIIb/IIIa-induced thrombocytopenia, different doses of JON1 and JON3 antibodies were tested. Interestingly, the protective effect of STIM2 ablation was dose-dependent in case of JON1-induced thrombocytopenia (remaining platelet counts on day 1 in WT mice 47.1 ± 21.0% vs. 89.5 ± 20.1% in *Stim2*$^{-/-}$ mice, $P<0.001$, for 4 µg JON1; 56.1 ± 10.5% vs. 65.4± 9.5%, $P>0.05$, for 11 µg). In contrast, the protective effect of STIM2-deficiency was not dose-dependent in JON3-induced thrombocytopenia (remaining platelet counts on day 1 in WT mice 52.5 ± 8.9% vs. 73.4 ± 16.4% in *Stim2*$^{-/-}$ mice, $P<0.01$, for 4 µg JON3; 37.5 ± 13.3% vs. 63.9 ± 5.6%, $P<0.01$, for 11 µg; see Figure 3-27).

It has previously been demonstrated that anti-GPIIb/IIIa antibodies are unique among antiplatelet antibodies because a bolus injection of a high dose triggers, in addition to thrombocytopenia, an (eventually lethal) acute systemic reaction by FcγR-dependent mechanisms [146, 194, 196]. Systemic anaphylaxis leads to a breakdown of the circulation which results in severe hypothermia, since mice do have an unfortunate mass to surface ratio. To determine the relative contribution of the two STIM isoforms in the pathology of IgG-mediated anaphylaxis, 100 µg JON3 or JON1 were injected into WT, *Stim1*$^{-/-}$, *Stim2*$^{-/-}$ and *Orai1*$^{-/-}$ mice and body temperature was monitored. In agreement with previous observations,

WT mice developed an anaphylactic shock and severe hypothermia within minutes upon intravenous injection. In contrast, *Stim1*$^{-/-}$ mice were completely protected against anti-GPIIb/IIIa-induced anaphylaxis (after 30 min 32.7 ± 1.0°C vs. 36.8 ± 0.3°C, P<0.001, for JON1 and 32.4 ± 0.4°C vs. 36.9 ± 0.2°C, P<0.001, for JON3-induced anaphylaxis; Figure 3-28). Again this protection was comparable to mice lacking the FcRγ-chain (31.1 ± 1.1°C vs. 36.5 ± 0.4°C, P<0.001, for JON1 and 32.0 ± 1.2°C vs. 36.6 ± 0.3°C, P<0.001, for JON3-induced anaphylaxis; see Figure 3-28). Mice lacking STIM2 were moderately protected against JON-mediated anaphylaxis (after 30 min 32.5 ± 0.7°C vs. 34.0 ± 0.8°C, P<0.01, for JON1 and 32.9 ± 0.8°C vs. 35.2 ± 1.8°C, P<0.001, for JON3-induced anaphylaxis; see Figure 3-28), indicating that STIM2 also contributes to this pathology. To exclude the possibility that the protective effect of STIM2-deficiency is not blood derived, STIM2-bone marrow chimeric mice were subjected to JON3-mediated anaphylaxis. Mice with STIM2-deficient bone marrow were protected against IgG-induced anaphylaxis (after 30 min 33.3 ± 0.8°C vs. 34.5 ± 0.6°C, P<0.05; not shown). This indicated that STIM2 contributes to IgG-mediated anaphylactic responses.

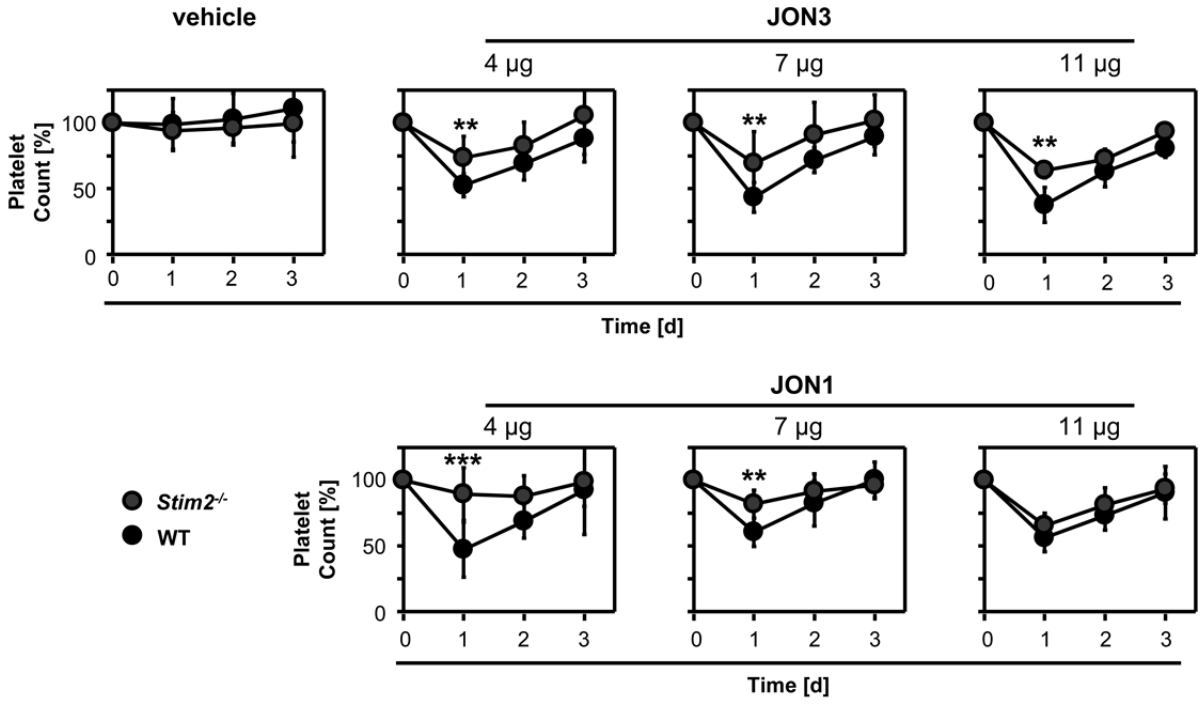

Figure 3-27: *Stim2*$^{-/-}$ mice are slightly protected against antiplatelet IgG-induced thrombocytopenia. *Stim2*$^{-/-}$ and wildtype mice received the indicated amounts of JON3 (rat IgG1) or JON1 (rat IgG2b; both directed against GPIIb/IIIa) or vehicle i.v. and platelet counts were monitored. The results shown are mean normalized platelet counts ± SD of at least 4 mice per group. * P<0.05; ** P<0.01; *** P<0.001.

Mice lacking the SOCE channel pore Orai1 were likewise protected against JON1- (30 min after injection: 31.9 ± 1.4°C vs. 34.8 ± 1.9°C, *P*<0.01) and JON3-induced anaphylaxis (31.4 ± 1.8°C vs. 36.2 ± 0.7°C, *P*<0.001; Figure 3-28).

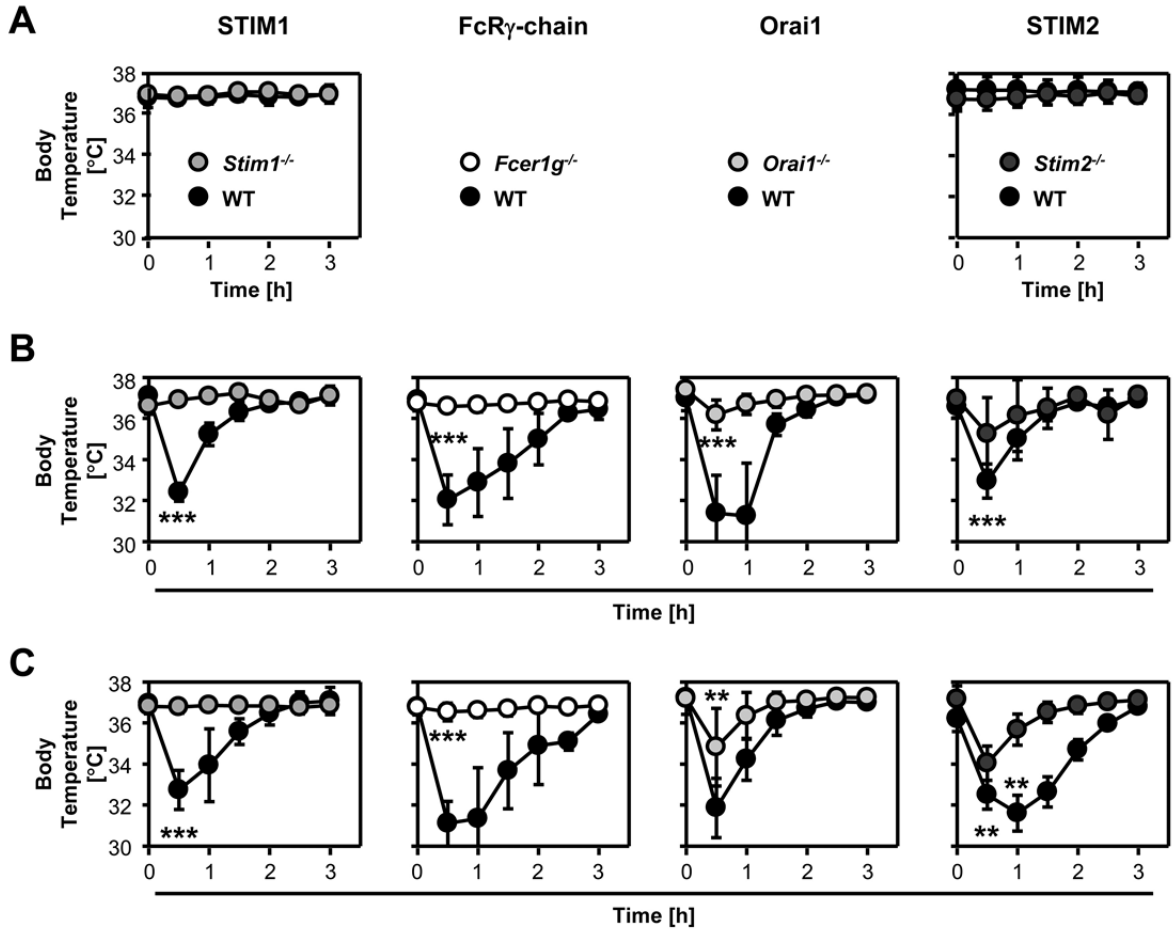

Figure 3-28: SOCE downstream of the FcRγ-chain is critical for antiplatelet IgG-induced anaphylaxis. *Stim1*$^{-/-}$, *Fcer1g*$^{-/-}$, *Stim2*$^{-/-}$, *Orai1*$^{-/-}$ and corresponding control mice received vehicle (A), 100 µg JON3 (B) or JON1 (C) and body temperature was monitored with a rectal probe. The results shown are mean body temperature ± SD (n≥4 mice per group). * *P*<0.05; ** *P*<0.01; *** *P*<0.001 compared to corresponding controls.

The more common way to trigger anaphylactic reactions is the IgE-mediated response of mast cells. Therefore, IgE-mediate anaphylaxis in both *Stim*-deficient mouse lines was investigated. Mice were primed by intravenous injection of anti-DNP IgE, followed by *i.v.* injection of the DNP-antigen 24 h later. This provoked a profound anaphylactic response in WT mice (20 min after injection of DNP: 33.7 ± 0.2°C), as assessed by measuring the body temperature, while *Stim1*$^{-/-}$ mice were protected (36.8 ± 0.4°C, *P*<0.001; Figure 3-29A). Mice lacking STIM2 were protected as well, albeit to a lesser extent (20 min after injection of DNP: 32.3 ± 0.4°C in WT vs. 34.8 ± 1.3°C in *Stim2*$^{-/-}$ mice, *P*<0.01; Figure 3-29B).

These results for *Stim1*$^{-/-}$ mice have already been reported by others [125] and were associated with an abolished SOCE in STIM1-deficient mast cells. To understand the

phenotype observed in STIM2-deficient mice calcium fluxes of *bone marrow-derived* (BMMC) and *peritoneal mast cells* (PMC) were measured. Neither in response to thapsigargin, nor in response to FcεR activation (via IgE priming and subsequent crosslinking through addition of the corresponding antigen) revealed any differences between WT and *Stim2*$^{-/-}$ mast cells (data not shown). This study reported similar observations in macrophages, where calcium fluxes were not altered in *Stim2*$^{-/-}$ macrophages (Figure 3-24), while the STIM2-deficient mice were protected against FcγR-related pathologies (Figure 3-27). However, to confirm that the observed phenotype of STIM2-deficient mice results from defective mast cell responses the IgE-mediated anaphylaxis, experiments were repeated using bone marrow chimeric mice. For this purpose lethally irradiated wildtype mice were transplanted either with wildtype or with *Stim2*$^{-/-}$ bone marrow. 11 weeks after transplantation IgE-mediated anaphylaxis was triggered as described above. Both groups of mice developed hypothermia within 20 min after injection of DNP (Figure 3-29C), indicating that the protective effect of STIM2-deficiency is not caused by the lack of STIM2 in blood cells.

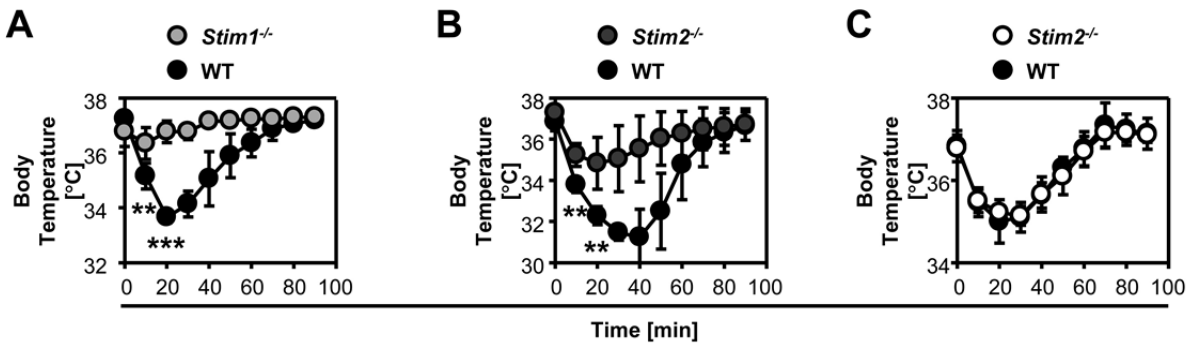

Figure 3-29: Hematopoietic STIM1-, but not STIM2-deficiency protects from IgE-induced anaphylaxis. *Stim1*$^{-/-}$ bone marrow chimeric (A), *Stim2*$^{-/-}$ (B), *Stim2*$^{-/-}$ bone marrow chimeric (C) and corresponding control mice received 30 µg anti-DNP IgE 24 h prior to the experiment. At time point 0, mice received 250 µg DNP-HSA and body temperature was monitored with a rectal probe. The results shown are mean body temperature ± SD (n≥4 mice per group). * P<0.05; ** P<0.01; *** P<0.001.

4 Discussion

Platelet activation, coagulation and subsequent thrombus formation at sites of vascular injury are essential to limit blood loss. This is underscored by numerous inheritable gene defects which impair platelet activation or blood coagulation and ultimately lead to severe bleeding disorders [reviewed in 197]. Likewise, acquired diseases which result in low platelet counts, e.g. immune or heparin-induced thrombocytopenia, increase the risk of spontaneous bleeding. On the other hand, uncontrolled thrombus formation can result in complete vessel occlusion, the main cause of heart attacks and stroke [198]. These two diseases are the most frequent *cardiovascular diseases* (CVDs). CVDs are the leading cause of mortality with 17.1 million deaths worldwide (which represents 29% of all global deaths) [198]. Therefore, platelet signaling has become an important field of basic clinical research over the last decades and many therapeutical drugs for prevention of CVDs, such as aspirin and clopidogrel, act via inhibition of platelet function. Nevertheless, the number of humans dying from CVDs is expected to rise despite multiple therapeutic options [198]. This emphasizes the need for a better understanding of platelet signaling and the mechanisms underlying thrombus formation in order to identify new potential molecular targets.

Despite some general concerns about the transferability of results from mice to humans and some differences in the expression of platelet receptors (e.g. PARs and FcγRIIA), the mouse has become an essential model system for thrombosis research. This is mainly based on the small size of mice, their high fertility and the existence of multiple *in vivo* models for thrombosis [reviewed in 199] and ischemic stroke [reviewed in 200] established in this species. Another major advantage of mice is the availability of genetic methods that allow targeted manipulations in the murine genome. The analyses of genetically modified mice have become instrumental for thrombosis research, since this approach enables not only the "phenocopy" of human diseases, e.g. Bernard-Soulier syndrome [20, 23] or Glanzmann thrombasthenia [201], but also the study of gene deficiencies for which no human correlate exists (e.g. *Gp5*$^{-/-}$ or *Pld1*$^{-/-}$ mice). Especially the latter approach has helped to identify several potential targets for antithrombotic therapy [202, 203].

In this thesis, the role of GPV and PLD1 for platelet function and thrombus formation was investigated in the respective knockout mice. Further, the relevance of SOCE for FcγR-signaling and immune thrombocytopenia was assessed. The results presented here revealed GPV as a critical modulator of thrombus formation and hemostasis. It was also demonstrated that PLD1 is required for efficient GPIb-mediated integrin activation. Additionally, an essential role of SOCE in FcγR-signaling and platelet clearance was revealed. Thus, GPV and PLD1

might serve as new potential targets for the treatment of CVDs, while targeting STIM1 and the SOCE machinery could open up new avenues for the treatment of ITP.

4.1 GPV – a Critical Modulator of Thrombus Formation and Hemostasis

This study confirmed that GPV contributes to platelet collagen responses. However, the most intriguing findings are the results of the *in vivo* models, which reveal an unexpected role of GPV as modulator of platelet activation and thrombus formation. Lack of GPV can compensate for the ablation of all collagen receptors in thrombosis, ischemic stroke and hemostasis, thus establishing GPV as a key player in platelet physiology. Hence, targeting GPV may serve as potential new treatment in certain bleeding complications, like intracranial hemorrhage.

Platelets lacking GPV were slightly but significantly increased in size compared with wildtype platelets (Table 3-1) which is in contrast to the first reports about the two *Gp5*$^{-/-}$ mouse lines [25, 63]. However, the difference might have been too small for the experimental methods used at that time and a small shift in FSC/SSC characteristic in knockout platelets compared to controls can be observed in the dot plot figures of the original paper [25]. Increased thrombin responsiveness of *Gp5*$^{-/-}$ platelets has been demonstrated by Ramakrishnan *et al.* [63] and confirmed later by Moog *et al.* using the same mouse strain which had been used for this study [66], albeit it is now backcrossed to the C57Bl/6 background. This thesis confirmed the increased thrombin responsiveness of GPV-deficient platelets in flow cytometry (Figure 3-1) and aggregation studies (Figure 3-2). Ramakrishnan *et al.* ascribed the increased thrombin responsiveness of GPV-deficient platelets to GPIb as a thrombin receptor which is unmasked by the lack of GPV [64, 204]. Despite the well-established capacity of GPIb to bind thrombin [reviewed in 27], this hypothesis seems to be overstated from today's point of view: Ramakrishnan *et al.* used a PAR1 inhibitor on murine *Gp5*$^{-/-}$ platelets to support the importance of GPIb-signaling upon thrombin stimulation [64]. Since mouse platelets express Par3 instead of PAR1 [205] and lack of the principal thrombin receptor, Par4, abolishes thrombin signaling in platelets, GPIb is probably not of major importance for the signaling process itself [14, 206]. Further, according to the two α-thrombin/GPIbα-N crystal structures [207, 208], the GPIb binding site for thrombin should not be affected by GPV. In addition, Nonne *et al.* reported that lack of GPV does not alter the capacity of platelets to bind thrombin [67]. Therefore, the increased thrombin responsiveness of *Gp5*$^{-/-}$ mice most likely results from the absence of GPV as thrombin substrate, thereby

shifting the thrombin threshold required for platelet activation towards lower thrombin concentrations, as initially postulated [63].

In line with previous reports [70, 74, 76], *Itga2*$^{-/-}$ platelets responded normally to all tested agonists except collagen (Figure 3-1). In response to Horm collagen, a suspension of fibrillar equine tendon collagen (mainly type I and to a lesser extent type III [3]), the aggregation response of *Itga2*$^{-/-}$ platelets was delayed, even though the same aggregation maximum was reached (Figure 3-2). This effect was more pronounced at low collagen concentrations, which was in line with previous observations [70, 74, 76]. Moog *et al.* reported slightly delayed and reduced aggregation responses of *Gp5*$^{-/-}$ platelets towards low doses of bovine collagen type I [66]. This study did not reproduce these findings using Horm collagen in GPV single-deficient platelets (Figure 3-2). However, double-deficient platelets lacking GPV and $\alpha2\beta1$ displayed an increased lag time between the addition of collagen and maximal aggregation in comparison with $\alpha2\beta1$ single-deficient platelets, without affecting the maximal aggregation response (Figure 3-2). These results reveal partially redundant functions of the $\alpha2\beta1$ integrin and GPV in collagen signaling, thereby expanding the role of GPV in collagen responses proposed by Moog *et al.* [66]. Though, in a whole blood perfusion system no effect of GPV-deficiency (independent of $\alpha2\beta1$ expression) could be demonstrated (Figure 3-3), making it more likely that GPV supports the interaction between GPVI and collagen under static conditions, which is not required (or not functional) under flow conditions.

The literature is somewhat in-consistent about the relevance of $\alpha2\beta1$ for adhesion to collagen under flow (see 1.3.1). Of note, both studies which reported no effect of $\alpha2\beta1$-deficiency on adhesion on fibrillar collagen used conditional *Itgb1*$^{-/-}$ mice, in which the expression of the Cre recombinase had to be induced to generate $\beta1$- (and hence $\alpha2\beta1$-) deficient platelets [73, 74]. Sarratt *et al.* speculated that a diminutive proportion of $\beta1$-expressing platelets, resulting from hematopoietic stem cells which escaped Cre induction, might be sufficient to prevent observable defects in flow adhesion assays [72]. The results presented here with strongly reduced (Figure 3-3), but not abolished adhesion (as observed with GPVI-deficient platelets, not shown), are comparable with the other reports on $\alpha2$-deficient platelets [70-72, 209].

One aim of this study was to reevaluate the role of GPV in thrombosis models, since the published results are somewhat contradictory. While Moog *et al.* reported delayed time to occlusion in *Gp5*$^{-/-}$ mice subjected to $FeCl_3$-induced injury [66], others stated that thrombus formation starts earlier in GPV-deficient mice and results in reduced mean occlusion times [65]. A third study, which used laser-injury to study the relevance of GPV-deficiency in thrombosis, stated that the severity of the injury decides whether *Gp5*$^{-/-}$ mice do have a pro-

or anti-thrombotic phenotype [67]. This might explain why the two aforementioned groups obtained conflicting results, albeit using the same model. However, conflicting results in ferric chloride-injury models about the relevance of GPVI have been reported as well (see below), demonstrating that technical differences might result in different outcomes. Nevertheless, the current thesis confirmed the pro-thrombotic phenotype of GPV-deficient mice (Figure 3-4). Unlike Ni *et al.* [65], we did not observe increased embolization in *Gp5*$^{-/-}$ mice, a difference which might result from platelet labeling procedures (*ex vivo* vs. *in vivo*) or different genetic backgrounds of the mice (Sv129/B6 vs. C57Bl/6). The latter explanation appears to be more likely since we observed higher frequency of emboli in *Gp5*$^{-/-}$ mice on Sv129/B6 background as well (Pleines *et al.*, unpublished).

Since aggregation studies revealed a partial functional redundancy between $\alpha 2\beta 1$ and GPV, mice lacking both glycoproteins were subjected to the ferric chloride-injury model. Interestingly, this did not reveal any additive effect when both receptors were absent. Instead, the phenotype of $\alpha 2\beta 1$/GPV double-deficient mice reflects the phenotype of the *Gp5*$^{-/-}$ mice (Figure 3-4). However, unlike Kuijpers *et al.* [71], no increased embolization in mice lacking $\alpha 2\beta 1$ was observed (independent of the expression of GPV). Similar to the results obtained with *Gp5*$^{-/-}$ mice (see above) this difference can probably be ascribed to the different genetic background, since their mice had a mixed Sv129/B6 background. The concomitant deficiency of $\alpha 2\beta 1$ and GPV did not alter the observed *in vivo* phenotype. Hence, it was investigated whether GPV-deficiency would amplify the phenotype observed in mice lacking the principal collagen receptor GPVI. Absence of GPVI was reported to protect mice from thrombosis in this model by several groups [55, 85 and Bender et al., unpublished, 210], although another group questioned these results [175]. In line with the aforementioned reports, GPVI-depletion resulted in delayed thrombus formation and protection from occlusion in WT and *Itga2*$^{-/-}$ mice (Figure 3-6). Surprisingly, these effects could be reversed if GPV was deleted, resulting in accelerated platelet adhesion and thrombus formation compared to wildtype mice, despite the lack of GPVI, or GPVI and $\alpha 2\beta 1$. Due to the controversies regarding the ferric chloride model the effect of combined deficiency of GPVI and GPV was assessed in an additional thrombosis model. The mechanical injury model of the abdominal aorta was chosen, since thrombus formation in this model is mainly driven by collagen [176]. As expected GPVI-depletion protected wildtype mice in this thrombosis model (Figure 3-7). In contrast, mice lacking GPV and GPVI were not protected and occluded comparable to untreated wildtype mice (Figure 3-7). Hence, the capacity of GPV-deficiency to “overrule” the loss of GPVI was confirmed in a second thrombosis model.

Combined deficiency of GPV and CLEC-2 did not alter the occlusion rate (Figure 3-8). However, beginning of thrombus formation started earlier in CLEC-2-depleted *Gp5*$^{-/-}$ mice.

This confirmed the results obtained in single-deficient *Gp5*$^{-/-}$ mice and underlined the notion that CLEC-2 is dispensable for the initial phase of thrombus formation [166]. In contrast, to the first description of the CLEC-2-depleting antibody, INU1, which was carried out with NMRi mice [166], C57Bl/6 mice were used for this study. In this mouse strain a subpopulation of mice displayed stable thrombus formation despite the lack of CLEC-2 and additional GPV-deficiency led to accelerated thrombus formation. This suggests that under certain rheological conditions thrombus formation and vessel occlusion can occur independently of CLEC-2. In these cases GPV decelerates thrombus formation.

Similarly, lack of GPV resulted in earlier beginning of thrombus formation in GPIb-blocked mice (Figure 3-8). This was, however, not associated with an altered endpoint, since GPIb-blockade prevented thrombus formation independently of GPV expression. Therefore, it can be concluded that GPV-deficiency cannot reverse the effect of a non-functional GPIb-vWF interaction in thrombus formation.

Similarly, hirudin treatment abolished thrombus formation in wildtype and *Gp5*$^{-/-}$ mice subjected to the ferric chloride-injury model (not shown), which is in line with similar results obtained after severe laser-injury [67]. To assess whether the increased thrombin responsiveness of *Gp5*$^{-/-}$ platelets *in vitro* results in thrombus formation under conditions of reduced local thrombin levels *in vivo*, FXII/GPV-double-deficient mice were generated. Genetic ablation of *F12* prevented thrombus formation which is in line with earlier studies [178]. The protective effect of FXII-deficiency could not be circumvented by the lack of GPV (Figure 3-9). This suggests that the reduced thrombin levels in *F12*$^{-/-}$ mice are too low to facilitate complete vessel occlusion even in *Gp5*$^{-/-}$ mice with platelets which display increased thrombin responsiveness. Alternatively, FXII has a role in thrombus formation beyond thrombin generation. In either case, lack of GPV cannot circumvent the absence of FXII in arterial thrombosis.

The results obtained with the tMCAO model (Figure 3-10) indicated that GPV is not anti-thrombotic *per se*, since GPV-deficiency did not alter the infarct size after 30 or 60 min of tMCAO. However, GPV is required for a protective effect of GPVI-deficiency in this model, while it is not required for the protective effect of GPIb-blockade. These results underscore the results obtained in arterial thrombosis models (see above) and expand them to ischemic stroke.

Hemostasis is the central function of platelets. Thus, it was tested whether GPV-deficiency has any impact on tail bleeding times. Comparable to the results in thrombosis models, lack

of GPV reduces tail bleeding times (Figure 3-11). A similar reduced tail bleeding time was reported earlier by one group [63], while a second group did not observe a difference between wildtype and *Gp5*$^{-/-}$ mice [25]. However, the number of animals used was much smaller in the latter study [25]. None of the published studies have investigated the effect of GPV-deficiency on concomitant defects.

A previous study demonstrated that the lack of $\alpha 2\beta 1$ did not and GPVI-depletion only slightly prolonged tail bleeding times, while the combined deficiency resulted in a severe hemostatic defect [86]. The current study reproduced these findings and demonstrated that GPV-deficiency fully reverses the effects of the concomitant absence of the two main collagen receptors (Figure 3-11). As reported previously CLEC-2-depletion prolongs tail bleeding times in wildtype mice. However, this effect was not visible in *Gp5*$^{-/-}$ mice indicating that the relevance of GPV might be more pronounced in hemostasis than in thrombosis. While the combined depletion of GPVI and CLEC-2 resulted in dramatic hemostatic effects in wildtype mice, hemostasis in *Gp5*$^{-/-}$ mice was not affected by the loss of both platelet ITAM receptors (Figure 3-11). P0p/B treatment reproduces the bleeding phenotype observed in transgenic mice lacking functional GPIb [211]. Like in arterial thrombosis GPV-deficiency cannot compensate for the loss of GPIb in hemostasis, underscoring the paramount importance of GPIb in hemostasis and thrombosis [34].

In summary, these data demonstrate for the first time that GPV-deficiency can fully compensate for the lack of the platelet activating collagen receptor GPVI and the collagen-binding integrin $\alpha 2\beta 1$ in models of arterial thrombosis, ischemic stroke and hemostasis. Thus, it is tempting to generalize these findings: GPV might be some sort of “master-regulator” in the initiation of thrombus formation but with limited impact during thrombus propagation / stabilization. GPV-deficiency compensates for the lack of GPVI and $\alpha 2\beta 1$ (this study) and was somewhat resistant towards $P2Y_{12}$-blockade in severe laser-injury [67], indicating that GPV-deficiency can (at least partially) compensate for reduced ADP-reinforcement during thrombus formation. The increased initial platelet attachment in *Gp5*$^{-/-}$ mice upon GPIb-blockade (p0p/B) also supports this notion. In contrast, lack of GPV was ineffective in compensating CLEC-2-depletion or deficiency of FXII, which have both been suggested to be required for thrombus propagation, rather than thrombus initiation [166, 178]. Again, the results obtained with p0p/B-treated mice support this model, because GPIb was demonstrated to be essential for incorporation of platelets into growing thrombi [33].

The effects of GPV-deficiency in compensating the loss of several other receptors in tail bleeding assays (see above) clearly demonstrate that the relevance of GPV for hemostasis even exceeds its role in arterial thrombosis.

The mechanism underlying the compensatory effect of GPV-deficiency remains unclear. At first sight, the increased thrombin responsiveness of *Gp5*$^{-/-}$ platelets might explain the phenotypes resulting from GPV-deficiency. This model is further supported by the findings of Mangin *et al.* showing that thrombin can overcome the thrombosis effects of GPVI-deficiency [212]. Similarly, the results with hirudin-treated animals might support the notion that the effect of GPV-deficiency can be ascribed to the increased thrombin responsiveness. On the other hand, it is not surprising that the complete inhibition of thrombin blocks platelet activation and thrombus formation despite GPV-deficiency. Like GPIb or the αIIbβ3 integrin, thrombin is fundamental for thrombus formation [1], which makes it difficult to interpret the data obtained from the hirudin experiments. Likewise, it is not surprising that a combined defect, like GPVI-deficiency and hirudin treatment in the study of Mangin *et al.* [212], has stronger effects than the ones observed upon single-deficiency. The strongest argument against increased thrombin responsiveness as explanation for the observed effects of GPV ablation, are the results obtained with mice lacking FXII and GPV: FXII contributes to thrombin generation via the contact activation pathway; consequently, this pathway is defective in *F12*$^{-/-}$ mice. The extrinsic pathway of thrombin generation via tissue factor and FVII is unaffected [178] or even upregulated in a compensatory manner in mice lacking FXII [179]. Therefore, one would expect to see an effect of GPV-deficiency in a *F12*$^{-/-}$ background, since thrombin is still generated, albeit to a lesser extent than in wildtype mice. The fact that no differences between GPV/FXII-double-deficient and *F12*$^{-/-}$ mice were visible, makes it unlikely that the thrombin responsiveness of *Gp5*$^{-/-}$ platelets is the fundamental characteristic of *Gp5*$^{-/-}$ mice. Nevertheless, currently different approaches are followed up to address the role of thrombin on the effects of GPV-deficiency *in vivo*. One approach is the generation of peptides containing the thrombin cleavage site of GPV to use this in thrombosis models. If the injection of these peptides prevented the effect of GPV-deficiency, this would strongly support the thrombin model. Another possibility is the use of anti-GPV antibodies. If one of the antibodies reproduced the *Gp5*$^{-/-}$ phenotypes without preventing thrombin cleavage of GPV, this would disprove the thrombin hypothesis. However, the latter approach might be hampered by thrombocytopenia, since anti-GPV antibodies were reported to be involved in drug-induced and gold-induced thrombocytopenia [213, 214]. If the thrombin responsiveness was not the reason for the observed effects of GPV-deficiency, what else might explain the phenotype? One explanation might be that the lack of GPV supports or enables interactions

between GPIb-IX and one of its ligands. GPIb is known to bind vWF, thrombin, P-selectin, Mac-1, factor XI, factor XII, HMWK and protein C [reviewed in 27]. GPIb-vWF interactions were unaltered in *Gp5*$^{-/-}$ platelets as compared to wildtype platelets [66, 215 and this study] and thrombin binding capacity of platelets was not affected by GPV-deficiency [67], it appears unlikely that one of these ligands is responsible for the *Gp5*$^{-/-}$ phenotypes. Despite their role in thrombosis, FXI [216], FXII [178] and HMWK [217] are all dispensable for hemostasis making it unlikely that they contribute to the effects of GPV-deficiency. Since a severe reduction of protein C causes thrombosis *per se* [218], this GPIb-interaction partner can probably also be excluded in respect to the *Gp5*$^{-/-}$ phenotypes. A role for MAC-1 in thrombosis or hemostasis has not been reported, excluding it from the list of likely candidates. The remaining ligand P-selectin is involved in thrombosis [219], increased levels of soluble P-selectin propagate ischemic stroke [220] and lack of P-selectin prolongs tail bleeding times [221]. In combination, this makes P-selectin the most likely candidate to explain the *Gp5*$^{-/-}$ phenotype. Of course, it has to be demonstrated whether the absence of GPV indeed results in more pronounced GPIb-P-selectin interactions. To address this, flow adhesion assays on P-selectin will be performed and P-selectin blocking antibodies will be tested in *Gp5*$^{-/-}$ mice. A third possibility to explain the *Gp5*$^{-/-}$ phenotype might be the interaction between GPV and a hitherto unrecognized inhibitory ligand of GPV, which would of course not be able to interact with platelets in *Gp5*$^{-/-}$ mice.

Independent of the mechanism the findings presented here are interesting, because different events can result in GPV shedding from WT platelets. Thus, more or less GPV-deficient platelets are generated at sites of thrombus formation. Locally produced thrombin [61], ADAM17 upon platelet activation [222] and under certain conditions ADAM10 [223], which is activated upon platelet activation or downstream of FXa [224], are all able to shed GPV from the platelet membrane. This raises the possibility that local GPV-shedding might shift the balance of platelet activation towards a pro-thrombotic phenotype thereby promoting thrombus formation. One effect of this could be the counter-regulation of GPVI shedding, since both glycoproteins have been reported to be shed upon thrombotic events such as ischemic stroke [225, 226]. This might be a counteraction against the proposed negative feedback of coagulation on GPVI signaling [227]. To investigate the physiological role of GPV shedding in more detail a transgenic mouse line bearing GPV with a mutated thrombin cleavage site, making it insensitive to thrombin cleavage, will be generated and analyzed.

From the clinical perspective the compensatory capacity of GPV-deficiency seems to be only slightly relevant at first sight. To our knowledge no GPV-deficient patients have been described, making it unlikely that an anti-GPVI therapy would fail due to GPV "overruling". The poor effect of GPV-deficiency in p0p/B-treated mice questions an effect of GPV-blockade in treating von Willebrand disease or similar bleeding disorders, even if it were possible to reproduce a GPV-deficient like phenotype using small molecule inhibitors, anti-GPV antibodies or to induce GPV shedding. However, one clinically highly relevant field of such a therapy could be the prevention of *intracranial hemorrhage* (ICH). ICH is the result of a rupture of a weakened blood vessel and subsequent bleeding into the surrounding brain [228]. Apart from hypertension, hyperglycemia is a risk factor for poor outcomes after ICH. A recent study by Liu *et al.* [229] identified plasma kallikrein, a component of the plasma contact activation pathway (also called Fletcher factor), as key player in hyperglycemia-induced ICH. Plasma kallikrein binds and blocks the GPVI-binding sites of collagen, especially in the presence of high glucose concentrations or under hyperosmolar conditions, thereby preventing platelet activation via GPVI. Liu *et al.* demonstrated that local administration of CRP reduced the hematoma expansion under these conditions, thus demonstrating that GPVI-stimulation is beneficial [229]. The data presented in this thesis demonstrates that GPV-deficiency can compensate for the loss of GPVI. Therefore, it seems possible that GPV-deficiency could compensate for the decreased GPVI-signaling during hyperglycemia. Hence, GPV-deficiency – or a comparable anti-GPV treatment – would be likewise effective under these conditions; thus making GPV-depletion a potential treatment for ICH.

4.2 PLD1 is Indispensable for Proper Shear-Dependent αIIbβ3 Integrin Activation

The results presented in this thesis show that PLD1 is required for proper αIIbβ3 integrin inside-out signaling and stable thrombus formation, particularly under high shear flow conditions. PLD1-deficiency resulted in protection of arterial thrombosis and ischemic brain infarction in experimental models. This indicates that PLD1 may be a fundamental mediator in thrombotic processes and a novel therapeutic target for the treatment of these diseases.

PLD has been implicated in facilitating several cellular functions, including endocytosis and exocytosis (degranulation), cytoskeletal reorganization and cell proliferation and migration [reviewed in 97, 98]. This even spurred speculations that PLD-deficiency might be lethal

[230]. However, mice lacking PLD1 or PLD2 are viable, healthy and fertile, a finding that has meanwhile been reported by others as well [231, 232]. This suggests that deficiency of one isoform can be functionally compensated by the other isoform or any of the other signaling enzymes that increase the production or decrease the catabolism of PA, such as DAG kinases, LysoPA acetyltransferases and PA phosphatases [reviewed in 233].

Studies on the function of phospholipase D isoforms were hampered by the lack of knockout mice or specific inhibitors. Therefore, correlation experiments to link measured PLD activity and certain cellular events were used to conclude about the functions of PLD. The method of choice to characterize the participation of PLD in signaling cascades, was the use of the primary alcohol n-butanol, to divert PLD activity to produce phosphatidylbutanol at the expense of PA [230]. However, 1-butanol only partially prevents PA production even at the maximal applicable concentrations and 1-butanol and phosphatidylbutanol have off-target effects on cell behaviors [100]. Nonetheless, this approach led to the suggestion that PLD might play a role in platelet degranulation [104], which was demonstrated for the secretion of vWF from endothelial cells [234]. Holinstat *et al.* reported that stimulation of PAR-1 activated human platelets in a PLD- and PA-dependent manner [107]. They proposed a positive feedback loop within PAR-1 mediated integrin activation, wherein PKC activates PLD; PLD-derived PA is converted into DAG, thereby reinforcing the activation of PKC and CalDAG-GEF (*Ca^{2+} and Diacylglycerol regulated guanine nucleotide exchange factor I*) [106]. The data presented in this thesis showed a requirement for PLD1 and PA in both G protein– and ITAM–dependent αIIbβ3 integrin activation and, in addition, revealed that the enzyme functions in GPIb-triggered signaling events that enable platelet adhesion under high shear and pathophysiological conditions. According to Holinstat's model [106], with PLD and PKC in one feedback loop, one would expect that degranulation should be impaired as well. However, this study did not reveal any requirement for PLD1 in the process of degranulation of platelet α-granules and dense granules.

The mechanism by which PLD1 and PA facilitate inside-out activation of αIIbβ3 integrin is incompletely understood. Intriguingly though, Powner *et al.* have suggested a potential mechanism for a related process in neutrophils, presenting evidence that the association of talin with a different integrin, MAC-1 (CD11b/CD18, $\alpha_M\beta$2), requires PLD activity [235]. Talin binds to CD11b, the α-subunit of MAC-1, in a PIP_2-dependent manner [236] and PA stimulates PIP_2 production by PI4P5 kinases (PI4K) [237]. Addition of cell-permeable PIP_2 rescues talin binding and CD11b activation in 1-butanol–treated neutrophils, suggesting involvement of PLD action in this step of the integrin activation process. More recently a similar role for PLD1-generated PA has been demonstrated for another β2-integrin, namely LFA-1 (CD11a/CD18, $\alpha_L\beta$2), in human T cells [238]. This study shows that chemokine

receptor activation leads to PLD1 activation via the Rho GTPases Rac1 and RhoA and subsequent stimulation of PI4K-C in a PA-dependent fashion. The authors speculated that PLD interacts with α-actinin which subsequently interacts with LFA-1 to favor the extended low-intermediate-affinity state of the integrin, a process which was independent of PI4K. In addition, the PI4K-C derived PIP_2 was essential for the transition of LFA-1 to the high-affinity state [238] which is in line with model of Powner *et al.* for PLD-triggered integrin activation [235].

This present study revealed that in *Pld1*$^{-/-}$ platelets, recruitment and initial attachment to collagen, a process driven mainly by GPIb, GPVI and integrins, appeared to be normal, whereas subsequent, stable platelet-platelet interaction was defective. This indicated that the first layer of platelets is sufficiently activated, presumably through the GPVI-collagen interaction, to firmly attach to the matrix. However, in upper layers of the growing thrombus, PLD1-deficiency results in impaired platelet activation. Activation of newly recruited platelets on the surface of adherent platelets relies on signals derived from GPIb-vWF interactions and released secondary mediators, specifically ADP and TxA_2. The data in this thesis show that lack of PLD1 affects this activation process, particularly under high shear conditions, suggesting a role of PLD1 in signaling events downstream of GPIb that lead to αIIbβ3 activation. A hypothetical model for the role of PLD1 in αIIbβ3 integrin activation based on the aforementioned studies on β2 integrins is depicted in Figure 4-1.

Furthermore, *Pld1*$^{-/-}$ platelets displayed a reduction in collagen-vWF–dependent phosphatidylserine exposure under high shear condition, which is facilitated by GPIb and αIIbβ3 activation [186]. Thus, it can be concluded that PLD1-deficiency also impairs coagulation.

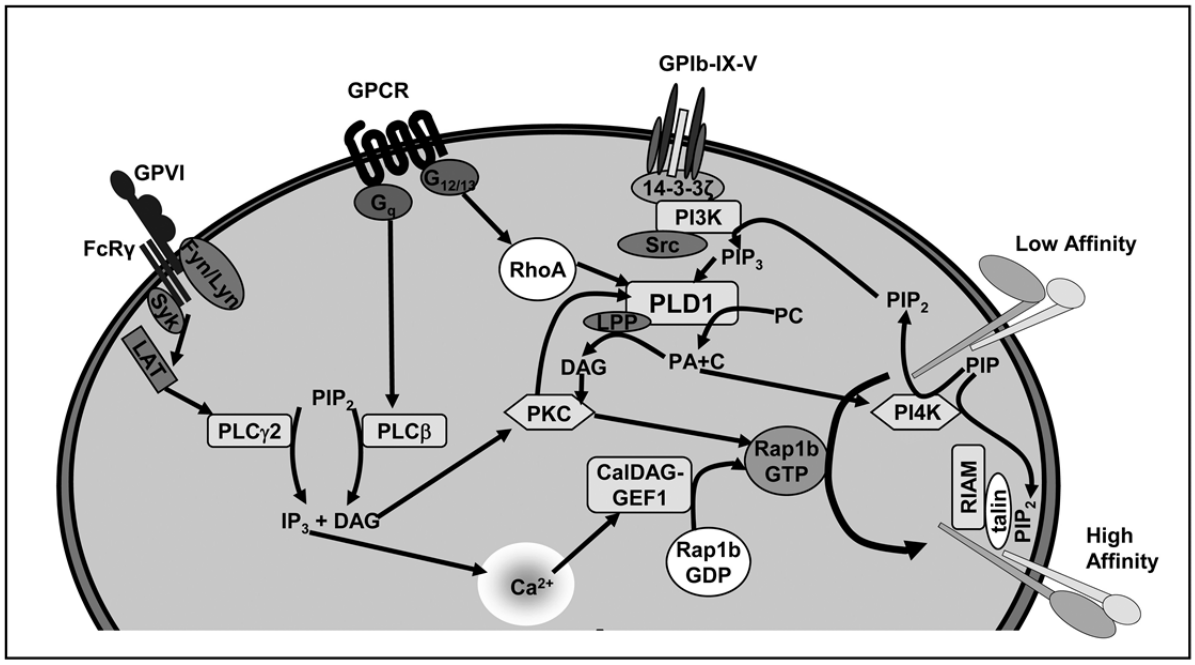

Figure 4-1: Proposed signaling pathways linking PLD1 to integrin activation. Crosslinking of GPVI activates the ITAM-signaling pathway leading to PLCγ2 activation, whereas stimulation of G protein-coupled receptors triggers PLCβ activation via the G_q pathway. Both PLC isoforms hydrolyze *phosphatidylinositol-4,5-bisphosphate* (PIP_2) to *inositol-1,4,5-trisphosphate* (IP_3) and *diacylglycerol* (DAG). IP_3 releases Ca^{2+} from the intracellular stores and triggers *store-operated calcium entry* (SOCE). Elevated Ca^{2+} activates *Ca^{2+} and Diacylglycerol regulated guanine nucleotide exchange factor I* (CalDAG-GEF1) and subsequently Rap1b, whereas DAG activates protein kinase C (PKC), which activates PLD1. PLD1 hydrolyzes *phosphatidylcholine* (PC) to *phosphatidic acid* (PA) and *choline* (C). PA can be converted into DAG via lipid *phosphate phosphatase-1* (LPP) and thereby stimulates PKC, establishing a positive feedback loop between PKC and PLD1. Additionally, PA activates *phosphoinositol-4-phosphate kinase* (PI4K), which converts *phosphatidylinositol-4-phosphate* (PIP) into PIP_2, which is required for PLD activity as well (second feedback loop). GPIb signaling involves *phosphoinositol-3-kinase* (PI3K) which converts PIP_2 into PIP_3, thus activating PLD1. GPCRs activate Rho via the $G_{12/13}$ pathway and Rho GTPases may also activate PLD1. Talin1, which translocates to the plasma membrane upon binding *Rap1–GTP-interacting adaptor molecule* (RIAM), requires PIP_2 to interact with the cytoplasmic tail of β integrins, thereby promoting inside-out activation. Modified from Stegner and Nieswandt, 2011 [8].

The unaltered bleeding times in *Pld1*$^{-/-}$ mice indicate that PLD1 is not essential for normal hemostasis. Based on this result, the enzyme is a candidate target for antithrombotic agents that might not be associated with increased bleeding. This would be of particular interest for the treatment or prophylaxis of ischemic stroke where the risk of intracranial bleeding is a major limitation of current antithrombotic treatment [239].

Blockade of pathologic platelet activity and platelet receptor-ligand interactions has demonstrated that platelets play a fundamental role in cerebral ischemic events, one of the leading causes of death in industrialized countries [180]. It has been shown previously that inhibition of GPIb or GPVI efficiently ameliorated lesion formation in the tMCAO model of ischemic stroke in mice. Although this approach did not induce intracranial hemorrhage, increased bleeding times were observed for the animals [56]. In contrast, although the protection from lesion formation seen in *Pld1*$^{-/-}$ mice was comparable to that achieved by

GPIb inhibition (>70% reduction in infarct size [56]), tail bleeding times were not affected, suggesting that hemostasis was normal. Thus, despite the lack of a clear correlation between bleeding time and risk of clinical hemorrhages [181], PLD1 or targets downstream of PLD1 action might be a preferable target for safe inhibition of thrombotic activity in the arterial system. However, data obtained in murine models of arterial thrombosis or focal cerebral ischemia cannot be directly extrapolated to human patients. Together, our studies reveal an important role for PLD1 in shear-dependent αIIbβ3 integrin activation and platelet aggregate formation and indicate that inhibition of the enzyme might be an effective strategy to prevent intra-arterial occlusive thrombus formation.

4.3 SOCE is Essential for Proper T Cell and Fcγ-Receptor Activation

The data presented in this thesis confirmed parallel reports [129] that both STIM isoforms regulate SOCE in T cells. Further, this work demonstrated that SOCE is functional in macrophages and required for FcγR-mediated phagocytosis. STIM1 is an essential mediator of SOCE in macrophages and required for immune thrombocytopenia and IgG-mediated anaphylaxis. This thesis showed that STIM2 and Orai1 contribute to the pathology of ITP and IgG-mediated anaphylaxis.

Oh-Hora *et al.* were unable to detect STIM2 protein in naïve CD4-positive T cells, but reported that T cell activation led to increased expression of STIM2 [129]. In contrast to their results, we were able to detect considerable amounts of STIM2 already in naïve T cells (Figure 3-23A, inlay). One explanation might be differences in the immuno-blotting protocols. The more likely reason is, however, the different genetic background of the *Stim2*$^{-/-}$ mice. Their mice were on a C57Bl/6 background, while our mice had a mixed Sv129/B6 background. These differences might also explain the different mortality of the two mouse lines. The authors reported that all *Stim2*$^{-/-}$ mice died within 5 weeks [129]. In the *Stim2*$^{-/-}$ mouse line analyzed in the present study, homozygous knockout mice reached the age of 6-8 weeks, before the first mice died spontaneously [169]. However, backcrossing of our mice to C57Bl/6 background decreased the survival rate (not shown).

In line with previous reports [129, 131], this study confirmed that the lack of STIM1 blunted TG- or TCR-stimulation induced SOCE (Figure 3-23). This resulted in defective *interleukin* (IL) 2 and *interferon* (IFN) γ production [129, 188], whereupon the quality of the stimulus seems to influence the severity of the observed phenotype [131, 188].

In contrast to previous reports [129], here a considerable reduction in CD3-triggered SOCE of CD4 positive T cells (Figure 3-23) and thymocytes from STIM2-deficient mice was observed (not shown). These differences between the data presented here and findings of Oh-Hora *et al.* can be most likely attributed to the different STIM2 protein levels observed in the different mouse lines. Also Oh-Hora *et al.* did observe effects of STIM2-deficiency when they stimulated T cells for a longer period of time, resulting in impaired IL-2 and IFNγ production [129]. The analysis of *Stim2*$^{-/-}$ T cells from mice used in this study did not reveal altered IL-2 production. However, IFNγ and IL-17 production were reduced in neuroantigen-specific *Stim2*$^{-/-}$ T cells. Additionally, proliferation of *Stim2*$^{-/-}$ splenocytes was impaired *in vitro* [188]. It has been demonstrated that STIM2 contributes to the pathology of EAE, a model of multiple sclerosis. Considering these findings, one could speculate that both STIM isoforms are also relevant in platelet specific T cells in ITP. However, this needs to be demonstrated in a T cell-driven model of this pathology.

Neither this study (Figure 3-23 and data not shown), nor Oh-Hora *et al.* [129] reported any differences in basal calcium levels of *Stim2*$^{-/-}$ T cells. This indicated that STIM2 is probably not required as a regulator of basal calcium levels in T cells, as proposed by Brandman *et al.* [135].

Lack of STIM1 [129, 131], STIM2 [129, 188, 240] or Orai1 [126, 130] seems to be dispensable for normal T and B cell development, thereby contradicting the long-standing hypothesis that SOCE is required for T cell development [133]. Nevertheless, STIM1-deficient [132], but not Orai1-deficient [120], human patients or mice lacking both STIM isoforms [129] have substantially reduced Treg numbers, which might explain the observed lymphoproliferation and autoimmunity phenotypes [133]. This suggests that SOCE is essential for the development of this specific T cell subset, while its absence can be compensated during general T cell development.

The thapsigargin measurements with peritoneal lavage cells clearly demonstrated that SOCE is functional in macrophages (Figure 3-24A, B). These results revealed that STIM1 is the essential Ca^{2+}-sensor, while Orai1 seems to be the main CRAC channel, at least in naïve peritoneal macrophages. STIM2 seems to be dispensable for TG or 2.4G2-induced SOCE in peritoneal lavage cells, even though the protein is expressed in these cells [240]. The results obtained with macrophages from *Stim1*$^{-/-}$ mice upon 2.4G2 crosslinking, which activates FcγRIII and FcγRIIb, demonstrated that SOCE is indeed the major route of Ca^{2+}-entry upon activation of Fcγ receptors (Figure 3-24C, D). To our knowledge this study is the first to provide definite proof for the relevance of SOCE in macrophages. Since STIM2-deficiency

did not impair SOCE, it seems likely that the remaining calcium entry in *Stim1*$^{-/-}$ macrophages upon FcγR activation originates from non-SOCE, probably triggered via DAG [241]. Lack of STIM1 also impaired store-release, while Orai1-deficiency had no effect. STIM2-deficient macrophages had a tendency to increased store-release (Figure 3-24). The reduced store-release in *Stim1*$^{-/-}$ macrophages indicated that calcium levels within the ER were reduced. This suggested a role for STIM1 in maintaining ER calcium levels. However, the observed basal calcium levels in macrophages are rather low and thus close to the detection limit of the fluorimeter. This makes it difficult to draw definitive conclusions about the role of the STIM isoforms in regulating basal calcium levels. Genetic ablation of *Stim1* resulted in increased blood monocyte and resident *peritoneal monocyte* (PM) counts [195], however this might also be a secondary defect. Monocyte counts in STIM2-deficient mice were grossly normal [240] and PM from wildtype, *Stim1*$^{-/-}$ or *Stim2*$^{-/-}$ mice were microscopically indistinguishable [195, 240]. Thus, we conclude that the isolated loss of either STIM isoform is not essential for monocyte/macrophage development or transmigration into the peritoneum. However, lack of either STIM isoform did affect the expression pattern of FcγR (Figure 3-25). STIM1-deficiency shifted the FcγRIII/FcγRIV ratio towards FcγRIV and since the 2.4G2 signals were unaltered, despite reduced FcγRIII-values, it seems likely that *Stim1*$^{-/-}$ macrophages have increased levels of FcγRIIb as well. Lack of STIM2 resulted in increased FcγRIII and FcγRIV expression levels (Figure 3-25). This suggests that this STIM isoform is involved in the regulation of FcγR expression, despite normal calcium fluxes (Figure 3-24). *Fcer1g*$^{+/-}$ macrophages, which express only 50% of normal FcRγ-chain levels and consequently bear only 50% of wildtype FcγRIII levels, were not impaired in phagocytosis assays [195]. Therefore, the alterations in the FcγR levels of STIM-mutant mice should not impair the phagocytic capacity of STIM-deficient macrophages.

STIM1-deficiency abrogated phagocytosis *in vitro*, demonstrating that rises of intracellular Ca^{2+} levels $[Ca^{2+}]_i$ are essential for FcγR-mediated phagocytosis [195], thus supporting an essential role of Ca^{2+}-mobilization of this process. Recently this key finding has been confirmed by a second group which assessed the relevance of SOCE for FcγR-mediated phagocytosis in granulocyte-like HL-60 cells [242]. The results obtained with *Stim1*$^{-/-}$ mice in the ITP model suggested that STIM1 is equally important as the absence of the activating FcγR (Figure 3-26). These data demonstrated that STIM1 and elevated $[Ca^{2+}]_i$ are essential for FcγR-mediated phagocytosis *in vivo*. Similar results were obtained in a model of *autoimmune hemolytic anemia* (AIHA) [195]. STIM1-deficient macrophages failed to generate bioactive C5a, but were able to produce considerable amounts of cytokines [195]. Thus, it can be concluded that cytokine production does not solely rely on SOCE [195].

Orai1-deficiency moderately protected against JON3- (IgG1) but not from JON1-mediated (IgG2b) thrombocytopenia (Figure 3-26). The effect of Orai1-deficiency was considerably lower than the effect of STIM1-deficiency. Hence, it can be concluded that STIM1 is of greater relevance to immune thrombocytopenia than Orai1. The differences between STIM1- and Orai1-deficiency could be explained in different ways: (I) Other CRAC channels, such as Orai2 or Orai3 might compensate for the lack of Orai1. (II) Ca^{2+} elevations resulting from store-release, which is reduced in *Stim1*$^{-/-}$, but not in *Orai1*$^{-/-}$ macrophages, could be sufficient to enable phagocytosis. This would be in line with early studies, indicating that chelation of extracellular Ca^{2+} only partially inhibited phagocytosis [153, 154]. Further support comes from a recent publication on FcγR-mediated phagocytosis in granulocyte-like cells. The authors concluded that store-release is required for FcγR-mediated phagocytosis, while extracellular Ca^{2+} – and therefore SOCE – is not important [242]. However, calcium measurements with FcγR stimulation and *in vitro* phagocytosis assays with *Orai1*$^{-/-}$ macrophages are required to confirm this hypothesis. The observed difference between the two anti-GPIIb/IIIa antibodies is in line with the general observation that IgG2b antibodies, like JON1, possess a higher activity than antibodies of the IgG1 subclass *in vivo* [243]. This would indicate that JON1 induces stronger responses than JON3. Thus, raising the possibility that increased store-release and non-SOCE can fully compensate for the lack of Orai1. In this scenario JON3 would induce weaker responses, which depend on Orai1-mediated calcium influx. Another possibility would be that FcγRIII-triggered SOCE requires STIM1 and Orai1, while FcγRIV stimulation leads to calcium influx via STIM1 and a CRAC channel, other than Orai1. However, to my knowledge such a pathway-dependent selection of CRAC channels has not been reported yet. Again, more experiments have to be done to understand the underlying mechanisms of the different outcome in *Orai1*$^{-/-}$ mice.

Stim2$^{-/-}$ mice were protected against IgG-induced thrombocytopenia (Figure 3-27). Considering the calcium measurements these results are somewhat contradictory. However, calcium measurements were performed with peritoneal macrophages, whereas IgG-opsonized platelets are cleared by splenic macrophages [148]. Considering the diversity of different monocyte subsets [244], it might well be that STIM2 expression and/or its contribution to SOCE differs between the different macrophage / monocyte subtypes. In addition, it has been reported that STIM2 expression increases in peritoneal macrophages upon LPS stimulation [133] and similar changes of STIM2 expression have been observed in T cells [129]. This might also result in a greater relevance of STIM2 in splenic than in peritoneal macrophages. Calcium measurements with splenic macrophages of *Stim2*$^{-/-}$ mice could help to address this issue. Similar to the results with *Orai1*$^{-/-}$ mice, the effect of STIM2-deficiency differed between JON1- and JON3-mediated thrombocytopenia. While STIM2-

deficiency was protective at low doses of JON1 it had no effect at higher doses of JON1 (which were still too low to induce anaphylaxis). In contrast, lack of STIM2 was protective in JON3-induced thrombocytopenia independent of the dose tested (Figure 3-27). Again, one could argue with different pathogenicity of the two JON antibodies or with differences downstream of the respective FcγRs.

Previous work of our laboratory demonstrated that high doses of JON antibodies trigger Fc-dependent acute anaphylaxis, which is accompanied by the formation of microparticle-like structures [146, 194, 196]. These structures might resemble platelet-derived IgG immune complexes, which have been reported in HIV-1 related ITP in human patients [245]. Thus, high doses of JON antibodies triggered systemic anaphylaxis resembles a unique kind of type I inflammation. Therefore, mice lacking the FcRγ-chain and STIM1-deficient animals were challenged with high doses of JON antibodies. This caused an anaphylactic shock and severe hypothermia in control mice, but not in mice lacking the FcRγ-chain (Figure 3-28), which is in line with previous reports [194, 196, 246]. STIM1-deficiency was equally protective demonstrating that STIM1 is an essential effector downstream of FcγR in this pathology.

Also *Orai1*$^{-/-}$ mice were protected against JON-induced anaphylaxis (Figure 3-28) indicating that Orai1 is crucial for anti-GPIIb/IIIa triggered acute systemic reactions. The present concept links IgG-mediated anaphylaxis to the FcγR-macrophages - *platelet-activating factor* (PAF) axis [reviewed in 247]. In line with this, it has been demonstrated that PAF contributes to the anaphylactic response following JON-injection [146]. Therefore, one could speculate that Orai1 is required for the synthesis and/or release of this pro-inflammatory phospholipid. The requirement of extracellular Ca^{2+} for the proper synthesis and release of PAF in neutrophils [248] might support this hypothesis. Comparable results of Orai1-deficiency have been reported in mast cells [126]: Lack of Orai1 resulted in defective secretion of lipid mediators and impaired degranulation.

Deficiency of STIM2 protected mice from JON-induced anaphylaxis, albeit to a lesser extent than the lack of STIM1 (Figure 3-28). This indicated that STIM2 contributes to the systemic responses triggered by IgG-GPIIb/IIIa immune complexes. The protective effect of STIM2-deficiency is blood-borne, because IgG-mediated anaphylaxis was also ameliorated in *Stim2*$^{-/-}$ bone marrow chimeric mice as well (not shown).

To investigate whether STIM2-deficiency was protective in IgE-mediated anaphylaxis as well, *Stim2*$^{-/-}$ mice were assessed in this model. Lack of STIM2 ameliorated the IgE-triggered anaphylaxis (Figure 3-29). For comparison, *Stim1*$^{-/-}$ mice were subjected to the same experiment, revealing that these mice were completely protected (Figure 3-29), thus confirming previous reports [125]. This data indicated that STIM2 might be a co-regulator of SOCE downstream of FcεR. In an attempt to assess the relevance of STIM2 more directly, Ca^{2+}-measurements with *Stim2*$^{-/-}$ mast cells were performed (not shown). Neither thapsigargin, nor FcεR-crosslinking induced calcium fluxes were altered in *Stim2*$^{-/-}$ mast cells. In contrast, lack of STIM1 impaired store-release and abolished SOCE, leading to defective mast cell degranulation [125]. Likewise, Orai1-defiency causes blunted SOCE and impaired degranulation downstream of FcεR stimulation [126]. However, as evident by the macrophage study of these thesis (see above), unaltered Ca^{2+}-fluxes in naïve cells are not necessarily linked to normal responses *in vivo*. Hence, bone marrow chimeric *Stim2*$^{-/-}$ mice were generated and their response towards IgE-induced anaphylaxis were assessed (Figure 3-29). This time no effects of STIM2-deficiency could be observed, indicating that the protective effect of STIM2-deficiency in constitutive knockout animals was not related to mast cell function. Preliminary results with histamine ELISA measurements following FcεR-crosslinking (with anti-DNP-IgE and DNP) *in vivo*, support this notion, since no difference in histamine serum levels could be observed (not shown). Histamine is the primary mediator of IgE-induced anaphylaxis, but PAF also contributes to the pathology [247]. However, given the results with *Stim2*$^{-/-}$ bone marrow chimeric animals upon IgG-induced anaphylaxis it seems unlikely that the PAF-response is responsible for the phenotype of *Stim2*$^{-/-}$ mice in IgE-triggered hypothermia. Most likely the histamine response is altered, if STIM2 is missing in non-hematopoietic cells. First attempts to test this directly by injecting histamine to induce anaphylaxis turned out to be technically challenging and have been unsuccessful so far. Nevertheless, one might speculate that body thermoregulation via histamine receptor bearing neurons in the hypothalamus [249] are affected in *Stim2*$^{-/-}$ mice. This is especially tempting in the light of the results obtained in *Stim2*$^{-/-}$ neurons [169], which revealed that STIM2 is the predominant STIM isoform in the brain.

In summary, the results obtained in this study, together with the published literature [5, 109] establish STIM1 as an essential Ca^{2+}-sensor within the ER and as central regulator of SOCE in all hematopoietic cells. STIM2 seems to be dispensable for the activation of mast cells (this study) and platelets [169, 250], but acts as a co-regulator of SOCE in macrophages and T cells [see above & 188]. To date, a central role of STIM2 as Ca^{2+}-sensor and regulator of SOCE has only been reported for two cell types: One study originates from our laboratory,

which revealed that STIM2, but not STIM1, is the essential regulator of neuronal SOCE (termed CCE, *capacitive Ca^{2+}-entry*). STIM2-deficiency protected against hypoxic conditions *in vitro* and *in vivo*, making *Stim2*$^{-/-}$ mice less susceptible to focal cerebral ischemia [169]. The second study suggested that STIM2, but not STIM1, is the essential mediator of SOCE in murine dendritic cells [251]. Of note, both reports state that Orai1 is dispensable [169] or of minor importance [251] in the respective cell type, raising the interesting possibility that the STIM2-Orai2 axis might be the pendant to the classical STIM1-Orai1 axis, in these cells.

The data presented in this thesis establish a role for Orai1 in FcγR-signaling, indicating that it is at least one of the CRAC channels in macrophages. Likewise, an essential role of Orai1 has already been reported for mast cells [126], platelets [128] and human T cells [120], while its role for murine T cells is under discussion [126, 130].

Given the broad variety of immune cell effector functions that rely on SOCE and considering that dysregulation of Ca^{2+}-signaling is involved in autoimmune and inflammatory disorders [252], interfering with SOCE might be a feasible approach to treat autoimmune diseases, or allergic responses [see also 119]. Despite the crucial importance of SOCE, STIM1-deficiency does not affect all immune responses, because *Stim1*$^{-/-}$ mice were able to mount humoral immune responses [131], indicating that at least short-time treatments might have a justifiable risk profile. In view of the comparable mild phenotype of *Stim2*$^{-/-}$ mice, STIM2 might be a relatively safe target in treating pathologies like multiple sclerosis or immune thrombocytopenia. The practicability of an ITP-treatment that targets molecules downstream of Fcγ receptors has recently been demonstrated with the use of a Syk inhibitor [253]. Inhibition of the tyrosine kinase Syk impairs ITAM-signaling downstream of FcγR (see Figure 1-7) and at least partially restored platelet count in a murine ITP model and in a subset of patients with refractory ITP. However, this treatment had some side effects that were detected in liver function tests [253]. In contrast, STIM1- or STIM2-deficiency did not affect standard liver parameters in mice [188], suggesting that STIMs could be a preferable target for the treatment of ITP. On the other hand, human patients lacking STIM1 suffer from AIHA and ITP [132]. This indicates that STIM1-deficiency did not prevent phagocytosis of red blood cells or platelets in these patients, possibly due to a different relevance of STIM1 for macrophage function in human and mice. Of note, bone marrow chimeric mice were analyzed which still expressed Stim1 in non-hematopoietic cells, while the human patients completely lacked STIM1. However, this does not offer a direct explanation for the discrepancies between the reported effects of STIM1-deficiency in mice and human patients.

4.4 Concluding Remarks

The work presented here reveals an unexpected role of GPV in modulating thrombus formation and shows that PLD1 is required for shear-dependent integrin activation. In addition, evidence for a crucial role for SOCE and the two STIM isoforms in FcγR-activation as well as in immune thrombocytopenia is provided.

The major findings are:

GPV and thrombus formation:

- GPV and α2β1 have partially redundant functions in collagen-triggered platelet aggregation
- GPV limits thrombus formation and hemostasis
- GPV-deficiency permits thrombus formation in mice lacking the two major collagen receptors GPVI and α2β1
- Lack of GPV prevents a protective effect of GPVI-deficiency in ischemic stroke
- GPV-deficiency restores the hemostatic function of mice lacking both ITAM-receptors

Function of PLD1 in platelets

- *Pld1*$^{-/-}$ and *Pld2*$^{-/-}$ mice are viable, fertile and apparently healthy
- PLD1 is responsible for the inducible PLD-activity in platelets
- PLD1 contributes to proper integrin activation under static conditions
- PLD1 is essential for proper GPIb-mediated integrin activation
- Mice deficient in PLD1 are protected against arterial thrombosis and ischemic stroke
- Lack of PLD1 does not result in hemostatic defects

Role of SOCE in T cell receptor and FcγR activation

- Both STIM isoforms contribute to calcium mobilization downstream of T cell receptor activation
- FcγR stimulation results in store-operated calcium entry
- FcγR-triggered SOCE is mediated by STIM1 and probably Orai1
- SOCE is essential for immune thrombocytopenia
- Both STIM isoforms contribute to platelet clearance during ITP
- SOCE via STIM1 and Orai1 is essential for IgG-mediated systemic anaphylaxis

- STIM2 contributes to IgG-mediated, but not to IgE-mediated systemic anaphylaxis

4.5 Outlook

This study could not provide the information how GPV regulates thrombus formation. Analysis of mice treated with anti-GPV antibodies and flow adhesion studies on P-selectin could help to understand the role of GPV. The generation and analysis of mice with a mutated thrombin-cleavage site within GPV will shed new light on the function of GPV in thrombus formation.

Genetic ablation of PLD1 resulted in abolished inducible PLD activity in platelets, while the basal PLD activity, which is mostly mediated by PLD2, remained unaltered. Therefore, platelet function of PLD2-deficient mice will be investigated. To understand whether both PLD isoforms have redundant functions, double-deficient mice will be analyzed in future. Further studies are planned in our laboratory to investigate the function of PLD not only in platelets and megakaryocytes, but also in cells of the immune system. This includes the study of PLD1-deficient T cells in a model of multiple sclerosis and the analysis of *Pld1*$^{-/-}$ macrophages in ITP. Furthermore, a PLD assay, which enables activity measurements in intact cells, will be established. These measurements in wildtype and PLD-deficient platelets will provide information about the isoform specificity of the different signaling pathways. Likewise, analyses of platelets from mice lacking proposed regulators of PLD, e.g. Rho GTPases, might reveal whether these proteins indeed influence PLD activity in the tested signaling pathways.

The process of calcium mobilization upon FcγR stimulation is still poorly understood. Further studies on macrophages deficient in STIM2 or Orai1 will provide deeper insight in the relevance of these components of the SOCE machinery.

5 References

1 Ruggeri ZM. Platelets in atherothrombosis. *Nature Medicine*. 2002; **8**: 1227-34.

2 Savage B, Saldivar E, Ruggeri ZM. Initiation of platelet adhesion by arrest onto fibrinogen or translocation on von Willebrand factor. *Cell*. 1996; **84**: 289-97.

3 Nieswandt B, Watson SP. Platelet-collagen interaction: is GPVI the central receptor? *Blood*. 2003; **102**: 449-61.

4 Watson SP, Herbert JM, Pollitt AY. GPVI and CLEC-2 in haemostasis and vascular integrity. *JThrombHaemost*. 2010; **8**: 1456-67.

5 Varga-Szabo D, Braun A, Nieswandt B. Calcium signaling in platelets. *JThrombHaemost*. 2009; **7**: 1057-66.

6 Gruner S, Prostredna M, Schulte V, Krieg T, Eckes B, Brakebusch C, Nieswandt B. Multiple integrin-ligand interactions synergize in shear-resistant platelet adhesion at sites of arterial injury in vivo. *Blood*. 2003; **102**: 4021-7.

7 Varga-Szabo D, Pleines I, Nieswandt B. Cell adhesion mechanisms in platelets. *Arteriosclerosis, Thrombosis, and Vascular Biology*. 2008; **28**: 403-12.

8 Stegner D, Nieswandt B. Platelet receptor signaling in thrombus formation. *J Mol Med*. 2011; **89**: 109-21.

9 Heemskerk JW, Kuijpers MJ, Munnix IC, Siljander PR. Platelet collagen receptors and coagulation. A characteristic platelet response as possible target for antithrombotic treatment. *Trends in Cardiovascular Medicine*. 2005; **15**: 86-92.

10 Lentz BR. Exposure of platelet membrane phosphatidylserine regulates blood coagulation. *Prog Lipid Res*. 2003; **42**: 423-38.

11 Muller F, Mutch NJ, Schenk WA, Smith SA, Esterl L, Spronk HM, Schmidbauer S, Gahl WA, Morrissey JH, Renne T. Platelet polyphosphates are proinflammatory and procoagulant mediators in vivo. *Cell*. 2009; **139**: 1143-56.

12 Kannemeier C, Shibamiya A, Nakazawa F, Trusheim H, Ruppert C, Markart P, Song Y, Tzima E, Kennerknecht E, Niepmann M, von Bruehl ML, Sedding D, Massberg S, Gunther A, Engelmann B, Preissner KT. Extracellular RNA constitutes a natural procoagulant cofactor in blood coagulation. *ProcNatlAcadSciUSA*. 2007; **104**: 6388-93.

13 Coughlin SR. Thrombin signalling and protease-activated receptors. *Nature*. 2000; **407**: 258-64.

14 Sambrano GR, Weiss EJ, Zheng YW, Huang W, Coughlin SR. Role of thrombin signalling in platelets in haemostasis and thrombosis. *Nature*. 2001; **413**: 74-8.

15 Offermanns S. Activation of platelet function through G protein-coupled receptors. *Circulation Research*. 2006; **99**: 1293-304.

16 Hart MJ, Jiang X, Kozasa T, Roscoe W, Singer WD, Gilman AG, Sternweis PC, Bollag G. Direct stimulation of the guanine nucleotide exchange activity of p115 RhoGEF by Galpha13. *Science*. 1998; **280**: 2112-4.

17 Cantley LC. The phosphoinositide 3-kinase pathway. *Science*. 2002; **296**: 1655-7.

18 Offermanns S, Toombs CF, Hu YH, Simon MI. Defective platelet activation in G alpha(q)-deficient mice. *Nature*. 1997; **389**: 183-6.

19 Shattil SJ, Kim C, Ginsberg MH. The final steps of integrin activation: the end game. *NatRevMolCell Biol*. 2010; **11**: 288-300.

20 Lopez JA, Andrews RK, fshar-Kharghan V, Berndt MC. Bernard-Soulier syndrome. *Blood*. 1998; **91**: 4397-418.

21 Luo SZ, Mo X, Afshar-Kharghan V, Srinivasan S, Lopez JA, Li R. Glycoprotein Ibalpha forms disulfide bonds with 2 glycoprotein Ibbeta subunits in the resting platelet. *Blood*. 2007; **109**: 603-9.

22 Canobbio I, Balduini C, Torti M. Signalling through the platelet glycoprotein Ib-V-IX complex. *Cell Signal*. 2004; **16**: 1329-44.

23 Ware J, Russell S, Ruggeri ZM. Generation and rescue of a murine model of platelet dysfunction: the Bernard-Soulier syndrome. *ProcNatlAcadSciUSA*. 2000; **97**: 2803-8.

24 Kato K, Martinez C, Russell S, Nurden P, Nurden A, Fiering S, Ware J. Genetic deletion of mouse platelet glycoprotein Ibbeta produces a Bernard-Soulier phenotype with increased alpha-granule size. *Blood*. 2004; **104**: 2339-44.

25 Kahn ML, Diacovo TG, Bainton DF, Lanza F, Trejo J, Coughlin SR. Glycoprotein V-deficient platelets have undiminished thrombin responsiveness and Do not exhibit a Bernard-Soulier phenotype. *Blood*. 1999; **94**: 4112-21.

26 Clemetson KJ. A short history of platelet glycoprotein Ib complex. *Thromb Haemost*. 2007; **98**: 63-8.

27 Ruggeri ZM, Zarpellon A, Roberts JR, Mc Clintock RA, Jing H, Mendolicchio GL. Unravelling the mechanism and significance of thrombin binding to platelet glycoprotein Ib. *Thromb Haemost*. 2010; **104**: 894-902.

28 Andrews RK, Munday AD, Mitchell CA, Berndt MC. Interaction of calmodulin with the cytoplasmic domain of the platelet membrane glycoprotein Ib-IX-V complex. *Blood*. 2001; **98**: 681-7.

29 Bergmeier W, Piffath CL, Cheng G, Dole VS, Zhang Y, von Andrian UH, Wagner DD. Tumor necrosis factor-alpha-converting enzyme (ADAM17) mediates GPIbalpha shedding from platelets in vitro and in vivo. *Circulation Research*. 2004; **95**: 677-83.

30 Maxwell MJ, Westein E, Nesbitt WS, Giuliano S, Dopheide SM, Jackson SP. Identification of a 2-stage platelet aggregation process mediating shear-dependent thrombus formation. *Blood*. 2007; **109**: 566-76.

31 Nesbitt WS, Westein E, Tovar-Lopez FJ, Tolouei E, Mitchell A, Fu J, Carberry J, Fouras A, Jackson SP. A shear gradient-dependent platelet aggregation mechanism drives thrombus formation. *Nature Medicine*. 2009; **15**: 665-73.

32 Ruggeri ZM, Orje JN, Habermann R, Federici AB, Reininger AJ. Activation-independent platelet adhesion and aggregation under elevated shear stress. *Blood*. 2006; **108**: 1903-10.

33 Bergmeier W, Piffath CL, Goerge T, Cifuni SM, Ruggeri ZM, Ware J, Wagner DD. The role of platelet adhesion receptor GPIbalpha far exceeds that of its main ligand, von Willebrand factor, in arterial thrombosis. *ProcNatlAcadSciUSA*. 2006; **103**: 16900-5.

34 Ruggeri ZM, Mendolicchio GL. Adhesion mechanisms in platelet function. *Circulation Research*. 2007; **100**: 1673-85.

35 Howard MA, Firkin BG. Ristocetin--a new tool in the investigation of platelet aggregation. *Thromb Diath Haemorrh*. 1971; **26**: 362-9.

36 Brinkhous KM, Read MS, Fricke WA, Wagner RH. Botrocetin (venom coagglutinin): reaction with a broad spectrum of multimeric forms of factor VIII macromolecular complex. *Proc Natl Acad Sci U S A*. 1983; **80**: 1463-6.

37 Rathore V, Stapleton MA, Hillery CA, Montgomery RR, Nichols TC, Merricks EP, Newman DK, Newman PJ. PECAM-1 negatively regulates GPIb/V/IX signaling in murine platelets. *Blood*. 2003; **102**: 3658-64.

38 Liu J, Fitzgerald ME, Berndt MC, Jackson CW, Gartner TK. Bruton tyrosine kinase is essential for botrocetin/VWF-induced signaling and GPIb-dependent thrombus formation in vivo. *Blood*. 2006; **108**: 2596-603.

39 Yin H, Liu J, Li Z, Berndt MC, Lowell CA, Du X. Src family tyrosine kinase Lyn mediates VWF/GPIb-IX-induced platelet activation via the cGMP signaling pathway. *Blood*. 2008; **112**: 1139-46.

40 Elvers M, Stegner D, Hagedorn I, Kleinschnitz C, Braun A, Kuijpers ME, Boesl M, Chen Q, Heemskerk JW, Stoll G, Frohman MA, Nieswandt B. Impaired alpha(IIb)beta(3) integrin activation and shear-dependent thrombus formation in mice lacking phospholipase D1. *SciSignal*. 2010; **3**: ra1.

41 Bergmeier W, Rackebrandt K, Schroder W, Zirngibl H, Nieswandt B. Structural and functional characterization of the mouse von Willebrand factor receptor GPIb-IX with novel monoclonal antibodies. *Blood*. 2000; **95**: 886-93.

42 Ozaki Y, Asazuma N, Suzuki-Inoue K, Berndt MC. Platelet GPIb-IX-V-dependent signaling. *JThrombHaemost*. 2005; **3**: 1745-51.

43 Kasirer-Friede A, Moran B, Nagrampa-Orje J, Swanson K, Ruggeri ZM, Schraven B, Neel BG, Koretzky G, Shattil SJ. ADAP is required for normal alphaIIbbeta3 activation by VWF/GP Ib-IX-V and other agonists. *Blood*. 2007; **109**: 1018-25.

44 Bodnar RJ, Xi X, Li Z, Berndt MC, Du X. Regulation of glycoprotein Ib-IX-von Willebrand factor interaction by cAMP-dependent protein kinase-mediated phosphorylation at Ser 166 of glycoprotein Ib(beta). *J Biol Chem*. 2002; **277**: 47080-7.

45 Falati S, Edmead CE, Poole AW. Glycoprotein Ib-V-IX, a receptor for von Willebrand factor, couples physically and functionally to the Fc receptor gamma-chain, Fyn, and Lyn to activate human platelets. *Blood*. 1999; **94**: 1648-56.

46 Wu Y, Suzuki-Inoue K, Satoh K, Asazuma N, Yatomi Y, Berndt MC, Ozaki Y. Role of Fc receptor gamma-chain in platelet glycoprotein Ib-mediated signaling. *Blood*. 2001; **97**: 3836-45.

47 Canobbio I, Bertoni A, Lova P, Paganini S, Hirsch E, Sinigaglia F, Balduini C, Torti M. Platelet activation by von Willebrand factor requires coordinated signaling through thromboxane A2 and Fc gamma IIA receptor. *J Biol Chem*. 2001; **276**: 26022-9.

48 Kasirer-Friede A, Cozzi MR, Mazzucato M, De ML, Ruggeri ZM, Shattil SJ. Signaling through GP Ib-IX-V activates alpha IIb beta 3 independently of other receptors. *Blood*. 2004; **103**: 3403-11.

49 Du X, Fox JE, Pei S. Identification of a binding sequence for the 14-3-3 protein within the cytoplasmic domain of the adhesion receptor, platelet glycoprotein Ib alpha. *J Biol Chem*. 1996; **271**: 7362-7.

50 Wu Y, Asazuma N, Satoh K, Yatomi Y, Takafuta T, Berndt MC, Ozaki Y. Interaction between von Willebrand factor and glycoprotein Ib activates Src kinase in human platelets: role of phosphoinositide 3-kinase. *Blood*. 2003; **101**: 3469-76.

51 Yap CL, Anderson KE, Hughan SC, Dopheide SM, Salem HH, Jackson SP. Essential role for phosphoinositide 3-kinase in shear-dependent signaling between platelet glycoprotein Ib/V/IX and integrin alpha(IIb)beta(3). *Blood*. 2002; **99**: 151-8.

52 Munday AD, Berndt MC, Mitchell CA. Phosphoinositide 3-kinase forms a complex with platelet membrane glycoprotein Ib-IX-V complex and 14-3-3zeta. *Blood*. 2000; **96**: 577-84.

53 Du X. Signaling and regulation of the platelet glycoprotein Ib-IX-V complex. *Curr Opin Hematol*. 2007; **14**: 262-9.

54 Li Z, Zhang G, Feil R, Han J, Du X. Sequential activation of p38 and ERK pathways by cGMP-dependent protein kinase leading to activation of the platelet integrin alphaIIb beta3. *Blood*. 2006; **107**: 965-72.

55 Massberg S, Gawaz M, Gruner S, Schulte V, Konrad I, Zohlnhofer D, Heinzmann U, Nieswandt B. A crucial role of glycoprotein VI for platelet recruitment to the injured arterial wall in vivo. *Journal of Experimental Medicine*. 2003; **197**: 41-9.

56 Kleinschnitz C, Pozgajova M, Pham M, Bendszus M, Nieswandt B, Stoll G. Targeting platelets in acute experimental stroke: impact of glycoprotein Ib, VI, and IIb/IIIa blockade on infarct size, functional outcome, and intracranial bleeding. *Circulation*. 2007; **115**: 2323-30.

57 Kleinschnitz C, De Meyer SF, Schwarz T, Austinat M, Vanhoorelbeke K, Nieswandt B, Deckmyn H, Stoll G. Deficiency of von Willebrand factor protects mice from ischemic stroke. *Blood*. 2009; **113**: 3600-3.

58 Dong JF, Gao S, Lopez JA. Synthesis, assembly, and intracellular transport of the platelet glycoprotein Ib-IX-V complex. *J Biol Chem*. 1998; **273**: 31449-54.

59 Li CQ, Dong JF, Lanza F, Sanan DA, Sae-Tung G, Lopez JA. Expression of platelet glycoprotein (GP) V in heterologous cells and evidence for its association with GP Ib alpha in forming a GP Ib-IX-V complex on the cell surface. *J Biol Chem*. 1995; **270**: 16302-7.

60 Fredrickson BJ, Dong JF, McIntire LV, Lopez JA. Shear-dependent rolling on von Willebrand factor of mammalian cells expressing the platelet glycoprotein Ib-IX-V complex. *Blood*. 1998; **92**: 3684-93.

61 Ravanat C, Morales M, Azorsa DO, Moog S, Schuhler S, Grunert P, Loew D, Van Dorsselaer A, Cazenave JP, Lanza F. Gene cloning of rat and mouse platelet glycoprotein V: identification of megakaryocyte-specific promoters and demonstration of functional thrombin cleavage. *Blood*. 1997; **89**: 3253-62.

62 Dong JF, Sae-Tung G, Lopez JA. Role of glycoprotein V in the formation of the platelet high-affinity thrombin-binding site. *Blood*. 1997; **89**: 4355-63.

63 Ramakrishnan V, Reeves PS, Deguzman F, Deshpande U, Ministri-Madrid K, DuBridge RB, Phillips DR. Increased thrombin responsiveness in platelets from mice lacking glycoprotein V. *ProcNatlAcadSciUSA*. 1999; **96**: 13336-41.

64 Ramakrishnan V, Deguzman F, Bao M, Hall SW, Leung LL, Phillips DR. A thrombin receptor function for platelet glycoprotein Ib-IX unmasked by cleavage of glycoprotein V. *ProcNatlAcadSciUSA*. 2001; **98**: 1823-8.

65 Ni H, Ramakrishnan V, Ruggeri ZM, Papalia JM, Phillips DR, Wagner DD. Increased thrombogenesis and embolus formation in mice lacking glycoprotein V. *Blood*. 2001; **98**: 368-73.

66 Moog S, Mangin P, Lenain N, Strassel C, Ravanat C, Schuhler S, Freund M, Santer M, Kahn M, Nieswandt B, Gachet C, Cazenave JP, Lanza F. Platelet glycoprotein V binds to collagen and participates in platelet adhesion and aggregation. *Blood*. 2001; **98**: 1038-46.

67 Nonne C, Hechler B, Cazenave JP, Gachet C, Lanza F. Reassessment of in vivo thrombus formation in glycoprotein V deficient mice backcrossed on a C57Bl/6 strain. *J Thromb Haemost*. 2008; **6**: 210-2.

68 Savage B, mus-Jacobs F, Ruggeri ZM. Specific synergy of multiple substrate-receptor interactions in platelet thrombus formation under flow. *Cell*. 1998; **94**: 657-66.

69 Santoro SA. Identification of a 160,000 dalton platelet membrane protein that mediates the initial divalent cation-dependent adhesion of platelets to collagen. *Cell*. 1986; **46**: 913-20.

70 Chen J, Diacovo TG, Grenache DG, Santoro SA, Zutter MM. The alpha(2) integrin subunit-deficient mouse: a multifaceted phenotype including defects of branching morphogenesis and hemostasis. *Am J Pathol*. 2002; **161**: 337-44.

71 Kuijpers MJ, Pozgajova M, Cosemans JM, Munnix IC, Eckes B, Nieswandt B, Heemskerk JW. Role of murine integrin alpha2beta1 in thrombus stabilization and embolization: contribution of thromboxane A2. *Thrombosis and Haemostasis*. 2007; **98**: 1072-80.

72 Sarratt KL, Chen H, Zutter MM, Santoro SA, Hammer DA, Kahn ML. GPVI and alpha2beta1 play independent critical roles during platelet adhesion and aggregate formation to collagen under flow. *Blood*. 2005; **106**: 1268-77.

73 Kuijpers MJ, Schulte V, Bergmeier W, Lindhout T, Brakebusch C, Offermanns S, Fassler R, Heemskerk JW, Nieswandt B. Complementary roles of glycoprotein VI and alpha2beta1 integrin in collagen-induced thrombus formation in flowing whole blood ex vivo. *FASEB Journal*. 2003; **17**: 685-7.

74 Nieswandt B, Brakebusch C, Bergmeier W, Schulte V, Bouvard D, Mokhtari-Nejad R, Lindhout T, Heemskerk JW, Zirngibl H, Fassler R. Glycoprotein VI but not alpha2beta1 integrin is essential for platelet interaction with collagen. *EMBO Journal*. 2001; **20**: 2120-30.

75 He L, Pappan LK, Grenache DG, Li Z, Tollefsen DM, Santoro SA, Zutter MM. The contributions of the alpha 2 beta 1 integrin to vascular thrombosis in vivo. *Blood*. 2003; **102**: 3652-7.

76 Holtkotter O, Nieswandt B, Smyth N, Muller W, Hafner M, Schulte V, Krieg T, Eckes B. Integrin alpha 2-deficient mice develop normally, are fertile, but display partially defective platelet interaction with collagen. *Journal of Biological Chemistry*. 2002; **277**: 10789-94.

77 Dumont B, Lasne D, Rothschild C, Bouabdelli M, Ollivier V, Oudin C, Ajzenberg N, Grandchamp B, Jandrot-Perrus M. Absence of collagen-induced platelet activation caused by compound heterozygous GPVI mutations. *Blood*. 2009; **114**: 1900-3.

78 Hermans C, Wittevrongel C, Thys C, Smethurst PA, Van GC, Freson K. A compound heterozygous mutation in glycoprotein VI in a patient with a bleeding disorder. *JThrombHaemost*. 2009; **7**: 1356-63.

79 Moroi M, Jung SM, Okuma M, Shinmyozu K. A patient with platelets deficient in glycoprotein VI that lack both collagen-induced aggregation and adhesion. *JClinInvest*. 1989; **84**: 1440-5.

80 Boylan B, Chen H, Rathore V, Paddock C, Salacz M, Friedman KD, Curtis BR, Stapleton M, Newman DK, Kahn ML, Newman PJ. Anti-GPVI-associated ITP: an acquired platelet disorder caused by autoantibody-mediated clearance of the GPVI/FcRgamma-chain complex from the human platelet surface. *Blood*. 2004; **104**: 1350-5.

81 Nieswandt B, Schulte V, Bergmeier W, Mokhtari-Nejad R, Rackebrandt K, Cazenave JP, Ohlmann P, Gachet C, Zirngibl H. Long-term antithrombotic protection by in vivo depletion of platelet glycoprotein VI in mice. *Journal of Experimental Medicine*. 2001; **193**: 459-69.

82 Schulte V, Rabie T, Prostredna M, Aktas B, Gruner S, Nieswandt B. Targeting of the collagen-binding site on glycoprotein VI is not essential for in vivo depletion of the receptor. *Blood*. 2003; **101**: 3948-52.

83 Lecut C, Schoolmeester A, Kuijpers MJ, Broers JL, van Zandvoort MA, Vanhoorelbeke K, Deckmyn H, Jandrot-Perrus M, Heemskerk JW. Principal role of glycoprotein VI in alpha2beta1 and alphaIIbbeta3 activation during collagen-induced thrombus formation. *Arteriosclerosis, Thrombosis, and Vascular Biology*. 2004; **24**: 1727-33.

84 Konishi H, Katoh Y, Takaya N, Kashiwakura Y, Itoh S, Ra C, Daida H. Platelets activated by collagen through immunoreceptor tyrosine-based activation motif play pivotal role in initiation and generation of neointimal hyperplasia after vascular injury. *Circulation*. 2002; **105**: 912-6.

85 Konstantinides S, Ware J, Marchese P, mus-Jacobs F, Loskutoff DJ, Ruggeri ZM. Distinct antithrombotic consequences of platelet glycoprotein Ibalpha and VI deficiency in a mouse model of arterial thrombosis. *JThrombHaemost*. 2006; **4**: 2014-21.

86 Gruner S, Prostredna M, Aktas B, Moers A, Schulte V, Krieg T, Offermanns S, Eckes B, Nieswandt B. Anti-glycoprotein VI treatment severely compromises hemostasis in mice with reduced alpha2beta1 levels or concomitant aspirin therapy. *Circulation*. 2004; **110**: 2946-51.

87 Morris AJ, Frohman MA, Engebrecht J. Measurement of phospholipase D activity. *Analytical Biochemistry*. 1997; **252**: 1-9.

88 Hammond SM, Altshuller YM, Sung TC, Rudge SA, Rose K, Engebrecht J, Morris AJ, Frohman MA. Human ADP-ribosylation factor-activated phosphatidylcholine-specific phospholipase D defines a new and highly conserved gene family. *J Biol Chem*. 1995; **270**: 29640-3.

89 Kodaki T, Yamashita S. Cloning, expression, and characterization of a novel phospholipase D complementary DNA from rat brain. *J Biol Chem*. 1997; **272**: 11408-13.

90 McDermott M, Wakelam MJ, Morris AJ. Phospholipase D. *Biochemistry and Cell Biology*. 2004; **82**: 225-53.

91 Vorland M, Holmsen H. Phospholipase D in human platelets: presence of isoenzymes and participation of autocrine stimulation during thrombin activation. *Platelets*. 2008; **19**: 211-24.

92 Kanaho Y, Funakoshi Y, Hasegawa H. Phospholipase D signalling and its involvement in neurite outgrowth. *Biochim Biophys Acta*. 2009; **1791**: 898-904.

93 Raghu P, Manifava M, Coadwell J, Ktistakis NT. Emerging findings from studies of phospholipase D in model organisms (and a short update on phosphatidic acid effectors). *Biochim Biophys Acta*. 2009; **1791**: 889-97.

94 Stuckey JA, Dixon JE. Crystal structure of a phospholipase D family member. *Nat Struct Biol*. 1999; **6**: 278-84.

95 Sung TC, Zhang Y, Morris AJ, Frohman MA. Structural analysis of human phospholipase D1. *J Biol Chem*. 1999; **274**: 3659-66.

96 Cazzolli R, Shemon AN, Fang MQ, Hughes WE. Phospholipid signalling through phospholipase D and phosphatidic acid. *IUBMB Life*. 2006; **58**: 457-61.

97 Oude Weernink PA, Lopez de Jesus M, Schmidt M. Phospholipase D signaling: orchestration by PIP2 and small GTPases. *Naunyn Schmiedebergs Arch Pharmacol*. 2007; **374**: 399-411.

98 Rudge SA, Wakelam MJ. Inter-regulatory dynamics of phospholipase D and the actin cytoskeleton. *Biochim Biophys Acta*. 2009; **1791**: 856-61.

99 Stace CL, Ktistakis NT. Phosphatidic acid- and phosphatidylserine-binding proteins. *Biochim Biophys Acta*. 2006; **1761**: 913-26.

100 Su W, Yeku O, Olepu S, Genna A, Park JS, Ren H, Du G, Gelb MH, Morris AJ, Frohman MA. 5-Fluoro-2-indolyl des-chlorohalopemide (FIPI), a phospholipase D pharmacological inhibitor that alters cell spreading and inhibits chemotaxis. *Molecular Pharmacology*. 2009; **75**: 437-46.

101 Vorland M, Thorsen VA, Holmsen H. Phospholipase D in platelets and other cells. *Platelets*. 2008; **19**: 582-94.

102 Rubin R. Phosphatidylethanol formation in human platelets: evidence for thrombin-induced activation of phospholipase D. *Biochem Biophys Res Commun*. 1988; **156**: 1090-6.

103 Chiang TM. Activation of phospholipase D in human platelets by collagen and thrombin and its relationship to platelet aggregation. *Biochim Biophys Acta*. 1994; **1224**: 147-55.

104 Martinson EA, Scheible S, Greinacher A, Presek P. Platelet phospholipase D is activated by protein kinase C via an integrin alpha IIb beta 3-independent mechanism. *Biochemical Journal*. 1995; **310 (Pt 2)**: 623-8.

105 Coorssen JR, Haslam RJ. GTP gamma S and phorbol ester act synergistically to stimulate both Ca(2+)-independent secretion and phospholipase D activity in permeabilized human platelets. Inhibition by BAPTA and analogues. *FEBS Lett*. 1993; **316**: 170-4.

106 Holinstat M, Preininger AM, Milne SB, Hudson WJ, Brown HA, Hamm HE. Irreversible platelet activation requires protease-activated receptor 1-mediated signaling to phosphatidylinositol phosphates. *Molecular Pharmacology*. 2009; **76**: 301-13.

107 Holinstat M, Voss B, Bilodeau ML, Hamm HE. Protease-activated receptors differentially regulate human platelet activation through a phosphatidic acid-dependent pathway. *Molecular Pharmacology*. 2007; **71**: 686-94.

108 Berridge MJ, Bootman MD, Roderick HL. Calcium signalling: dynamics, homeostasis and remodelling. *Nat Rev Mol Cell Biol*. 2003; **4**: 517-29.

109 Vig M, Kinet JP. Calcium signaling in immune cells. *Nat Immunol*. 2009; **10**: 21-7.

110 Cahalan MD. STIMulating store-operated Ca(2+) entry. *Nat Cell Biol*. 2009; **11**: 669-77.

111 Putney JW, Jr. A model for receptor-regulated calcium entry. *Cell Calcium*. 1986; **7**: 1-12.

112 Hoth M, Penner R. Depletion of intracellular calcium stores activates a calcium current in mast cells. *Nature*. 1992; **355**: 353-6.

113 Lewis RS, Cahalan MD. Mitogen-induced oscillations of cytosolic Ca2+ and transmembrane Ca2+ current in human leukemic T cells. *Cell Regul*. 1989; **1**: 99-112.

114 Zweifach A, Lewis RS. Mitogen-regulated Ca2+ current of T lymphocytes is activated by depletion of intracellular Ca2+ stores. *Proc Natl Acad Sci U S A*. 1993; **90**: 6295-9.

115 Parekh AB, Putney JW, Jr. Store-operated calcium channels. *Physiol Rev*. 2005; **85**: 757-810.

116 Liou J, Kim ML, Heo WD, Jones JT, Myers JW, Ferrell JE, Jr., Meyer T. STIM is a Ca2+ sensor essential for Ca2+-store-depletion-triggered Ca2+ influx. *Current Biology*. 2005; **15**: 1235-41.

117 Roos J, DiGregorio PJ, Yeromin AV, Ohlsen K, Lioudyno M, Zhang S, Safrina O, Kozak JA, Wagner SL, Cahalan MD, Velicelebi G, Stauderman KA. STIM1, an essential and conserved component of store-operated Ca2+ channel function. *Journal of Cell Biology*. 2005; **169**: 435-45.

118 Zhang SL, Yu Y, Roos J, Kozak JA, Deerinck TJ, Ellisman MH, Stauderman KA, Cahalan MD. STIM1 is a Ca2+ sensor that activates CRAC channels and migrates from the Ca2+ store to the plasma membrane. *Nature*. 2005; **437**: 902-5.

119 Baba Y, Kurosaki T. Physiological function and molecular basis of STIM1-mediated calcium entry in immune cells. *Immunol Rev*. 2009; **231**: 174-88.

120 Feske S, Gwack Y, Prakriya M, Srikanth S, Puppel SH, Tanasa B, Hogan PG, Lewis RS, Daly M, Rao A. A mutation in Orai1 causes immune deficiency by abrogating CRAC channel function. *Nature*. 2006; **441**: 179-85.

121 Vig M, Peinelt C, Beck A, Koomoa DL, Rabah D, Koblan-Huberson M, Kraft S, Turner H, Fleig A, Penner R, Kinet JP. CRACM1 is a plasma membrane protein essential for store-operated Ca2+ entry. *Science*. 2006; **312**: 1220-3.

122 Zhang SL, Yeromin AV, Zhang XH, Yu Y, Safrina O, Penna A, Roos J, Stauderman KA, Cahalan MD. Genome-wide RNAi screen of Ca(2+) influx identifies genes that regulate Ca(2+) release-activated Ca(2+) channel activity. *Proc Natl Acad Sci U S A*. 2006; **103**: 9357-62.

123 Lis A, Peinelt C, Beck A, Parvez S, Monteilh-Zoller M, Fleig A, Penner R. CRACM1, CRACM2, and CRACM3 are store-operated Ca2+ channels with distinct functional properties. *Curr Biol*. 2007; **17**: 794-800.

124 Grosse J, Braun A, Varga-Szabo D, Beyersdorf N, Schneider B, Zeitlmann L, Hanke P, Schropp P, Muhlstedt S, Zorn C, Huber M, Schmittwolf C, Jagla W, Yu P, Kerkau T, Schulze H, Nehls M, Nieswandt B. An EF hand mutation in Stim1 causes premature platelet activation and bleeding in mice. *JClinInvest*. 2007; **117**: 3540-50.

125 Baba Y, Nishida K, Fujii Y, Hirano T, Hikida M, Kurosaki T. Essential function for the calcium sensor STIM1 in mast cell activation and anaphylactic responses. *Nat Immunol*. 2008; **9**: 81-8.

126 Vig M, DeHaven WI, Bird GS, Billingsley JM, Wang H, Rao PE, Hutchings AB, Jouvin MH, Putney JW, Kinet JP. Defective mast cell effector functions in mice lacking the CRACM1 pore subunit of store-operated calcium release-activated calcium channels. *Nat Immunol*. 2008; **9**: 89-96.

127 Varga-Szabo D, Braun A, Kleinschnitz C, Bender M, Pleines I, Pham M, Renne T, Stoll G, Nieswandt B. The calcium sensor STIM1 is an essential mediator of arterial thrombosis and ischemic brain infarction. *Journal of Experimental Medicine*. 2008; **205**: 1583-91.

128 Braun A, Varga-Szabo D, Kleinschnitz C, Pleines I, Bender M, Austinat M, Bosl M, Stoll G, Nieswandt B. Orai1 (CRACM1) is the platelet SOC channel and essential for pathological thrombus formation. *Blood*. 2009; **113**: 2056-63.

129 Oh-Hora M, Yamashita M, Hogan PG, Sharma S, Lamperti E, Chung W, Prakriya M, Feske S, Rao A. Dual functions for the endoplasmic reticulum calcium sensors STIM1 and STIM2 in T cell activation and tolerance. *Nat Immunol*. 2008; **9**: 432-43.

130 Gwack Y, Srikanth S, Oh-Hora M, Hogan PG, Lamperti ED, Yamashita M, Gelinas C, Neems DS, Sasaki Y, Feske S, Prakriya M, Rajewsky K, Rao A. Hair loss and

defective T- and B-cell function in mice lacking ORAI1. *Mol Cell Biol*. 2008; **28**: 5209-22.

131 Beyersdorf N, Braun A, Vogtle T, Varga-Szabo D, Galdos RR, Kissler S, Kerkau T, Nieswandt B. STIM1-independent T cell development and effector function in vivo. *Journal of Immunology*. 2009; **182**: 3390-7.

132 Picard C, McCarl CA, Papolos A, Khalil S, Luthy K, Hivroz C, LeDeist F, Rieux-Laucat F, Rechavi G, Rao A, Fischer A, Feske S. STIM1 mutation associated with a syndrome of immunodeficiency and autoimmunity. *N Engl J Med*. 2009; **360**: 1971-80.

133 Feske S. ORAI1 and STIM1 deficiency in human and mice: roles of store-operated Ca2+ entry in the immune system and beyond. *Immunol Rev*. 2009; **231**: 189-209.

134 Parvez S, Beck A, Peinelt C, Soboloff J, Lis A, Monteilh-Zoller M, Gill DL, Fleig A, Penner R. STIM2 protein mediates distinct store-dependent and store-independent modes of CRAC channel activation. *FASEB J*. 2008; **22**: 752-61.

135 Brandman O, Liou J, Park WS, Meyer T. STIM2 is a feedback regulator that stabilizes basal cytosolic and endoplasmic reticulum Ca2+ levels. *Cell*. 2007; **131**: 1327-39.

136 Yuan JP, Zeng W, Dorwart MR, Choi YJ, Worley PF, Muallem S. SOAR and the polybasic STIM1 domains gate and regulate Orai channels. *Nat Cell Biol*. 2009; **11**: 337-43.

137 Cines DB, Bussel JB, Liebman HA, Luning Prak ET. The ITP syndrome: pathogenic and clinical diversity. *Blood*. 2009; **113**: 6511-21.

138 Neunert C, Lim W, Crowther M, Cohen A, Solberg L, Jr. Clinical guideline update on "Immune thrombocytopenia: an evidence based practice guideline developed by the American Society of Hematology". *Blood*. 2011.

139 Kuwana M, Ikeda Y. The role of autoreactive T-cells in the pathogenesis of idiopathic thrombocytopenic purpura. *International Journal of Hematology*. 2005; **81**: 106-12.

140 Ballem PJ, Segal GM, Stratton JR, Gernsheimer T, Adamson JW, Slichter SJ. Mechanisms of thrombocytopenia in chronic autoimmune thrombocytopenic purpura. Evidence of both impaired platelet production and increased platelet clearance. *J Clin Invest*. 1987; **80**: 33-40.

141 Chang M, Nakagawa PA, Williams SA, Schwartz MR, Imfeld KL, Buzby JS, Nugent DJ. Immune thrombocytopenic purpura (ITP) plasma and purified ITP monoclonal autoantibodies inhibit megakaryocytopoiesis in vitro. *Blood*. 2003; **102**: 887-95.

142 McMillan R, Nugent D. The effect of antiplatelet autoantibodies on megakaryocytopoiesis. *Int J Hematol*. 2005; **81**: 94-9.

143 Webster ML, Sayeh E, Crow M, Chen P, Nieswandt B, Freedman J, Ni H. Relative efficacy of intravenous immunoglobulin G in ameliorating thrombocytopenia induced by antiplatelet GPIIbIIIa versus GPIbalpha antibodies. *Blood*. 2006; **108**: 943-6.

144 Go RS, Johnston KL, Bruden KC. The association between platelet autoantibody specificity and response to intravenous immunoglobulin G in the treatment of patients with immune thrombocytopenia. *Haematologica*. 2007; **92**: 283-4.

145 Stasi R, Evangelista ML, Stipa E, Buccisano F, Venditti A, Amadori S. Idiopathic thrombocytopenic purpura: current concepts in pathophysiology and management. *Thromb Haemost*. 2008; **99**: 4-13.

146 Nieswandt B, Bergmeier W, Rackebrandt K, Gessner JE, Zirngibl H. Identification of critical antigen-specific mechanisms in the development of immune thrombocytopenic purpura in mice. *Blood*. 2000; **96**: 2520-7.

147 McMillan R. Antiplatelet antibodies in chronic adult immune thrombocytopenic purpura: assays and epitopes. *J Pediatr Hematol Oncol*. 2003; **25 Suppl 1**: S57-61.

148 Kuwana M, Okazaki Y, Ikeda Y. Splenic macrophages maintain the anti-platelet autoimmune response via uptake of opsonized platelets in patients with immune thrombocytopenic purpura. *JThrombHaemost*. 2009; **7**: 322-9.

149 Nimmerjahn F, Ravetch JV. Fcgamma receptors as regulators of immune responses. *Nat Rev Immunol*. 2008; **8**: 34-47.

150 Sung SS, Young JD, Origlio AM, Heiple JM, Kaback HR, Silverstein SC. Extracellular ATP perturbs transmembrane ion fluxes, elevates cytosolic [Ca2+], and inhibits phagocytosis in mouse macrophages. *J Biol Chem*. 1985; **260**: 13442-9.

151 Young JD, Ko SS, Cohn ZA. The increase in intracellular free calcium associated with IgG gamma 2b/gamma 1 Fc receptor-ligand interactions: role in phagocytosis. *Proc Natl Acad Sci U S A*. 1984; **81**: 5430-4.

152 Hishikawa T, Cheung JY, Yelamarty RV, Knutson DW. Calcium transients during Fc receptor-mediated and nonspecific phagocytosis by murine peritoneal macrophages. *J Cell Biol*. 1991; **115**: 59-66.

153 Ichinose M, Asai M, Sawada M. beta-Endorphin enhances phagocytosis of latex particles in mouse peritoneal macrophages. *Scand J Immunol*. 1995; **42**: 311-6.

154 Ichinose M, Asai M, Sawada M. Enhancement of phagocytosis by dynorphin A in mouse peritoneal macrophages. *J Neuroimmunol*. 1995; **60**: 37-43.

155 Di Virgilio F, Meyer BC, Greenberg S, Silverstein SC. Fc receptor-mediated phagocytosis occurs in macrophages at exceedingly low cytosolic Ca2+ levels. *J Cell Biol*. 1988; **106**: 657-66.

156 Greenberg S, el Khoury J, di Virgilio F, Kaplan EM, Silverstein SC. Ca(2+)-independent F-actin assembly and disassembly during Fc receptor-mediated phagocytosis in mouse macrophages. *J Cell Biol*. 1991; **113**: 757-67.

157 McNeil PL, Swanson JA, Wright SD, Silverstein SC, Taylor DL. Fc-receptor-mediated phagocytosis occurs in macrophages without an increase in average [Ca++]i. *J Cell Biol*. 1986; **102**: 1586-92.

158 Chun J, Prince A. Activation of Ca2+-dependent signaling by TLR2. *J Immunol*. 2006; **177**: 1330-7.

159 Del Corno M, Liu QH, Schols D, de Clercq E, Gessani S, Freedman BD, Collman RG. HIV-1 gp120 and chemokine activation of Pyk2 and mitogen-activated protein kinases in primary macrophages mediated by calcium-dependent, pertussis toxin-insensitive chemokine receptor signaling. *Blood*. 2001; **98**: 2909-16.

160 Semenova SB, Kiselev KI, Mozhaeva GN. Low-conductivity calcium channels in the macrophage plasma membrane: activation by inositol-1,4,5-triphosphate. *Neurosci Behav Physiol*. 1999; **29**: 339-45.

161 Zhou X, Yang W, Li J. Ca2+- and protein kinase C-dependent signaling pathway for nuclear factor-kappaB activation, inducible nitric-oxide synthase expression, and tumor necrosis factor-alpha production in lipopolysaccharide-stimulated rat peritoneal macrophages. *J Biol Chem*. 2006; **281**: 31337-47.

162 Nimmerjahn F, Bruhns P, Horiuchi K, Ravetch JV. FcgammaRIV: a novel FcR with distinct IgG subclass specificity. *Immunity*. 2005; **23**: 41-51.

163 Holmes KL, Palfree RG, Hammerling U, Morse HC, 3rd. Alleles of the Ly-17 alloantigen define polymorphisms of the murine IgG Fc receptor. *Proc Natl Acad Sci U S A*. 1985; **82**: 7706-10.

164 Unkeless JC. Characterization of a monoclonal antibody directed against mouse macrophage and lymphocyte Fc receptors. *J Exp Med*. 1979; **150**: 580-96.

165 Leo O, Foo M, Sachs DH, Samelson LE, Bluestone JA. Identification of a monoclonal antibody specific for a murine T3 polypeptide. *Proc Natl Acad Sci U S A*. 1987; **84**: 1374-8.

166 May F, Hagedorn I, Pleines I, Bender M, Vogtle T, Eble J, Elvers M, Nieswandt B. CLEC-2 is an essential platelet-activating receptor in hemostasis and thrombosis. *Blood*. 2009; **114**: 3464-72.

167 Bergmeier W, Schulte V, Brockhoff G, Bier U, Zirngibl H, Nieswandt B. Flow cytometric detection of activated mouse integrin alphaIIbbeta3 with a novel monoclonal antibody. *Cytometry*. 2002; **48**: 80-6.

168 Pauer HU, Renne T, Hemmerlein B, Legler T, Fritzlar S, Adham I, Muller-Esterl W, Emons G, Sancken U, Engel W, Burfeind P. Targeted deletion of murine coagulation factor XII gene-a model for contact phase activation in vivo. *Thromb Haemost*. 2004; **92**: 503-8.

169 Berna-Erro A, Braun A, Kraft R, Kleinschnitz C, Schuhmann MK, Stegner D, Wultsch T, Eilers J, Meuth SG, Stoll G, Nieswandt B. STIM2 regulates capacitive Ca2+ entry in neurons and plays a key role in hypoxic neuronal cell death. *SciSignal*. 2009; **2**: ra67.

170 Dirnagl U. Bench to bedside: the quest for quality in experimental stroke research. *J Cereb Blood Flow Metab*. 2006; **26**: 1465-78.

171 Swanson RA, Morton MT, Tsao-Wu G, Savalos RA, Davidson C, Sharp FR. A semiautomated method for measuring brain infarct volume. *J Cereb Blood Flow Metab*. 1990; **10**: 290-3.

172 Bederson JB, Pitts LH, Tsuji M, Nishimura MC, Davis RL, Bartkowski H. Rat middle cerebral artery occlusion: evaluation of the model and development of a neurologic examination. *Stroke*. 1986; **17**: 472-6.

173 Moran PM, Higgins LS, Cordell B, Moser PC. Age-related learning deficits in transgenic mice expressing the 751-amino acid isoform of human beta-amyloid precursor protein. *Proc Natl Acad Sci U S A*. 1995; **92**: 5341-5.

174 Ravanat C, Strassel C, Hechler B, Schuhler S, Chicanne G, Payrastre B, Gachet C, Lanza F. A central role of GPIb-IX in the procoagulant function of platelets that is independent of the 45-kDa GPIbalpha N-terminal extracellular domain. *Blood*. 2010; **116**: 1157-64.

175 Eckly A, Hechler B, Freund M, Zerr M, Cazenave JP, Lanza F, Mangin P, Gachet C. Mechanisms underlying FeCl(3) -induced arterial thrombosis. *J Thromb Haemost*. 2011.

176 Gruner S, Prostredna M, Koch M, Miura Y, Schulte V, Jung SM, Moroi M, Nieswandt B. Relative antithrombotic effect of soluble GPVI dimer compared with anti-GPVI antibodies in mice. *Blood*. 2005; **105**: 1492-9.

177 Ni H, Denis CV, Subbarao S, Degen JL, Sato TN, Hynes RO, Wagner DD. Persistence of platelet thrombus formation in arterioles of mice lacking both von Willebrand factor and fibrinogen. *JClinInvest*. 2000; **106**: 385-92.

178 Renne T, Pozgajova M, Gruner S, Schuh K, Pauer HU, Burfeind P, Gailani D, Nieswandt B. Defective thrombus formation in mice lacking coagulation factor XII. *Journal of Experimental Medicine*. 2005; **202**: 271-81.

179 Hagedorn I, Schmidbauer S, Pleines I, Kleinschnitz C, Kronthaler U, Stoll G, Dickneite G, Nieswandt B. Factor XIIa inhibitor recombinant human albumin Infestin-4

abolishes occlusive arterial thrombus formation without affecting bleeding. *Circulation*. 2010; **121**: 1510-7.

180 Murray CJ, Lopez AD. Mortality by cause for eight regions of the world: Global Burden of Disease Study. *Lancet*. 1997; **349**: 1269-76.

181 Rodgers RP, Levin J. A critical reappraisal of the bleeding time. *Semin Thromb Hemost*. 1990; **16**: 1-20.

182 Cadroy Y, Hanson SR, Kelly AB, Marzec UM, Evatt BL, Kunicki TJ, Montgomery RR, Harker LA. Relative antithrombotic effects of monoclonal antibodies targeting different platelet glycoprotein-adhesive molecule interactions in nonhuman primates. *Blood*. 1994; **83**: 3218-24.

183 Bluestein D, Niu L, Schoephoerster RT, Dewanjee MK. Fluid mechanics of arterial stenosis: relationship to the development of mural thrombus. *AnnBiomedEng*. 1997; **25**: 344-56.

184 Reverter JC, Beguin S, Kessels H, Kumar R, Hemker HC, Coller BS. Inhibition of platelet-mediated, tissue factor-induced thrombin generation by the mouse/human chimeric 7E3 antibody. Potential implications for the effect of c7E3 Fab treatment on acute thrombosis and "clinical restenosis". *J Clin Invest*. 1996; **98**: 863-74.

185 Heemskerk JW, Vuist WM, Feijge MA, Reutelingsperger CP, Lindhout T. Collagen but not fibrinogen surfaces induce bleb formation, exposure of phosphatidylserine, and procoagulant activity of adherent platelets: evidence for regulation by protein tyrosine kinase-dependent Ca2+ responses. *Blood*. 1997; **90**: 2615-25.

186 Kuijpers MJ, Schulte V, Oury C, Lindhout T, Broers J, Hoylaerts MF, Nieswandt B, Heemskerk JW. Facilitating roles of murine platelet glycoprotein Ib and alphaIIbbeta3 in phosphatidylserine exposure during vWF-collagen-induced thrombus formation. *JPhysiol*. 2004; **558**: 403-15.

187 DiMinno G, Silver MJ. Mouse antithrombotic assay: a simple method for the evaluation of antithrombotic agents in vivo. Potentiation of antithrombotic activity by ethyl alcohol. *J Pharmacol Exp Ther*. 1983; **225**: 57-60.

188 Schuhmann MK, Stegner D, Berna-Erro A, Bittner S, Braun A, Kleinschnitz C, Stoll G, Wiendl H, Meuth SG, Nieswandt B. Stromal interaction molecules 1 and 2 are key regulators of autoreactive T cell activation in murine autoimmune central nervous system inflammation. *Journal of Immunology*. 2010; **184**: 1536-42.

189 Ma J, McCarl CA, Khalil S, Luthy K, Feske S. T-cell-specific deletion of STIM1 and STIM2 protects mice from EAE by impairing the effector functions of Th1 and Th17 cells. *Eur J Immunol*. 2010; **40**: 3028-42.

190 Woods VL, Jr., McMillan R. Platelet autoantigens in chronic ITP. *Br J Haematol*. 1984; **57**: 1-4.

191 He R, Reid DM, Jones CE, Shulman NR. Spectrum of Ig classes, specificities, and titers of serum antiglycoproteins in chronic idiopathic thrombocytopenic purpura. *Blood*. 1994; **83**: 1024-32.

192 Beardsley DS, Ertem M. Platelet autoantibodies in immune thrombocytopenic purpura. *Transfus Sci*. 1998; **19**: 237-44.

193 Clynes R, Ravetch JV. Cytotoxic antibodies trigger inflammation through Fc receptors. *Immunity*. 1995; **3**: 21-6.

194 Nieswandt B, Bergmeier W, Schulte V, Takai T, Baumann U, Schmidt RE, Zirngibl H, Bloch W, Gessner JE. Targeting of platelet integrin alphaIIbbeta3 determines systemic reaction and bleeding in murine thrombocytopenia regulated by activating and inhibitory FcgammaR. *International Immunology*. 2003; **15**: 341-9.

195 Braun A, Gessner JE, Varga-Szabo D, Syed SN, Konrad S, Stegner D, Vogtle T, Schmidt RE, Nieswandt B. STIM1 is essential for Fcgamma receptor activation and autoimmune inflammation. *Blood*. 2009; **113**: 1097-104.

196 Nieswandt B, Echtenacher B, Wachs FP, Schroder J, Gessner JE, Schmidt RE, Grau GE, Mannel DN. Acute systemic reaction and lung alterations induced by an antiplatelet integrin gpIIb/IIIa antibody in mice. *Blood*. 1999; **94**: 684-93.

197 Brown DL. Congenital bleeding disorders. *Curr Probl Pediatr Adolesc Health Care*. 2005; **35**: 38-62.

198 WHO. *Atlas of Heart Disease and Stroke*. Geneva, Switzerland: World Health Organization, 2004.

199 Whinna HC. Overview of murine thrombosis models. *Thrombosis Research*. 2008; **122 Suppl 1**: S64-S9.

200 Braeuninger S, Kleinschnitz C. Rodent models of focal cerebral ischemia: procedural pitfalls and translational problems. *ExpTranslStroke Med*. 2009; **1**: 8.

201 Hodivala-Dilke KM, McHugh KP, Tsakiris DA, Rayburn H, Crowley D, Ullman-Cullere M, Ross FP, Coller BS, Teitelbaum S, Hynes RO. Beta3-integrin-deficient mice are a model for Glanzmann thrombasthenia showing placental defects and reduced survival. *JClinInvest*. 1999; **103**: 229-38.

202 Becker RC, Smyth S. The evolution of platelet-directed pharmacotherapy. *J Thromb Haemost*. 2009; **7 Suppl 1**: 266-71.

203 Hagedorn I, Vogtle T, Nieswandt B. Arterial thrombus formation. Novel mechanisms and targets Novel mechanisms and targets. *Hamostaseologie*. 2010; **30**: 127-35.

204 Roth GJ. A new "kid" on the platelet thrombin receptor "block": glycoprotein Ib-IX-V. *Proc Natl Acad Sci U S A*. 2001; **98**: 1330-1.

205 Nakanishi-Matsui M, Zheng YW, Sulciner DJ, Weiss EJ, Ludeman MJ, Coughlin SR. PAR3 is a cofactor for PAR4 activation by thrombin. *Nature*. 2000; **404**: 609-13.

206 Hamilton JR, Cornelissen I, Coughlin SR. Impaired hemostasis and protection against thrombosis in protease-activated receptor 4-deficient mice is due to lack of thrombin signaling in platelets. *JThrombHaemost*. 2004; **2**: 1429-35.

207 Celikel R, McClintock RA, Roberts JR, Mendolicchio GL, Ware J, Varughese KI, Ruggeri ZM. Modulation of alpha-thrombin function by distinct interactions with platelet glycoprotein Ibalpha. *Science*. 2003; **301**: 218-21.

208 Dumas JJ, Kumar R, Seehra J, Somers WS, Mosyak L. Crystal structure of the GpIbalpha-thrombin complex essential for platelet aggregation. *Science*. 2003; **301**: 222-6.

209 Akar N, Duman T, Akar E, Deda G, Sipahi T. The alpha2 Gene alleles of the platelet collagen receptor integrin alpha2 beta1 in Turkish children with cerebral infarct. *Thrombosis Research*. 2001; **102**: 121-3.

210 Dubois C, Panicot-Dubois L, Merrill-Skoloff G, Furie B, Furie BC. Glycoprotein VI-dependent and -independent pathways of thrombus formation in vivo. *Blood*. 2006; **107**: 3902-6.

211 Kanaji T, Russell S, Ware J. Amelioration of the macrothrombocytopenia associated with the murine Bernard-Soulier syndrome. *Blood*. 2002; **100**: 2102-7.

212 Mangin P, Yap CL, Nonne C, Sturgeon SA, Goncalves I, Yuan Y, Schoenwaelder SM, Wright CE, Lanza F, Jackson SP. Thrombin overcomes the thrombosis defect associated with platelet GPVI/FcRgamma deficiency. *Blood*. 2006; **107**: 4346-53.

213 Joutsi-Korhonen L, Javela K, Hormila P, Kekomaki R. Glycoprotein V-specific platelet-associated antibodies in thrombocytopenic patients. *Clin Lab Haematol*. 2001; **23**: 307-12.

214 Garner SF, Campbell K, Metcalfe P, Keidan J, Huiskes E, Dong JF, Lopez JA, Ouwehand WH. Glycoprotein V: the predominant target antigen in gold-induced autoimmune thrombocytopenia. *Blood*. 2002; **100**: 344-6.

215 Kahn ML, Nakanishi-Matsui M, Shapiro MJ, Ishihara H, Coughlin SR. Protease-activated receptors 1 and 4 mediate activation of human platelets by thrombin. *JClinInvest*. 1999; **103**: 879-87.

216 Gailani D, Lasky NM, Broze GJ, Jr. A murine model of factor XI deficiency. *Blood Coagul Fibrinolysis*. 1997; **8**: 134-44.

217 Merkulov S, Zhang WM, Komar AA, Schmaier AH, Barnes E, Zhou Y, Lu X, Iwaki T, Castellino FJ, Luo G, McCrae KR. Deletion of murine kininogen gene 1 (mKng1) causes loss of plasma kininogen and delays thrombosis. *Blood*. 2008; **111**: 1274-81.

218 Lay AJ, Liang Z, Rosen ED, Castellino FJ. Mice with a severe deficiency in protein C display prothrombotic and proinflammatory phenotypes and compromised maternal reproductive capabilities. *J Clin Invest*. 2005; **115**: 1552-61.

219 Cambien B, Wagner DD. A new role in hemostasis for the adhesion receptor P-selectin. *Trends Mol Med*. 2004; **10**: 179-86.

220 Kisucka J, Chauhan AK, Zhao BQ, Patten IS, Yesilaltay A, Krieger M, Wagner DD. Elevated levels of soluble P-selectin in mice alter blood-brain barrier function, exacerbate stroke, and promote atherosclerosis. *Blood*. 2009; **113**: 6015-22.

221 Subramaniam M, Frenette PS, Saffaripour S, Johnson RC, Hynes RO, Wagner DD. Defects in hemostasis in P-selectin-deficient mice. *Blood*. 1996; **87**: 1238-42.

222 Rabie T, Strehl A, Ludwig A, Nieswandt B. Evidence for a role of ADAM17 (TACE) in the regulation of platelet glycoprotein V. *Journal of Biological Chemistry*. 2005; **280**: 14462-8.

223 Bender M, Hofmann S, Stegner D, Chalaris A, Bosl M, Braun A, Scheller J, Rose-John S, Nieswandt B. Differentially regulated GPVI ectodomain shedding by multiple platelet-expressed proteinases. *Blood*. 2010; **116**: 3347-55.

224 Al-Tamimi M, Grigoriadis G, Tran H, Paul E, Servadei P, Berndt MC, Gardiner EE, Andrews RK. Coagulation-induced shedding of platelet glycoprotein VI mediated by factor Xa. *Blood*. 2011.

225 Wolff V, Aleil B, Giroud M, Lorenzini JL, Meyer N, Wiesel ML, Cazenave JP, Lanza F. Soluble platelet glycoprotein V is a marker of thrombosis in patients with ischemic stroke. *Stroke*. 2005; **36**: e17-9.

226 Al-Tamimi M, Gardiner EE, Thom JY, Shen Y, Cooper MN, Hankey GJ, Berndt MC, Baker RI, Andrews RK. Soluble Glycoprotein VI Is Raised in the Plasma of Patients With Acute Ischemic Stroke. *Stroke*. 2011; **42**: 498-500.

227 Nieswandt B, Heemskerk JW. Dividing VI by X(a). *Blood*. 2011; **117**: 3704-5.

228 Brown DL, Morgenstern LB. Stopping the bleeding in intracerebral hemorrhage. *N Engl J Med*. 2005; **352**: 828-30.

229 Liu J, Gao BB, Clermont AC, Blair P, Chilcote TJ, Sinha S, Flaumenhaft R, Feener EP. Hyperglycemia-induced cerebral hematoma expansion is mediated by plasma kallikrein. *Nat Med*. 2011; **17**: 206-10.

230 Klein J. Functions and pathophysiological roles of phospholipase D in the brain. *J Neurochem*. 2005; **94**: 1473-87.

231 Dall'armi C, Hurtado-Lorenzo A, Tian H, Morel E, Nezu A, Chan RB, Yu WH, Robinson KS, Yeku O, Small SA, Duff K, Frohman MA, Wenk MR, Yamamoto A, Di Paolo G. The phospholipase D1 pathway modulates macroautophagy. *Nat Commun*. 2010; **1**: 142.

232 Oliveira TG, Chan RB, Tian H, Laredo M, Shui G, Staniszewski A, Zhang H, Wang L, Kim TW, Duff KE, Wenk MR, Arancio O, Di Paolo G. Phospholipase d2 ablation ameliorates Alzheimer's disease-linked synaptic dysfunction and cognitive deficits. *J Neurosci*. 2010; **30**: 16419-28.

233 Jenkins GM, Frohman MA. Phospholipase D: a lipid centric review. *Cell MolLife Sci*. 2005; **62**: 2305-16.

234 Disse J, Vitale N, Bader MF, Gerke V. Phospholipase D1 is specifically required for regulated secretion of von Willebrand factor from endothelial cells. *Blood*. 2009; **113**: 973-80.

235 Powner DJ, Pettitt TR, Anderson R, Nash GB, Wakelam MJ. Stable adhesion and migration of human neutrophils requires phospholipase D-mediated activation of the integrin CD11b/CD18. *Molecular Immunology*. 2007; **44**: 3211-21.

236 Martel V, Racaud-Sultan C, Dupe S, Marie C, Paulhe F, Galmiche A, Block MR, biges-Rizo C. Conformation, localization, and integrin binding of talin depend on its interaction with phosphoinositides. *Journal of Biological Chemistry*. 2001; **276**: 21217-27.

237 Honda A, Nogami M, Yokozeki T, Yamazaki M, Nakamura H, Watanabe H, Kawamoto K, Nakayama K, Morris AJ, Frohman MA, Kanaho Y. Phosphatidylinositol 4-phosphate 5-kinase alpha is a downstream effector of the small G protein ARF6 in membrane ruffle formation. *Cell*. 1999; **99**: 521-32.

238 Bolomini-Vittori M, Montresor A, Giagulli C, Staunton D, Rossi B, Martinello M, Constantin G, Laudanna C. Regulation of conformer-specific activation of the integrin LFA-1 by a chemokine-triggered Rho signaling module. *Nat Immunol*. 2009; **10**: 185-94.

239 Adams HP, Jr., Effron MB, Torner J, Davalos A, Frayne J, Teal P, Leclerc J, Oemar B, Padgett L, Barnathan ES, Hacke W. Emergency administration of abciximab for treatment of patients with acute ischemic stroke: results of an international phase III trial: Abciximab in Emergency Treatment of Stroke Trial (AbESTT-II). *Stroke*. 2008; **39**: 87-99.

240 Berna-Erro A. Generation and Characterization of Stromal Interaction Molecule 2 (STIM2)-deficient Mice. *Chair of Vascular Medicine, University Hospital Würzburg & Rudolf Virchow Center, DFG Research Center for Experimental Biomedicine, University of Würzburg, Würzburg, Germany*. Würzburg, Germany: University of Würzburg, 2009.

241 Bird GS, Aziz O, Lievremont JP, Wedel BJ, Trebak M, Vazquez G, Putney JW, Jr. Mechanisms of phospholipase C-regulated calcium entry. *Curr Mol Med*. 2004; **4**: 291-301.

242 Steinckwich N, Schenten V, Melchior C, Brechard S, Tschirhart EJ. An Essential Role of STIM1, Orai1, and S100A8-A9 Proteins for Ca2+ Signaling and Fc{gamma}R-Mediated Phagosomal Oxidative Activity. *J Immunol*. 2011; **186**: 2182-91.

243 Nimmerjahn F, Ravetch JV. Fcgamma receptors: old friends and new family members. *Immunity*. 2006; **24**: 19-28.

244 Auffray C, Sieweke MH, Geissmann F. Blood monocytes: development, heterogeneity, and relationship with dendritic cells. *Annu Rev Immunol*. 2009; **27**: 669-92.

245 Nardi M, Tomlinson S, Greco MA, Karpatkin S. Complement-independent, peroxide-induced antibody lysis of platelets in HIV-1-related immune thrombocytopenia. *Cell*. 2001; **106**: 551-61.

246 Ujike A, Ishikawa Y, Ono M, Yuasa T, Yoshino T, Fukumoto M, Ravetch JV, Takai T. Modulation of immunoglobulin (Ig)E-mediated systemic anaphylaxis by low-affinity Fc receptors for IgG. *J Exp Med*. 1999; **189**: 1573-9.

247 Finkelman FD. Anaphylaxis: lessons from mouse models. *J Allergy Clin Immunol*. 2007; **120**: 506-15; quiz 16-7.

248 Ludwig JC, Hoppens CL, McManus LM, Mott GE, Pinckard RN. Modulation of platelet-activating factor (PAF) synthesis and release from human polymorphonuclear leukocytes (PMN): role of extracellular albumin. *Arch Biochem Biophys*. 1985; **241**: 337-47.

249 Sakata T, Yoshimatsu H, Kurokawa M. Thermoregulation modulated by hypothalamic histamine in rats. *Inflamm Res*. 1997; **46 Suppl 1**: S35-6.

250 Gilio K, van Kruchten R, Braun A, Berna-Erro A, Feijge MA, Stegner D, van der Meijden PE, Kuijpers MJ, Varga-Szabo D, Heemskerk JW, Nieswandt B. Roles of platelet STIM1 and Orai1 in glycoprotein VI- and thrombin-dependent procoagulant activity and thrombus formation. *J Biol Chem*. 2010; **285**: 23629-38.

251 Bandyopadhyay BC, Pingle SC, Ahern GP. Store-operated Ca(2)+ signaling in dendritic cells occurs independently of STIM1. *J Leukoc Biol*. 2011; **89**: 57-62.

252 Feske S. Calcium signalling in lymphocyte activation and disease. *Nat Rev Immunol*. 2007; **7**: 690-702.

253 Podolanczuk A, Lazarus AH, Crow AR, Grossbard E, Bussel JB. Of mice and men: an open-label pilot study for treatment of immune thrombocytopenic purpura by an inhibitor of Syk. *Blood*. 2009; **113**: 3154-60.

6 Appendix

6.1 Abbreviations

AA	Amino acid
AC	Adenylyl cyclase
ACD	Acid-citrate-dextrose
ADAM	A disintegrin and metalloproteinase
ADP	Adenosine diphosphate
AIHA	Autoimmune hemolytic anemia
APC	Antigen presenting cell
ARF	ADP ribosylation factor
ATP	Adenosine triphosphate
BMMC	Bone marrow-derived mast cell
BSA	Bovine serum albumin
BSS	Bernard-Soulier syndrome
BTK	Bruton's tyrosine kinase
Ca^{2+}	Calcium
CalDAG-GEFI	Ca^{2+} and Diacylglycerol regulated guanine nucleotide exchange factor I
CCE	Capacitive calcium entry
CD	Cluster of differentiation
cGMP	Cyclic guanosine monophosphate
CISS	Constructed interference in steady state
CLEC-2	C-type lectin receptor 2
CRAC	Calcium release activated calcium
CRACM	Calcium release activated calcium modulator
CRP	Collagen-related peptide
CVD	Cardiovascular disease
DAG	Diacylglycerol

DKO	GPV/α2β1 double-deficient (mice)
DMEM	Dulbecco's modified Eagle's medium
DMSO	Dimethyl sulfoxide
DNP	2,4-dinitrophenol
EAE	Experimental autoimmune encephalomyelitis
ECM	Extracellular matrix
ER	Endoplasmic reticulum
ERK	Extracellular-signal-regulated kinases
ERM	Ezrin-radixin-myosin-like
F	Coagulation factor
FACS	Fluorescence-activated cell sorting
FcR	Fc receptor
FCS	Fetal calf serum
FITC	Fluorescein isothiocyanate
FSC	Forward scatter
GEF	Guanine nucleotide exchange factor
GP	Glycoprotein
GPCR	G protein-coupled receptors
HEPES	4-(2-hydroxyethyl)-1-piperazineethanesulfonic acid
HMWK	High-molecular weight kininogen
HSA	Human serum albumin
ICH	Intracranial hemorrhage
IFN	Interferon
Ig	Immunoglobulin
IL	Interleukin
IP	Immunoprecipitation
IP_3	Inositol-1,4,5-trisphosphate
IP_3R	IP_3 receptor

ITAM	Immunoreceptor tyrosine-based activating motif
ITIM	Immunoreceptor tyrosine-based inhibitory motif
ITP	Immune thrombocytopenia
IVIG	Intravenous immunoglobulin
LAT	Linker of activated T cells
LB	Luria-Bertani
LRR	Leucine-rich repeat
MAC-1	Macrophage-1 antigen
MACS	Magnetic-activated cell sorting
MFI	Mean fluorescence intensity
MHC	Major histocompatibility complex
MRI	Magnetic resonance imaging
PA	Phosphatidic acid
PAF	Platelet-activating factor
PAGE	Polyacrylamide gel electrophoresis
PAR	Protease-activated receptor
PAR-4	PAR4 activating peptide
PC	Phosphatidylcholine
PE	Phycoerythrin
PGI_2	Prostacyclin
PH	Pleckstrin homology
PI3K	Phosphoinositide-3-kinase
PIP_2	Phosphatidylinositol-4,5-bisphosphate
PIP_3	Phosphatidylinositol-3,4,5-triphosphate
PKC	Protein kinase C
PL	Phospholipase
PM	Peritoneal monocyte
PMC	Peritoneal mast cell

PRP	Platelet-rich plasma
PS	Phosphatidylserine
PX	Phox homology
Rho	Ras homolog gene family
RIAM	Rap1–GTP-interacting adaptor molecule
RT	Room temperature; in case of RT-PCR, RT indicates reverse transcription
SAM	Sterile alpha-motif
SDS	Sodium dodecyl sulfate
SERCA	Sarco/endoplasmic reticulum Ca^{2+}-ATPase
SFK	Src family kinases
SH2	Src homology domain 2
SLP-76	SH2 domain containing leukocyte protein of 76 kD
SOCE	Store-operated calcium entry
Sos	Son of sevenless homologue
SSC	Sideward scatter
STIM	Stromal interaction molecule
TBS	TRIS-buffered saline
TCR	T cell receptor
TF	Tissue factor
TG	Thapsigargin
TLR	Toll-like receptor
TM	Transmembrane
tMCAO	Transient middle cerebral artery occlusion
TP	Thromboxane A_2 receptor
TRIS	Tris(hydroxymethyl)aminomethane
TTC	2,3,5-triphenyltetrazolium chloride
TxA_2	Thromboxane A_2

vWF	Von Willebrand factor
WT	Wildtype

6.2 Acknowledgments

The work presented here was accomplished at the Chair of Vascular Medicine, University Hospital and Rudolf Virchow Center, DFG Research Center for Experimental Biomedicine, University of Würzburg, in the group of Prof. Bernhard Nieswandt.

During the period of my PhD project (May 2007 - April 2011), many people helped and supported me. Therefore I would like to thank:

- Prof. Bernhard Nieswandt for the possibility to work on these interesting topics in his laboratory and for his support, trust, encouragement and useful advice.
- Prof. Georg Krohne for helpful discussions and for reviewing my thesis.
- Prof. Johan W.M. Heemskerk for introducing me into procoagulant activity measurements and for critical discussions and helpful suggestions.
- The Graduate School of Life Sciences (GSLS) of the University of Würzburg and the German Excellence Initiative for financial support. I would further thank the team of GSLS for their support and for organizing all the transferable skills courses.
- All present and past members of the lab for their experimental support, useful discussions and the pleasant atmosphere in the Nieswandt group.
- Ina Hagedorn for her commitment to our joint projects, all the data of the arterial thrombosis models and for helpful discussions.
- Dr. Alejandro Berna-Erro for introducing me into the mouse-handling and for our successful analyses of the *Stim2* mice.
- Dr. Margitta Elvers for her support in the PLD project.
- Prof. Guido Stoll, PD Christoph Kleinschnitz, Dr. Peter Kraft and their team for the tMCAO analyses and helpful discussions.
- PD Dr. Sven Meuth, Michael Schuhmann (University Münster) and their colleagues for the pleasant and fruitful collaboration on the role of the STIM isoforms and PLD1 in EAE.
- Prof. J. Engelbert Gessner (Hanover Medical School) and his group for the successful collaboration on the macrophage / monocyte analysis and for providing the *Ferg1*$^{-/-}$, *FcgR2b*$^{-/-}$ and *FcgR3*$^{-/-}$ mice.

- Prof. François Lanza (Université de Strasbourg) for providing the *Gp5*$^{-/-}$ mice.
- Dr. Beate Eckes (University of Cologne) for the *Itga2*$^{-/-}$ mice.
- Dr. Attila Braun for all his ideas and help with cloning and stem cell culture.
- Dr. Markus Bender for helpful discussions, critical suggestion and continuous support.
- Juliana Goldmann for her kind help and excellent technical support.
- Sylvia Hengst for her kind help in resolving molecular biology problems and her help with the isotope lab.
- Stefanie Hartmann for all the antibodies and Fab fragments.
- Birgit Midloch for help with the stem cell culture.
- Timo Vögtle for his kind help with all immuno assays.
- All animal caretakers in the RVZ and ZEMM who took care of my mice, especially to Azer Achmedov, Marie Blum, Mario Müller, Evi Reichert and Valentina Zemskova. I also like to thank Dr. Dr. Katharina Remer and Dr. Heike Wagner for keeping the animal facilities running.
- All proof-readers of this thesis.
- Prof. Peter Presek and Marko Damm (University of Halle) for their help with the PLD assay.
- Prof. Michael Huber (RWTH Aachen) for purification and culturing of the STIM2 mast cells.
- All external collaboration partners not mentioned by name for giving me insights into new research fields and for important advice.
- I am very thankful for all support from my family and friends during these years, especially my parents for their continuous encouragements and help.
- Finally, and most importantly, my wife Iwona for her support, patience, love and our two wonderful children.

6.3 Publications

6.3.1 Articles

Schuhmann MK*, **Stegner D***, Berna-Erro A, Bittner S, Braun A, Kleinschnitz C, Stoll G, Wiendl H, Meuth SG, Nieswandt B. Stromal interaction molecules 1 and 2 are key regulators of autoreactive T cell activation in murine autoimmune central nervous system inflammation. *J Immunol.* 2010 Feb 1;184(3):1536-42.

Braun A*, Gessner JE*, Varga-Szabo D, Syed SN, Konrad S, **Stegner D**, Vögtle T, Schmidt RE, Nieswandt B. STIM1 is essential for Fcgamma receptor activation and autoimmune inflammation. *Blood*. 2009 Jan 29;113(5):1097-104.

Berna-Erro A*, Braun A*, Kraft R, Kleinschnitz C, Schuhmann MK, **Stegner D**, Wultsch T, Eilers J, Meuth SG, Stoll G, Nieswandt B. STIM2 regulates capacitive Ca2+ entry in neurons and plays a key role in hypoxic neuronal cell death. *Sci Signal.* 2009 Oct 20;2(93):ra67

Elvers M, **Stegner D**, Hagedorn I, Kleinschnitz C, Braun A, Kuijpers ME, Boesl M, Chen Q, Heemskerk JW, Stoll G, Frohman MA, Nieswandt B. Impaired alpha(IIb)beta(3) integrin activation and shear-dependent thrombus formation in mice lacking phospholipase D1. *Sci Signal.* 2010 Jan 5;3(103):ra1.

Gilio K*, van Kruchten R*, Braun A*, Berna-Erro A, Feijge MA, **Stegner D**, van der Meijden PE, Kuijpers MJ, Varga-Szabo D, Heemskerk JW, Nieswandt B. Roles of platelet STIM1 and Orai1 in glycoprotein VI- and thrombin-dependent procoagulant activity and thrombus formation. *J Biol Chem.* 2010 Jul 30;285(31):23629-38.

Bender M, Hofmann S, **Stegner D**, Chalaris A, Bösl M, Braun A, Scheller J, Rose-John S, Nieswandt B. Differentially regulated GPVI ectodomain shedding by multiple platelet-expressed proteinases. *Blood*. 2010 Oct 28;116(17):3347-55.

6.3.2 Review

Stegner D, Nieswandt B. Platelet receptor signaling in thrombus formation. *J Mol Med.* 2011 Feb;89(2):109-21.

6.3.3 Oral Presentations

Store-operated calcium entry is essential for FcγR activation and immune thrombocytopenia. XXIInd Congress of the International Society on Thrombosis and Hemostasis, July 2009, Boston (MA, USA).

Impaired αIIbβ3 integrin activation and shear dependent thrombus formation in mice lacking PLD1. 54. Jahrestagung der Gesellschaft für Thrombose und Hämostaseforschung, February 2010, Nuremberg (Germany).

6.3.4 Poster

Store-operated calcium entry is essential for FcγR activation and immune thrombocytopenia. GPCR Dimer Symposium, October 2009, Würzburg (Germany).

Store-operated calcium entry is essential for FcγR activation and immune thrombocytopenia. 54. Jahrestagung der Gesellschaft für Thrombose und Hämostaseforschung, February 2010, Nuremberg (Germany).

6.5 Affidavit

I hereby declare that my thesis entitled: "**Novel Aspects of Platelet Signaling and of the Pathogenesis of Immune Thrombocytopenia**" is the result of my own work. I did not receive any help or support from commercial consultants. All sources and / or materials applied are listed and specified in the thesis.

Furthermore, I verify that this thesis has not yet been submitted as part of another examination process neither in identical nor in similar form.

Würzburg, April 2011 _____

6.6 Eidesstattliche Erklärung

Hiermit erkläre ich an Eides statt, die Dissertation **„Neue Aspekte in Signalwegen von Blutplättchen und in der Pathogenese der Immunthrombozytopenie"** eigenständig, d.h. insbesondere selbstständig und ohne Hilfe eines kommerziellen Promotionsberaters, angefertigt und keine anderen als die von mir angegebenen Quellen und Hilfsmittel verwendet zu haben.

Ich erkläre außerdem, dass die Dissertation weder in gleicher noch in ähnlicher Form bereits in einem anderen Prüfungsverfahren vorgelegen hat.

Würzburg, April 2011 _____